Title:

Field Testing and Analysis of Blasts Utilizing Short Delays with Electronic Detonators

OSM Cooperative Agreement Number:

S09AP15632

Type of Report:

FINAL REPORT

Reporting Period Start Date:

09/01/2009

Reporting Period End Date:

03/31/2012

Principal Authors:

Dr. Braden Lusk
Dr. Jhon Silva
Kenneth K. Eltschlager

Date Report Issued:

September 2013

Address:

University of Kentucky
Mining and Minerals Resources Building, Lexington, KY
859-257-1105 (office)
859-323-1962 (fax)

Table of Contents

LIST OF FIGURES

DISCLAIMER

ABSTRACT

It is a common practice that the delay (timing) between explosives charges in a mining blast is decided according to the blaster's "experience" and often within the compulsory 8-ms rule. Usually, the timing for a shot based on the blaster experience does not imply that the selected timing is optimized for minimized vibration output. The same applies to timing selected based on the 8-ms rule. Timing for a shot is often selected based on a timing scenario that has been used several times at the operation over a long period of time. The time between charges chosen is that which is known to provide "good results." On the other hand, the 8-ms rule was developed using initiator technology that is no longer applicable in many cases (rule based in technologies developed more than 30 years ago). These facts indicate that with the emergence of electronic detonators it is necessary to rethink blasting as it pertains to timing.

In this study, three clear objectives were set:

1. Determination and documentation of the accuracy of delay times in two specific programmable electronic detonator systems in comparison to the desired (nominal) time programmed into the detonators.
2. Determination of accuracy in delay times for a select number of modern non-electric shock tube type millisecond delay series detonators.
3. Observation and analysis of surface coal mine blast that utilize short delays intervals (<3 milliseconds between charges) and comparison of the results to conventional delay designs at the same location.

To accomplish the objectives, field and laboratory tests were performed. Along with the analysis of field and lab results, it was necessary to perform a theoretical investigation of timing in blast design. During the laboratory stage, the accuracy of delay times in electronic detonator and non-electric shock tube systems were determined. The field tests were conducted at a surface coal mine in West Virginia. During the field testing phase of the research, several mine blasts were recorded and analyzed. Some of the shots utilized short delay intervals lower than 8 milliseconds between charges. Finally, a tool for analysis of the blasts involving timing in the process was developed and adapted from the signature hole technique. The description of all research phases, their findings and subsequent conclusions are included in this report.

ACKNOWLEDGEMENT

The authors acknowledge the assistance of government agencies; OSM, WVDEP, University of Kentucky and Patriot Coal Corporation, Guyan Mine. Much of the fieldwork and data reduction and analysis were performed by graduate student Jhon Silva. Rick Townsend of Nelson Brothers, LLC and the blasters at the Guyan Mine facilitated much of the data collection. Special thanks go to Ken Eltschlager Office of Surface Mining – Appalachian Region by his suggestions through this research and the discussions in order to improve this report.

1. EXECUTIVE SUMMARY

Nowadays, the usage of electronic and non-electric detonators in mine blasting is common; however there is a lack of technical information regarding the accuracy of both types of initiation systems. In this research, the accuracy of those initiation systems was measured. The accuracy of the electronic detonators was the result of the contrast between the actual firing time against the programmed time, while for the non-electric detonators the accuracy was the comparison between time specified from the maker (nominal delay) against the actual firing time. The result for non-electric detonators (two makers, A and B) is included in next table.

Non-electric Detonator Results						
	Non-electric Detonators A			Non-electric Detonators B		
Nominal Delay (ms)	9	1000	1400	25	100	700
Number of detonators Tested	68	60	67	59	65	59
Delay Average (ms)	11.342	1125.501	1418.766	27.751	102.730	715.710
Standard Deviation	4.594	6.550	19.054	0.765	11.250	6.195
Maximum (ms)	15.756	1146.782	1462.381	29.304	123.193	730.575
Minimum (ms)	1.534	1114.704	1367.035	26.155	79.835	697.925
Percent Error	26.023%	12.550%	1.340%	11.005%	2.730%	2.244%

The following figures are obtained when the probability density function of the normal distribution is used to express the results for short (9, 25 and 100ms) and long delays (700, 1000 and 1400ms).

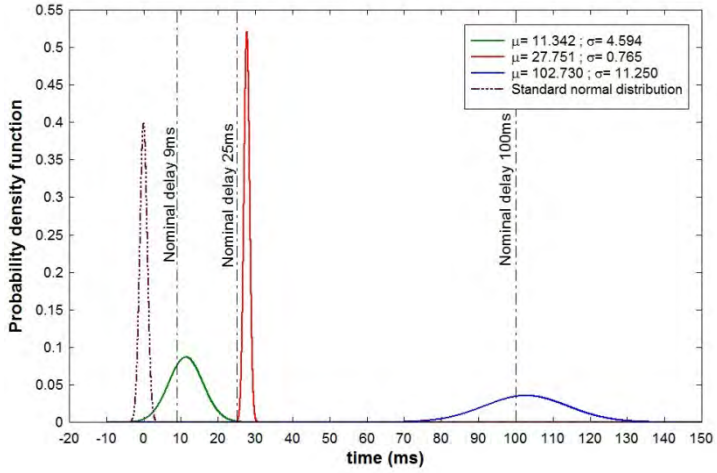

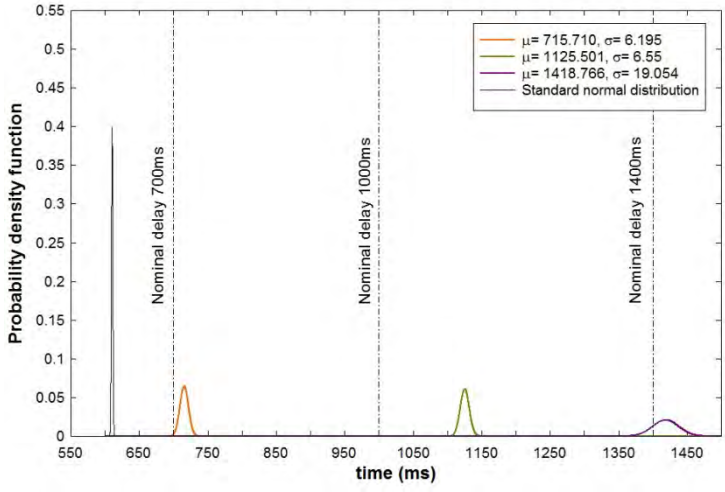

According to the results, none of the non-electric detonators are accurate; in all cases some degree of scatter is presented. For short delays, the less accurate non-electric detonator is the 9ms detonator (percent error 26%); on the other hand, the 25ms delay is the most precise (standard deviation 0.765). However, timing is not accurate (percent error 11%). In the case of long delays, 1000ms delays were less accurate than the delay of 1400ms.

In the case of electronic detonators, the results are included in the next table.

Electronic Detonator Results						
	Electronic Detonators A			Electronic Detonators B		
Programmed Delay (ms)	10	1000	8000	10	1000	8000
Number of detonators Tested	53	43	50	51	52	47
Delay Average (ms)	9.950	1000.543	8003.375	9.987	999.804	7998.589
Standard Deviation	0.092	0.321	3.751	0.030	0.107	0.851
Maximum (ms)	10.201	1001.120	8015.625	10.052	999.954	7999.400
Minimum (ms)	9.816	999.960	7995.190	9.910	999.460	7995.800
Percent Error	-0.501%	0.054%	0.042%	-0.130%	-0.020%	-0.018%

When the percent error and the standard deviations are used to compare the results between the two systems (non-electric and electronic), it is clear (as expected) that the electronic detonators are more accurate and precise than the non-electric systems. In the next figure, a comparison between the two systems for short delays is presented.

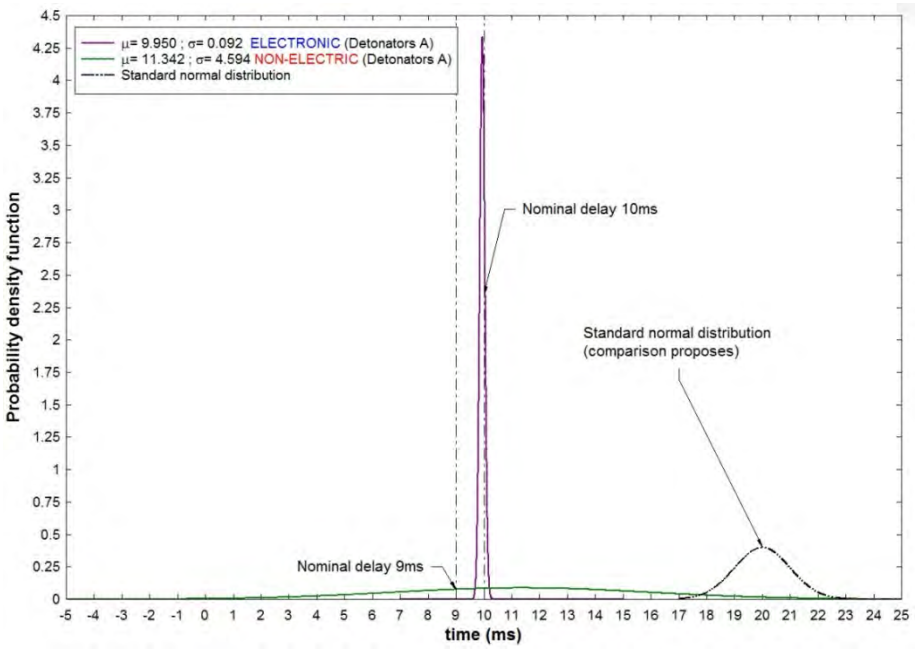

In the previous figure, the precision is given by the shape of the bell curve. For electronic systems, the shape is very sharp, around 10ms (very precise), while the shape for non-electric is very wide (imprecise). In the previous figure, a standard normal distribution was included (a standard normal distribution is a distribution having a standard deviation equal to one).

The traditional approach to control and estimate vibration levels in mine blasting is through the usage of scaled distance theories. The timing implicit to scaled distance approach is given by the 8ms rule. Using such rule, the maximum quantity of explosive allowed to

detonate should not be initiated at intervals of less than 8ms. Despite the common and extended use of the 8ms rule, such rule is not a guarantee that the vibration levels will be minimum or under control. To date, there is not a simple and friendly tool to analyze and estimate the effects of the use of initiation timing different than 8ms or a combination of different initiation times. Due to the lack of such tools in this research, a modification of the signature hole technique using a Monte Carlo was developed. The Monte Carlo based signature technique has four distinct steps:

1. Synthesis of signals (one unique signal for each charge or hole in the blast) from signature data using an equation developed. The signals are created with random variability in amplitude and frequency within a reasonable range to account for energy output variation from hole to hole.
2. Prediction of complete blast output utilizing unique synthetic hole output signal for each hole or charge in a blast sequence. The blast is simulated considering variations in wave travel time, initiation system accuracy, and nominal timing.
3. Monte Carlo iteration of complete blast vibration output. Number of iterations is determined based on convergence of data.
4. Creation of a peak particle velocity histogram. The histogram allows for determination of maximum and minimum expected particle velocities.

To verify the applicability of the methodology, several tests were performed in a surface coal mine in West Virginia. Next figure shows the contrast between the waveforms calculated using the proposed methodology and an actual reading for one of the production test shots.

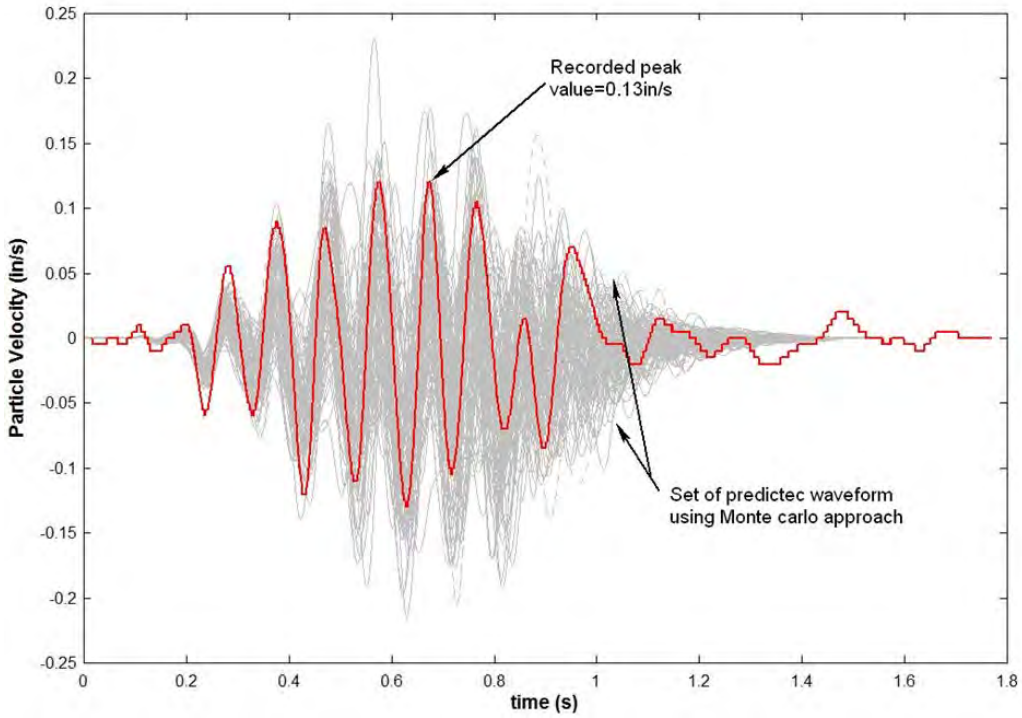

Utilizing this modified signature hole technique, timing scenarios can be adjusted to investigate the effects on blast vibration output for one specific site. This procedure allows for

assessment and definition of a "delay" and also allows for optimizing timing for minimizing vibration output.

Using the calibrated methodology, it was observed that when peak particle velocity and timing is analyzed, there is a range of optimum timing configurations within which the reduction in peak particle velocity values is negligible with respect to the changes in the delay timing. In other words, rather than one specific delay configuration, there is a range that would produce similar results. This provides for a target area in which timings can be adjusted to optimize fragmentation and other productivity and cost based metrics. The concept is illustrated in next figure.

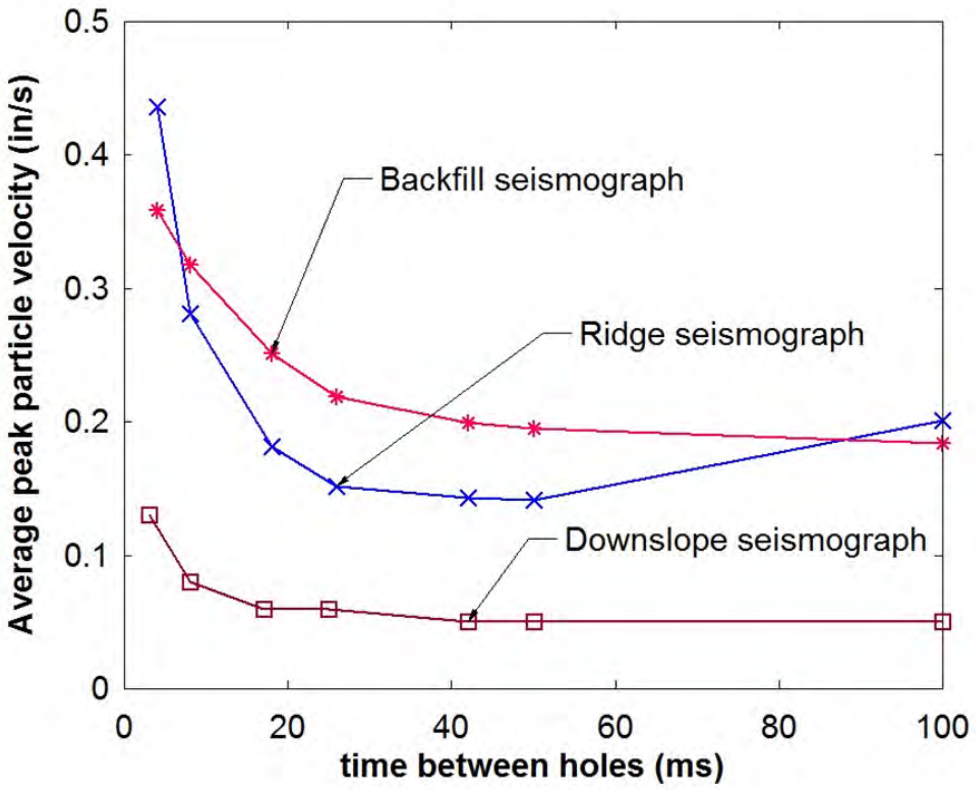

The optimum delay interval is site specific (backfill and ridge in previous figure) and depends on the vibration characteristics of the monitoring location.

Finally, in order to answer the question of what is a delay, from the ground vibration point of view, several aspects need to be addressed:

- Distance from the monitoring point to the production blast and different materials at the monitoring point affect the optimum delay timing of a production blast.
- Changes in main frequency of vibration. It is difficult to change the main frequency of ground vibration in a specific point through the change in the sequence of the initiation delay. In other words, the main frequency of vibration remains almost constant or in a narrow range of frequencies for different combinations of initiation delays at the same point. This can be explained if it is considered that the characteristics of the vibration in a specific place depends on

the dynamic properties of the place where the vibration take place more than the dynamic properties of the place where the production blast is generated.

- Tools to assess vibration levels. It is clear that through the application of the usage of scaled distance methodology and the implicit 8ms minimum delay between charges, it is impossible to study different timing combinations. It is necessary to migrate to another technique such as the modified signature hole technique proposed in this research. Other probabilistic methods are under development as well within the blast vibration research community. Through the use of these tools it is possible to establish a timing configuration with optimum delay intervals to minimize the ground vibrations.

Considering these aspects for a given blasthole geometry (one blasthole) and quantity of explosive detonated at the same time, an optimum delay can be defined as a timing configuration and blasthole sequence giving the minimum possible ground vibration levels for a specific monitoring point. The optimum configuration will distribute the energy around the main vibration frequency (avoiding energy concentrations around a main value) and it is expected that the vibration energy will be in lower ranges when compared to other timing configurations.

Practical application of the results of this study will allow for better control of vibration at points of interest surrounding a blast site. In the beginning phases of blasting, site response characteristics can be assessed. During this process seed waveforms can be collected to allow for simulation of vibration results at key interest points such as homes, schools, or historic structures. The initial blasts can also provide real time data for model validation. After the modeling process has been completed, the results can be used to determine an optimum delay interval to be used for the duration of the project.

2. INTRODUCTION

New technologies and products for mine blasting encourage mining professionals to rethink the traditional manner of application and design methodologies of blasting. Many research findings to date have focused on the advantages of the use of electronic detonators regarding improvements in the particle size distribution of the blasted material; blast vibration control (peak particle velocity reduction); geotechnical protection of the exposed rock mass when blasted; blasting safety improvement; etc. Nevertheless, the question about what is the appropriate delay when using electronic detonators persists.

It is a common practice that the delay (timing) between explosive charges for one specific shot be decided according to the blaster's "experience" or based on the mandatory 8-ms rule. Usually, the timing for a shot based on the blaster experience does not imply that the selected timing is the best timing for that particular shot or the most appropriate timing for that specific situation. The same applies to timing selected based on the 8-ms rule. Commonly if the timing for a shot is selected based on the blaster experience, the blaster will choose a timing scenario that has been used several times in previous shots over a long period of time. According to the blaster, the time between charges chosen is the timing that always provides good results. On the other hand, the 8-ms rule was developed using initiator technology that is no longer applicable in many cases (rule based in technologies developed more than 30 years ago). These facts indicate that with the emergence of electronic detonators it is necessary to rethink blasting as it pertains to timing.

In this study, three clear objectives were set:

1. Determination and documentation of the accuracy of delay times in two specific programmable electronic detonator systems in comparison to the desired (nominal) time programmed into the detonators.
2. Determination of accuracy in delay times for a select number of modern non-electric shock tube type millisecond delay series detonators.
3. Observation and analysis of surface coal mine blast that utilize short delay intervals (<3 milliseconds between charges) and comparison of the results to conventional delay designs at the same location.

In order to accomplish the objectives of this study, field and laboratory tests were executed. Along with the analysis of field and lab results, it was necessary to perform a theoretical investigation of timing in blast design. During the laboratory stage, the accuracy of delay times in electronic detonator and non-electric shock tube systems were determined. The activities comprising the field tests were conducted at a surface coal mine in West Virginia. During the field testing phase of the research, several mine blast were recorded and analyzed. Some of the shots utilized short delay intervals lower than 8 milliseconds between charges. Finally, a tool for analysis of the blasts involving timing in the process was developed. It was found that the most convenient methodology to modify (between all available methodologies involving timing in the design of a shot) was the signature hole method. The description of all research phases, their findings and subsequent conclusions are included in this report.

3. EXPERIMENTAL

Field and laboratory experiments were conducted to complete the research and accomplish the objectives. Objectives one and two (accuracy of detonators) were accomplished with laboratory testing. Objective three was completed in the field and with subsequent development of a model to predict vibrations.

3.1 Laboratory experiments

Traditionally there are few sources of technical information available about the accuracy of detonators for mining (electronic or non-electric). It is not disputed that there is a difference between the specific delay interval (nominal or programmed time) and the time at which a detonator fires. This difference is commonly known as cap scatter and is generally considered to be higher for non-electric detonators than for electronic detonators. The first two objectives in this project quantified the value of cap scatter for several initiation systems (determination of accuracy). The experimental setup and the findings are presented as follows.

3.1.1 Experimental setup

To test the detonator's accuracy, the break wire principle was used. At the moment of detonation, the break wire is severed, causing a loss of continuity through a signal in the wire. A counter-timer card triggered on this event and reported a detonation time. It was also necessary to determine the zero reference time for the event, or the time at which the detonator was initiated. The difference between the measured detonation time and the zero reference time represented the realized delay achieved by the detonator.

To collect the information from the detonator accuracy tests, a National Instruments PCI-6602 counter-timer card along with a custom software application developed in Labview was used. It included eight 32 bit counter channels and 32 configurable digital IO lines. With the onboard clock running at 80 megahertz, it was capable of measuring events down to 6.25; nanoseconds (6.25e-006ms) making it well suited for this testing. Six of the channels were configured for monitoring break wires. A seventh channel was used to monitor the control signals coming from the electronic initiator blasting machine.

The channels on the counter-timer card relied on two signals for measuring time. The first was the counter source, which was connected to a known internal timebase. It produced an 80 megahertz signal. The hardware counted every occurrence of a rising edge produced by the clock. The gate was the other important input used when performing period measurements. The gate signal determines when the hardware should report a count to the software application. This is demonstrated in Figure 1. The arm start trigger shown was used to determine when the counter started counting. It counts every edge received from the internal timebase. The gate was connected to the break wire. Once continuity was lost and that signal went low, the gate was asserted and the appropriate output was captured.

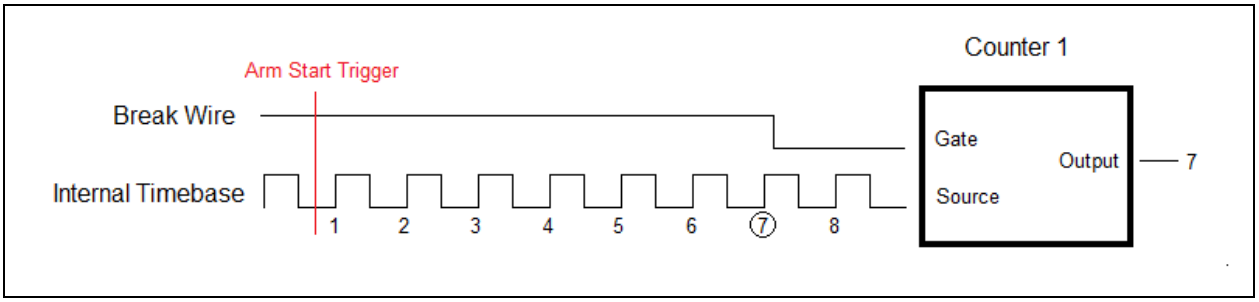

Figure 1 Illustration of Interaction between Break Wire and Counter

For the electronic detonator systems, the blasting machine communicated with the detonators using a low frequency AC signal. The necessary commands to program the detonator timing, arm them, and detonate them were sent via this signal (arm start signal). It was observed that communication is ceased prior to detonation, presumably because a fire signal has been transmitted to the detonators. This break in the signal was used to determine a zero reference time for the application to calculate the achieved delay timing. Figure 2 demonstrates this as realized in the counter time hardware. The arm start trigger, common across all counter channels, signaled the hardware to begin counting. It is important to note that all counters began counting at the same moment due to the arm start trigger, so they are effectively synchronized. Every falling edge on the signal generated from the blasting machine was captured at the gate. The corresponding count values were reported to the output for processing in the software application.

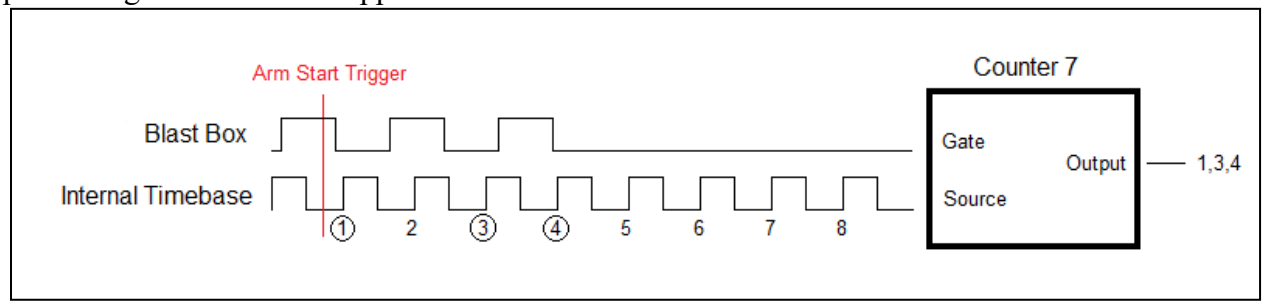

Figure 2: Blasting Machine Counter Interaction

For non-electric detonator systems, the zero reference time was determined in a similar fashion to the detonation time. The detonators being tested were connected via a bunch block. The bunch block ensured that the detonators under test shared a common start time. A break wire positioned within the bunch block captured this time which served as the zero reference time. This can be seen in Figure 3. The detonators being tested can be seen as the shock tube leading from the bunch block to the right of the figure (orange wires). The detonator used to initiate them can be seen as the shock tube leading into the bunch block from the left of the figure (yellow wire). The small wires (green wires) are the break wire which were positioned with and directly adjacent to the initiator.

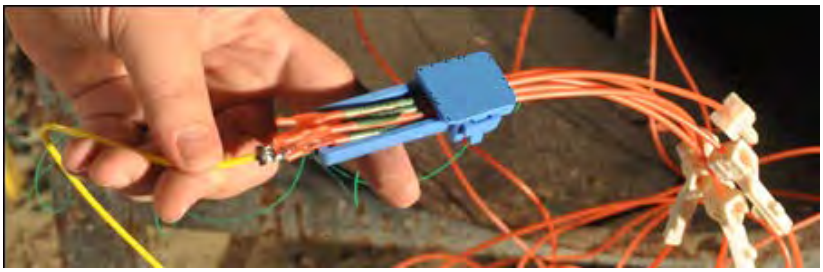

Figure 3: Bunch Block Configuration

Once the hardware captured the detonation and reported the corresponding counts, it would convert this value to time. Due to the synchronization, it is simply a matter of subtracting the two values and dividing the count by the frequency of the internal timebase. This was accomplished once the measured counts were transferred to the Labview application.

The Labview application was responsible for a number of activities. It provided a graphical user interface for the person conducting the test (Figure 4). Fields were included to record information pertinent to the testing. It also provided feedback to the user to ensure proper operation.

The application was also responsible for controlling the hardware. It configured the counter devices for the task. It controlled the various digital lines used to establish the levels in the break wires and manage the reset-set latches. Finally, it sets the arm start trigger to synchronize the channels on the card. Another function was calculating the times from the measured counts and accumulating those values. When convenient for the user, it generated a report including the test times and summary statistics.

To validate the data collected by this system, a Blaster Ranger high speed camera was used to document several of the tests using the appropriate frame rate. This footage was manually reviewed to conclude if the counter system was accurately collecting the times of detonation.

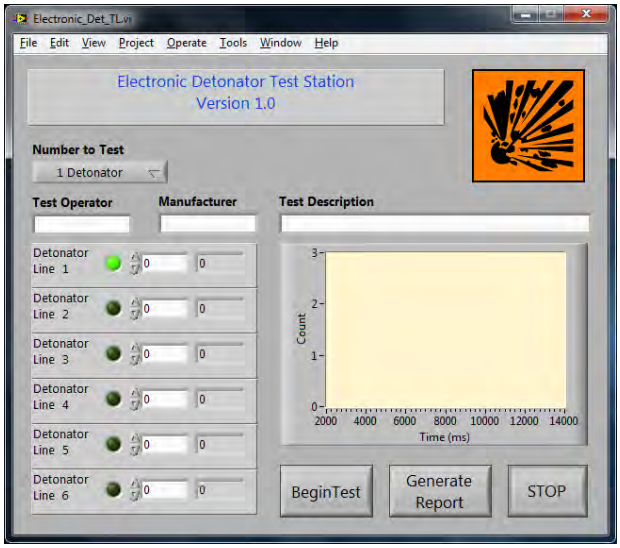

Figure 4: Graphical User Interface test setup

Viewing the video on a frame by frame basis allowed for the visual confirmation of when each detonator initiated relative to the others. The first detonator initiating in a test sample was considered time zero, with timing for each following detonator based on this reference point. This was done since the true time zero could not be obtained from the video data.

For each data set, the video was recorded at a specified frame rate, varying from 1,000 frames per second (fps) to as high as 16,000 fps. With the frame rate for each data set known, the time from one frame to the next could be calculated. For example, recording at 4,000 fps results in a time lapse of 0.25millisecond (ms) from frame to frame. Therefore, if the first detonator initiating is time zero and the following detonator is shown to detonate 10 frames later, it can then be calculated that the difference between the two detonators initiating is 2.5ms. This process was repeated for each subsequent detonator in the test sample.

In total, 674 detonators were tested. The detonators consisted of two electronic systems and two non-electric systems. When possible, different lots were procured to provide a more representative sample. Table 1 outlines the testing matrix.

Table 1 Detonator Matrix

Electronic Detonator Matrix						
Manufacture	**Electronic detonator A**			**Electronic detonator B**		
Programmed delay (ms)	10	1000	8000	10	1000	8000
Lots	3	3	3	3	3	4
Total detonators	53	43	50	51	52	47

Non-electric Detonator Matrix						
Manufacture	**Non-electric detonator A**			**Non-electric detonator B**		
Nominal delay (ms)	9	1000	1400	25	100	700
Lots	1	1	1	2	2	2
Total detonators	68	60	67	59	65	59

The purpose of different delays was to include a wide range, including short and long timing, to analyze the influence of the delay time in the accuracy of the initiation system for both non-electric and electronic.

With the high degree of automation built into the testing apparatus, the methodology proved to be fairly simple. The detonators to be tested were first loaded into the test cell consisting of short sections of steel pipe. The steel pipe served the purpose of deflecting the shrapnel away from adjacent test cells and directing it away from the break wire leads. A bar running the length of the test cells had small holes through which the detonators were placed (Figure 5).

Figure 5 Test Cells

The break wire used for all of the testing was Belden 30 AWG solid copper hook-up wire with polyvinyl chloride insulation. The break wire was held firmly against the tip of the detonator and secured with a piece of vinyl tape. Care was taken to ensure the break wire was placed running through the center of the tip. This technique is displayed in Figure 6.

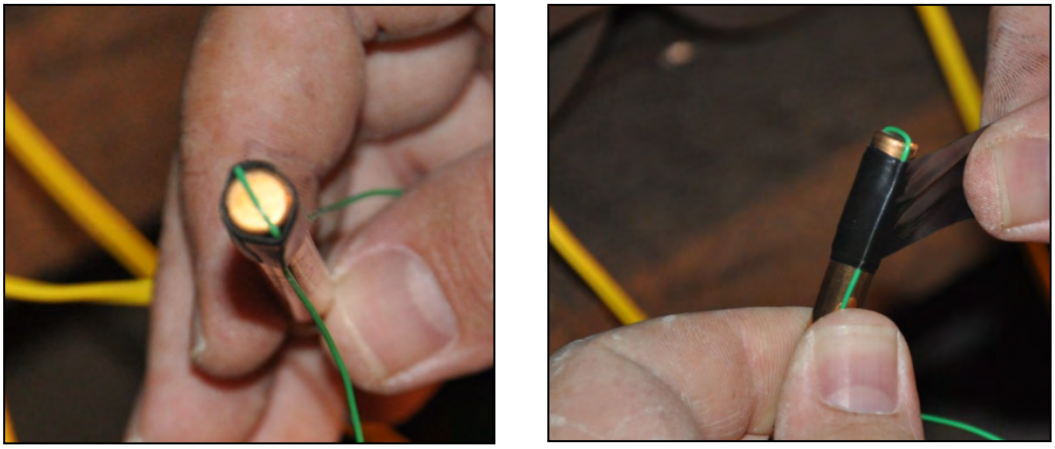

Figure 6 Break Wire Placement

Figure 7 shows detonators awaiting test in the test cells. Each detonator is shown with its own break wire ready for the test sequence.

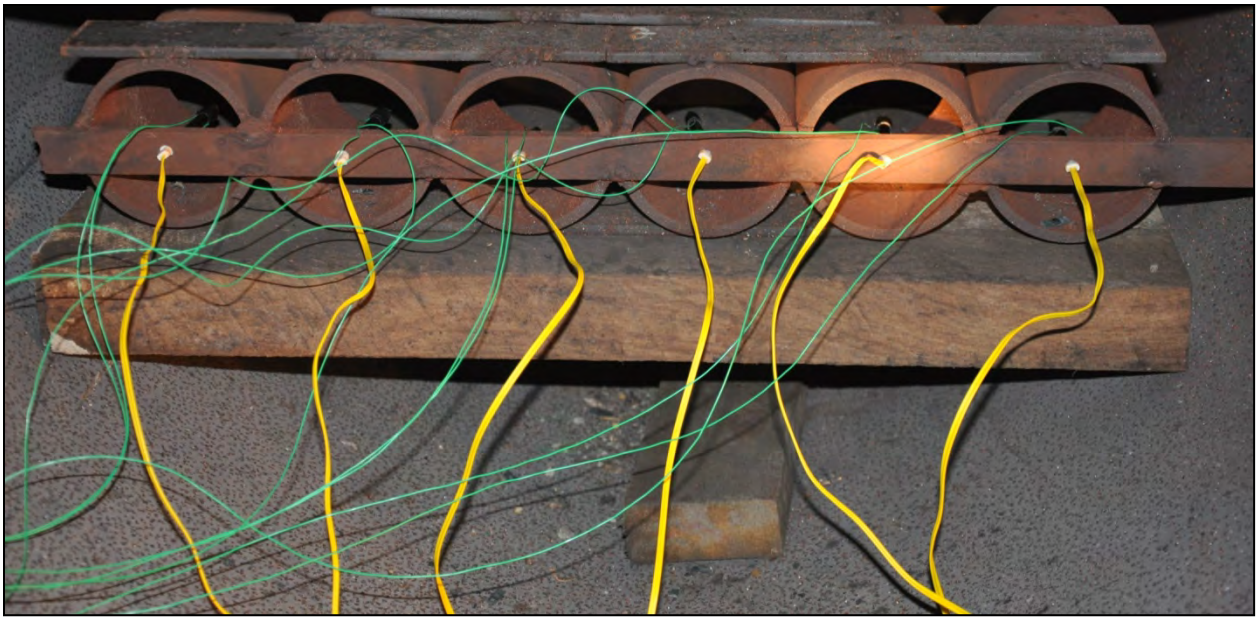

Figure 7 Detonators Awaiting Test

The following image shows the break out box, housing the interface electronics, with the break wires and blasting machine control wires attached (Figure 8).

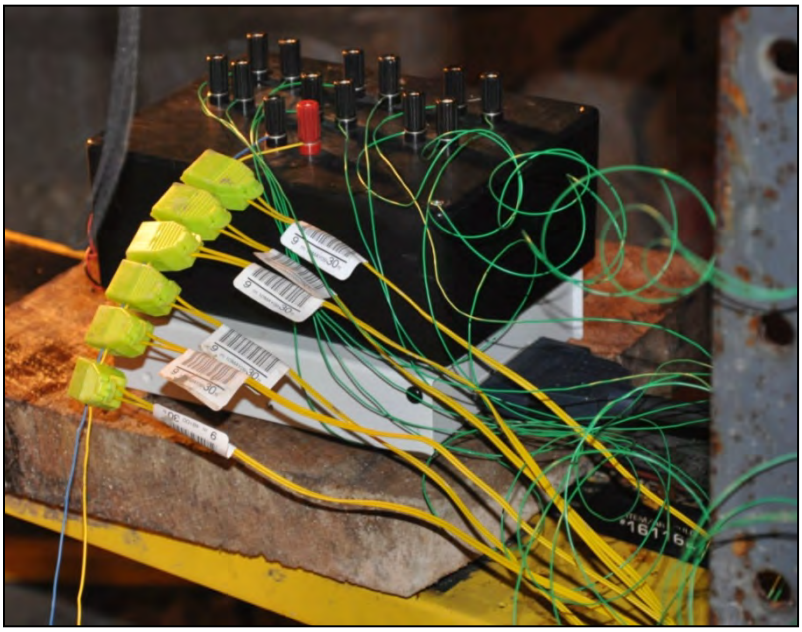

Figure 8: Electronics Break Out Box

For non-electric detonator testing, the detonator in the bunch block was placed under the test cell. After a number of misfires occurred the setup was changed. The bunch block was placed in a galvanized trash can filled with sand and buried. After this change in the experimental setup, no other misfires occurred.

3.1.2 Non-electric detonators results

The frame grabs shown in Figure 9 illustrate the detonation sequences for one test sample of non-electric detonators, in this case five detonators filmed at 4,000 fps. For this series, a detonation event is shown to occur at Frames 00, 08, 68, 105, and 121. The frame prior to each event is also shown for comparison purposes.

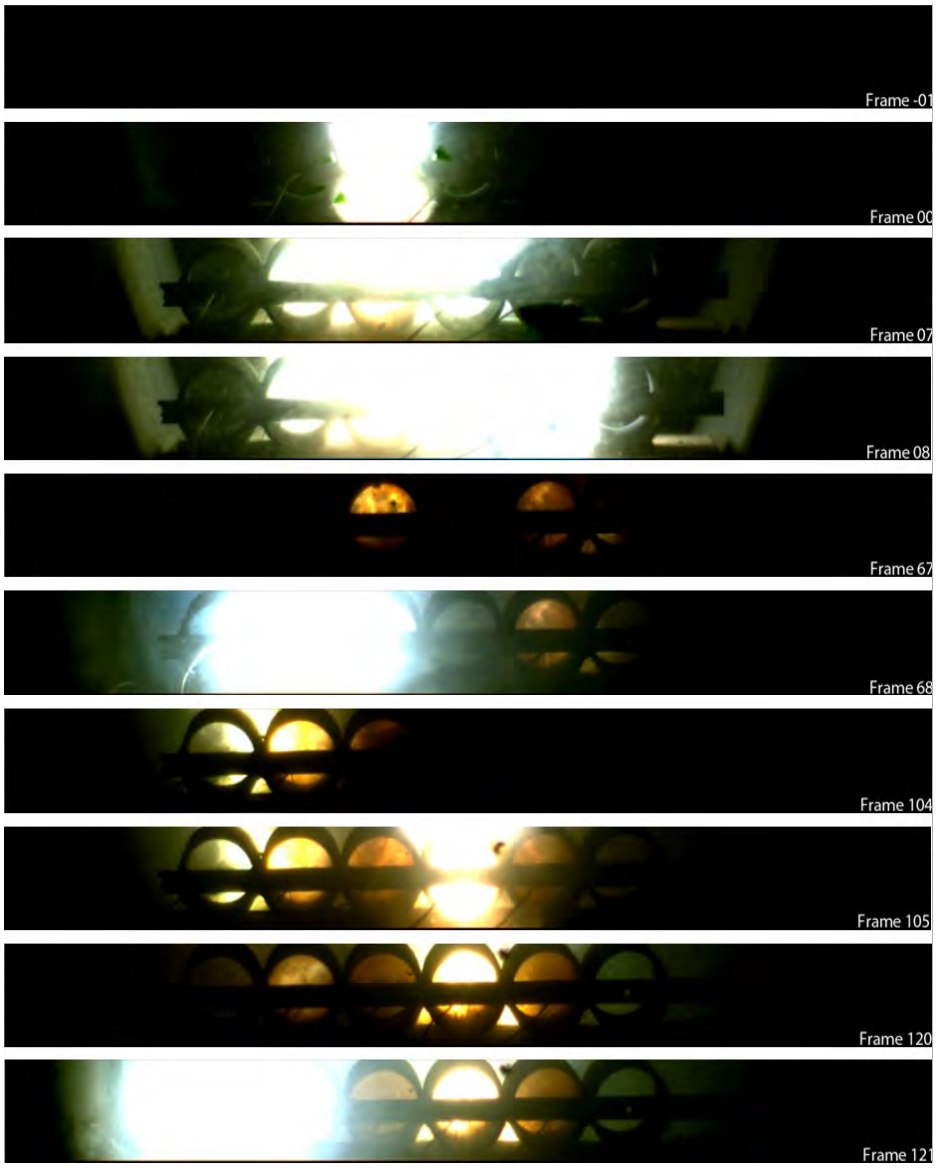

Figure 9 Frame grabs from non-electric sample showing detonation sequence

Table 2 provides a summary of the frame number at which a detonation event occurred, the calculated time using the given frame rate, and the time recorded by the testing system.

Table 2 Summary of Results for Non-Electric Validation Example

Non-electric 4000 fps			
Tube #	Frame Number	Calculated time using high speed video (ms)	System recorded time (ms)
1	0	0.00	0.00
2	8	2.00	1.76
3	68	17.00	16.82
4	105	26.25	26.13
5	121	30.25	30.57

It is important to note two temporal considerations when reviewing the visual analysis. One is that each frame represents a window of time created by the shutter speed. This window for a video shot at 4,000 fps is 0.25ms long. An event shown in a single frame could have occurred at any point in this window. The second consideration is that the detonation event is not an instantaneous one. There is a variable amount of time inherent in this process. This can be seen when comparing Frames 68 and 105 in Figure 9. Nevertheless, manual comparison of the video data allowed for a high degree of confidence in the data collected by the break wire system.

The results of the testing from the non-electric detonator systems are summarized in Table 3 and graphically in Figure 10, Figure 11 and Figure 12.

Table 3 Summary non-electric detonator results

Non-electric Detonator Results						
	Non-electric Detonators A			Non-electric Detonators B		
Nominal Delay (ms)	9	1000	1400	25	100	700
Number of detonators Tested	68	60	67	59	65	59
Delay Average (ms)	11.342	1125.501	1418.766	27.751	102.730	715.710
Standard Deviation	4.594	6.550	19.054	0.765	11.250	6.195
Maximum (ms)	15.756	1146.782	1462.381	29.304	123.193	730.575
Minimum (ms)	1.534	1114.704	1367.035	26.155	79.835	697.925
Percent Error	26.023%	12.550%	1.340%	11.005%	2.730%	2.244%

Normal distribution probability density function was chosen to compare the results. All non-electric detonator results are included in Figure 10. In this figure, it is clear, how the most precise delay time is presented at 25ms nominal delay. The average value for this detonator set shows a difference of 2.751ms when compared to the nominal time delay (25ms). The precision of this delay is reflected in the lower value of the standard deviation. Figure 10, also shows how the least accurate delay time is the 1000ms detonator. The difference between the nominal delay time and the average tested is around 125.501ms.

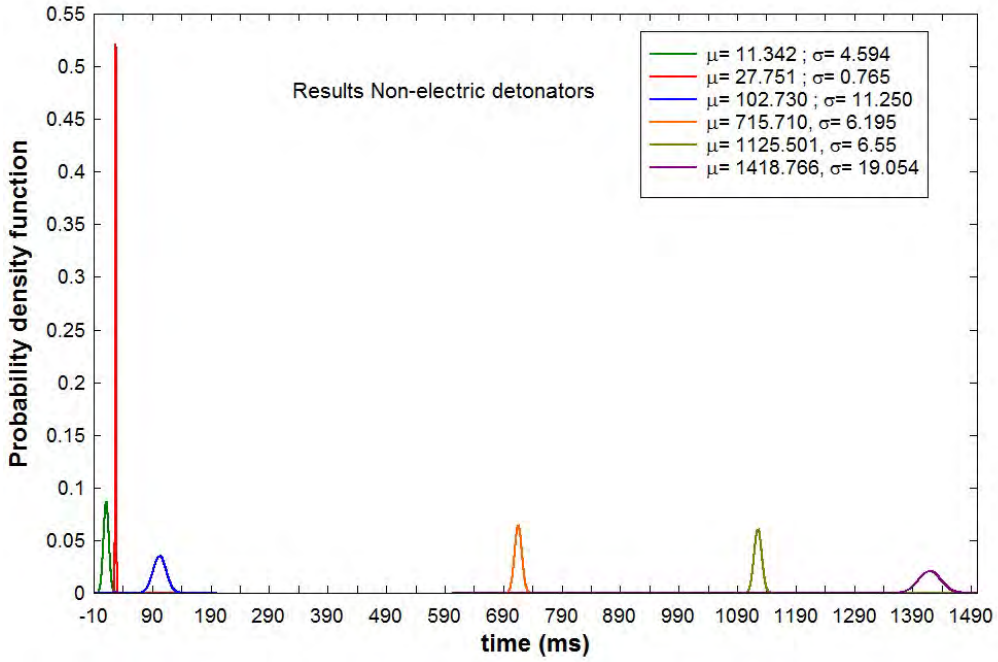

Figure 10 Normal distribution, density function, non-electric detonators tested.

Figure 10 was split to show the short and long delay periods separately in Figures 11 and 12 respectively.

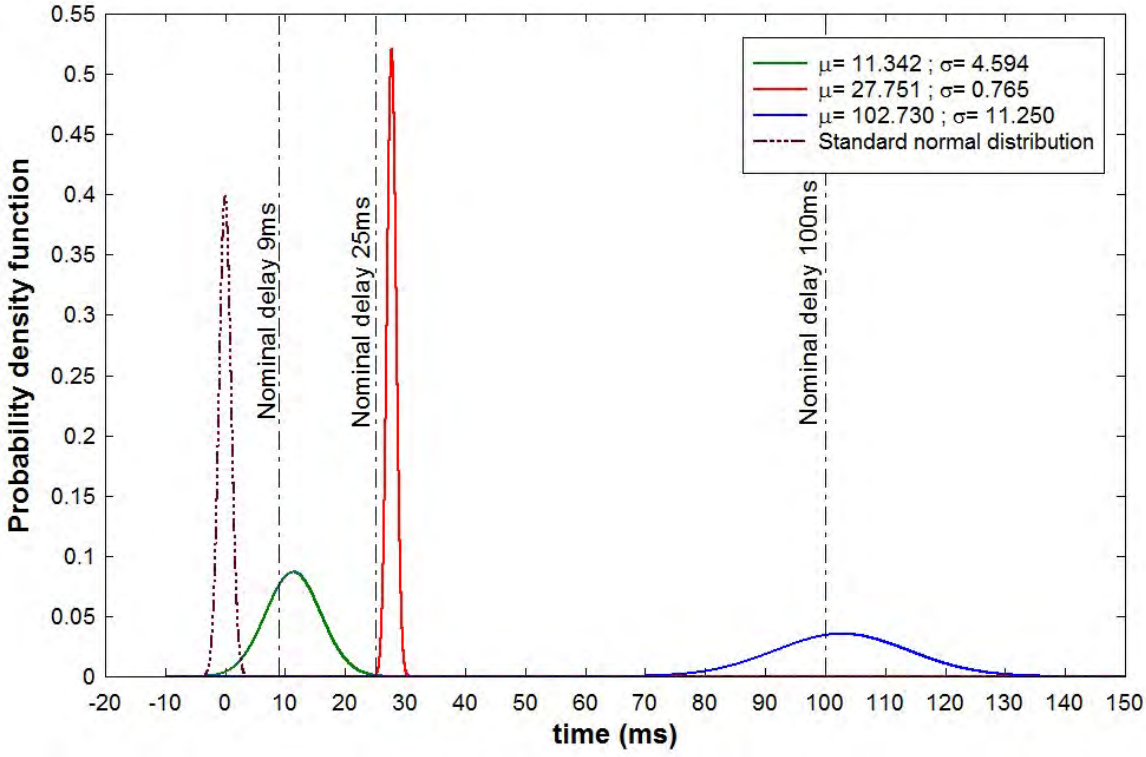

Figure 11 Normal distribution, density function, non-electric detonators at 9, 25 and 100 ms nominal delays.

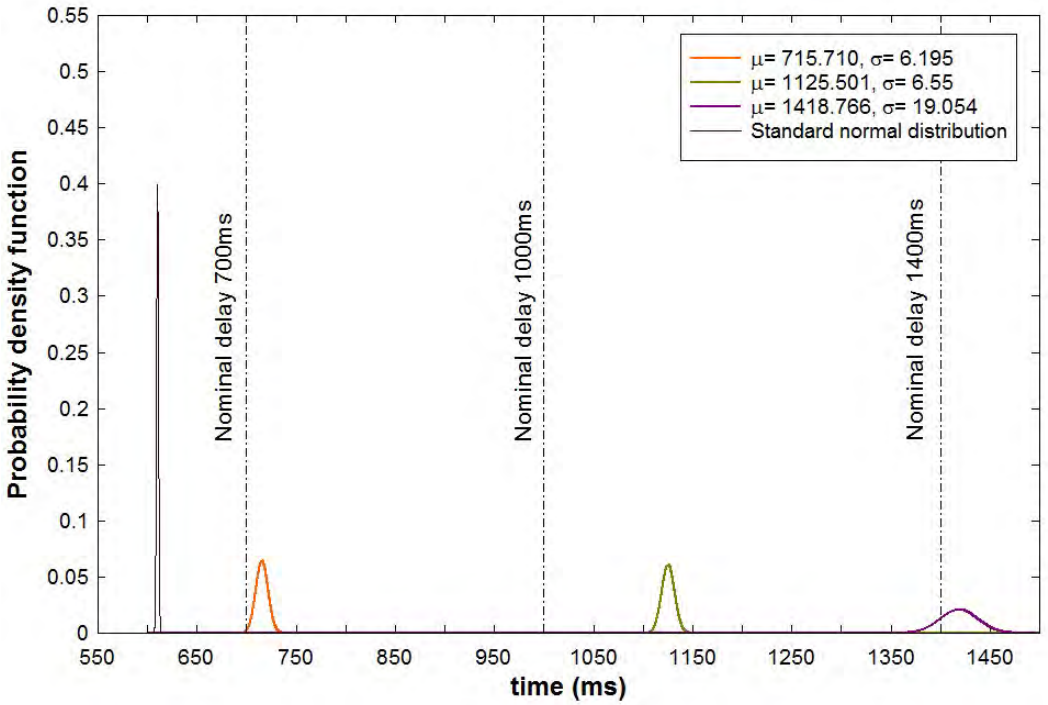

Figure 12 Normal distribution, density function for nominal delays, non-electric detonators at 700, 1000 and 1400 ms.

3.1.3 Electronic detonators results

High speed video data was also used to confirm testing results for the electronic detonator systems. Table 4 provides a summary of the frame number at which a detonation event occurred, the calculated time using the given frame rate, and the time recorded by the testing system for a single test event. These results were typical when comparing video data to the recording system.

Table 4 Summary of Results for Electronic Validation Example

Electronic 8000 fps			
Tube #	Frame Number	Calculated time using high speed video (ms)	System recorded time (ms)
1	0	0.00	0.00
2	11	1.38	1.48
3	18	2.25	2.26
4	22	2.75	2.27
5	26	3.25	2.76

The frame grabs shown in Figure 13 illustrate the detonation sequence for one test sample of electronic detonators, in this case five detonators filmed at 8,000 fps. For this series, a detonation event is shown to occur at Frames 00, 11, 18, 22, and 26. The frame prior to each event is also shown for comparison purposes.

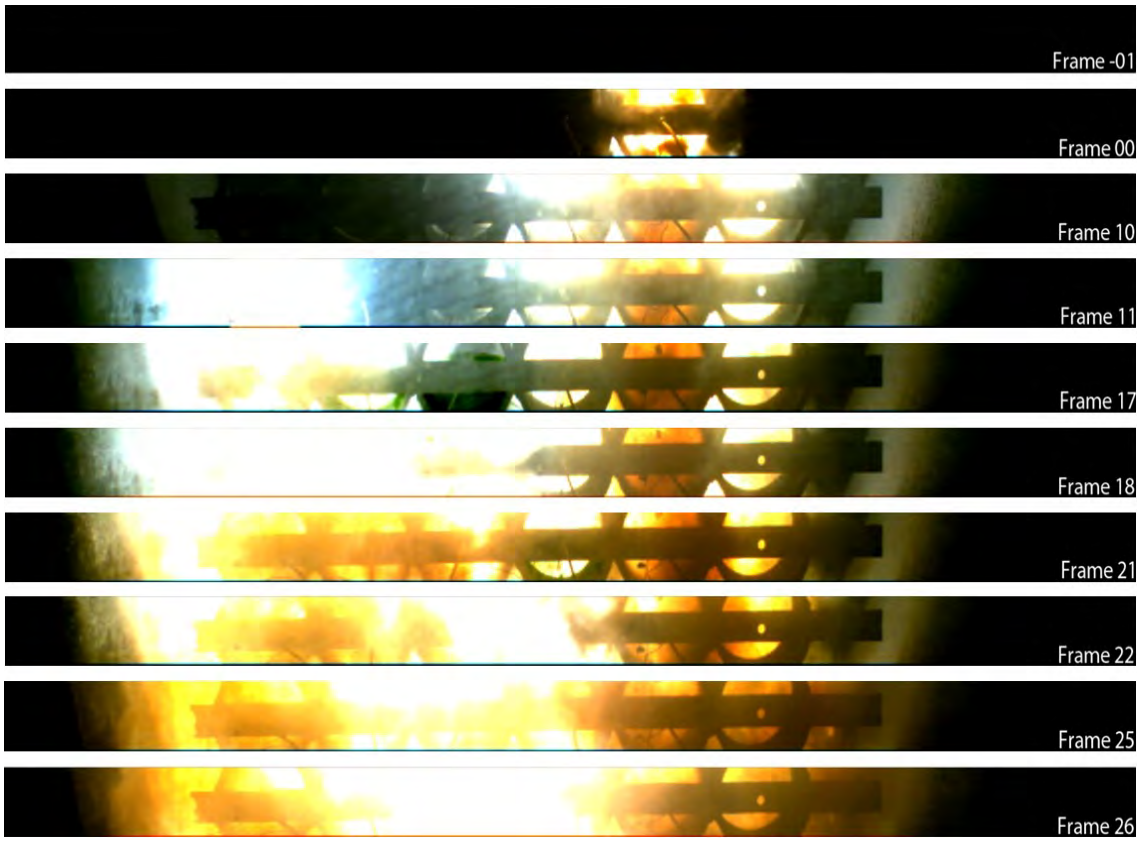

Figure 13: Frame grabs from electronic sample showing detonation sequence

The results of the testing from the electronic detonator systems are summarized in Table 5 and graphically from Figure 14 to Figure 17.

Table 5 Summary statistics electronic system

Electronic Detonator Results						
	Electronic Detonators A			Electronic Detonators B		
Programmed Delay (ms)	10	1000	8000	10	1000	8000
Number of detonators Tested	53	43	50	51	52	47
Delay Average (ms)	9.950	1000.543	8003.375	9.987	999.804	7998.589
Standard Deviation	0.092	0.321	3.751	0.030	0.107	0.851
Maximum (ms)	10.201	1001.120	8015.625	10.052	999.954	7999.400
Minimum (ms)	9.816	999.960	7995.190	9.910	999.460	7995.800
Percent Error	-0.501%	0.054%	0.042%	-0.130%	-0.020%	-0.018%

Normal distribution probability density function was chosen to compare the results. All electronic detonator results are included in Figure 14. In this figure, it is clear how detonators from system A are less accurate and precise when compared to system B. Also in this result, it is evident how the precision of electronic detonators decreases when the delay time increases.

It is evident when standard normal distribution is used to compare results in Figure 15 to Figure 17 (see how the shape of the standard normal distribution changes in those figures).

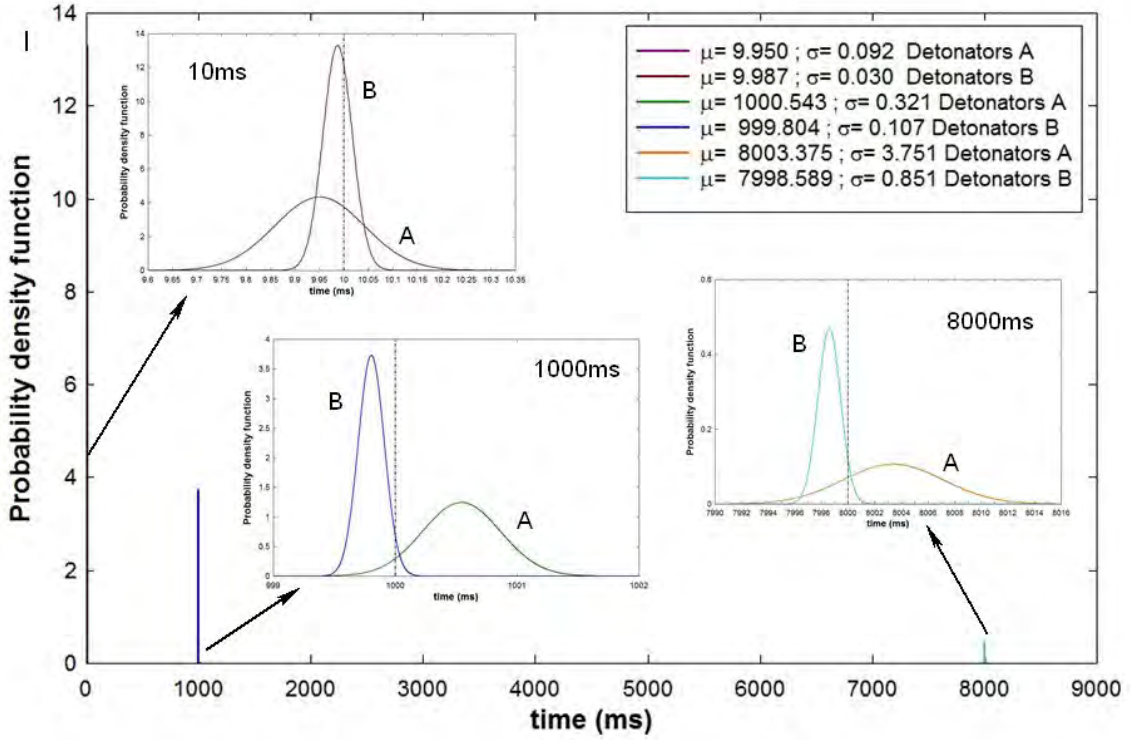

Figure 14 Normal distribution, density function, electronic detonators tested.

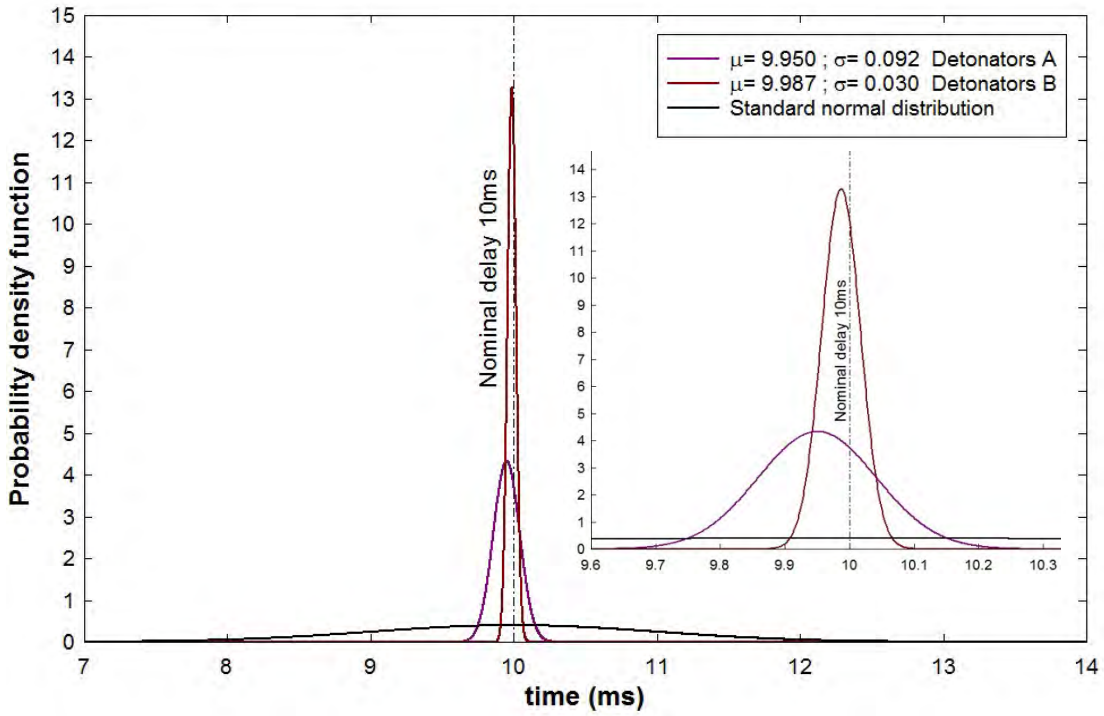

Figure 15 Normal distribution, density function, electronic detonators at 10ms Programmed delays.

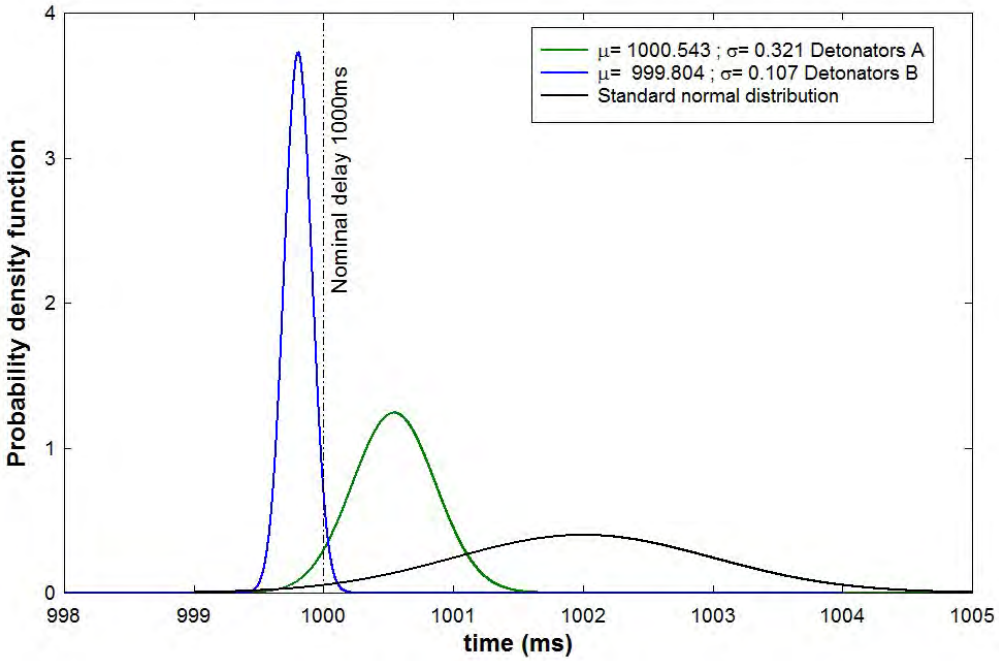

Figure 16 Normal distribution, density function, electronic detonators at 1000ms programmed delays.

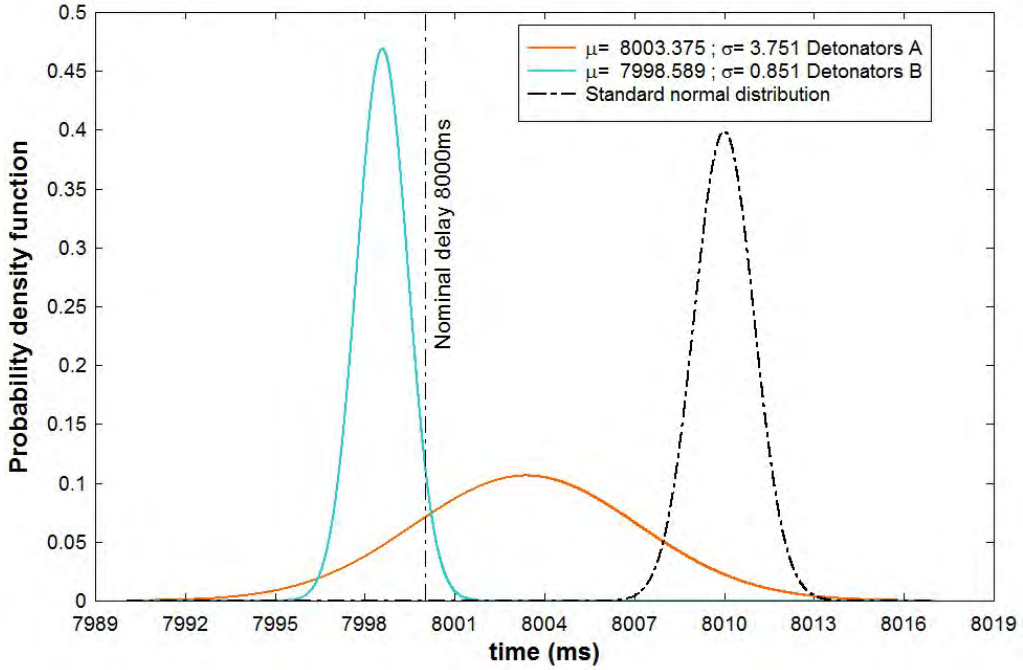

Figure 17 Normal distribution, density function, electronic detonators at 8000ms programmed delays.

Finally when non-electric and electronic initiation systems are compared side by side, at nominal delay time of 9 and 10ms respectively, Figure 18 is obtained.

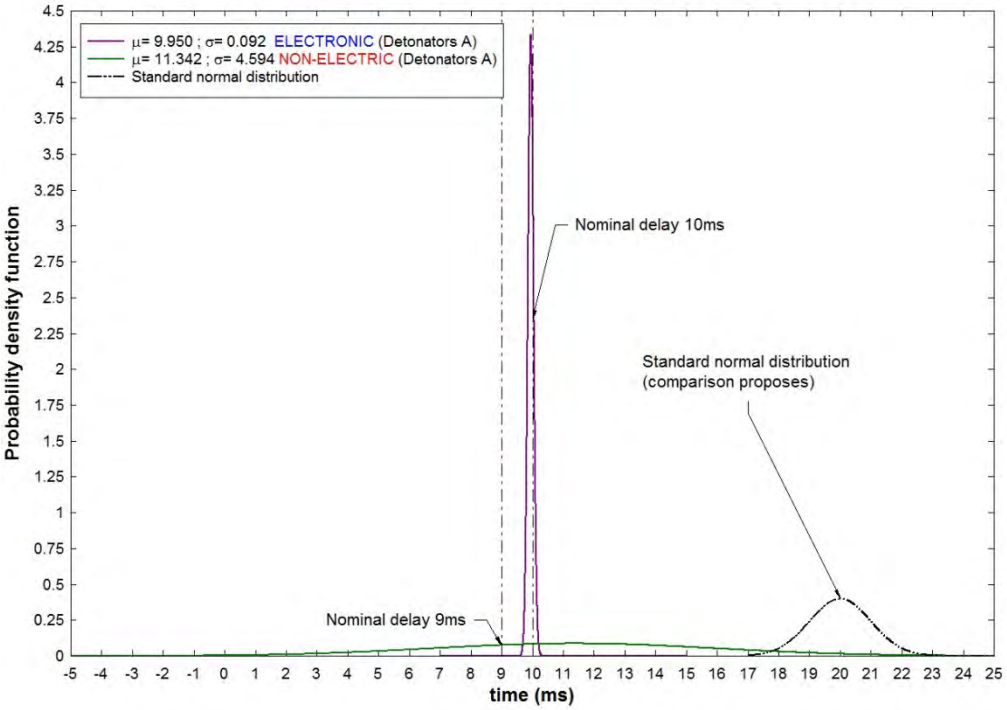

Figure 18 Comparison 9ms and 10ms nominal delay (non-electric Vs electronic)

Figure 18 shows clearly the difference between electronic and non-electric initiation systems regarding precision and accuracy.

The laboratory experiments quantified "cap scatter" for several initiation systems, and confirmed the basic assumption that electronic detonators have superior accuracy and precision. Furthermore, the data was useful as input for a theoretical model described later in this report.

3.2 Field Experiments

To complete objective three, a seismograph network was installed in a surface coal mine in West Virginia. The ground vibration levels and airblast for several production shots were recorded. Along with production shots, some shots were specifically designed to use short delay intervals between charges. Two specific periods were utilized for data collection at the mine. The first period of information collection was between summer and fall 2010 while the second period of field tests occurred in summer 2011.

3.2.1 Site description

Field instrumentation was placed at the Patriot Coal Corporation, Guyan mine, in Logan County West Virginia. This operation is a typical surface coal mine; the mine utilizes the truck and shovel/loader mining method. The coal is sourced from the Five Block, Stockton and Coalburg seams, with a 15 to 1 average overburden coal ratio. (Source: Patriot Coal Corporation). The Coalburg seam has been previously mined underground at this site. Figure 19 shows the location of the site where the information was collected.

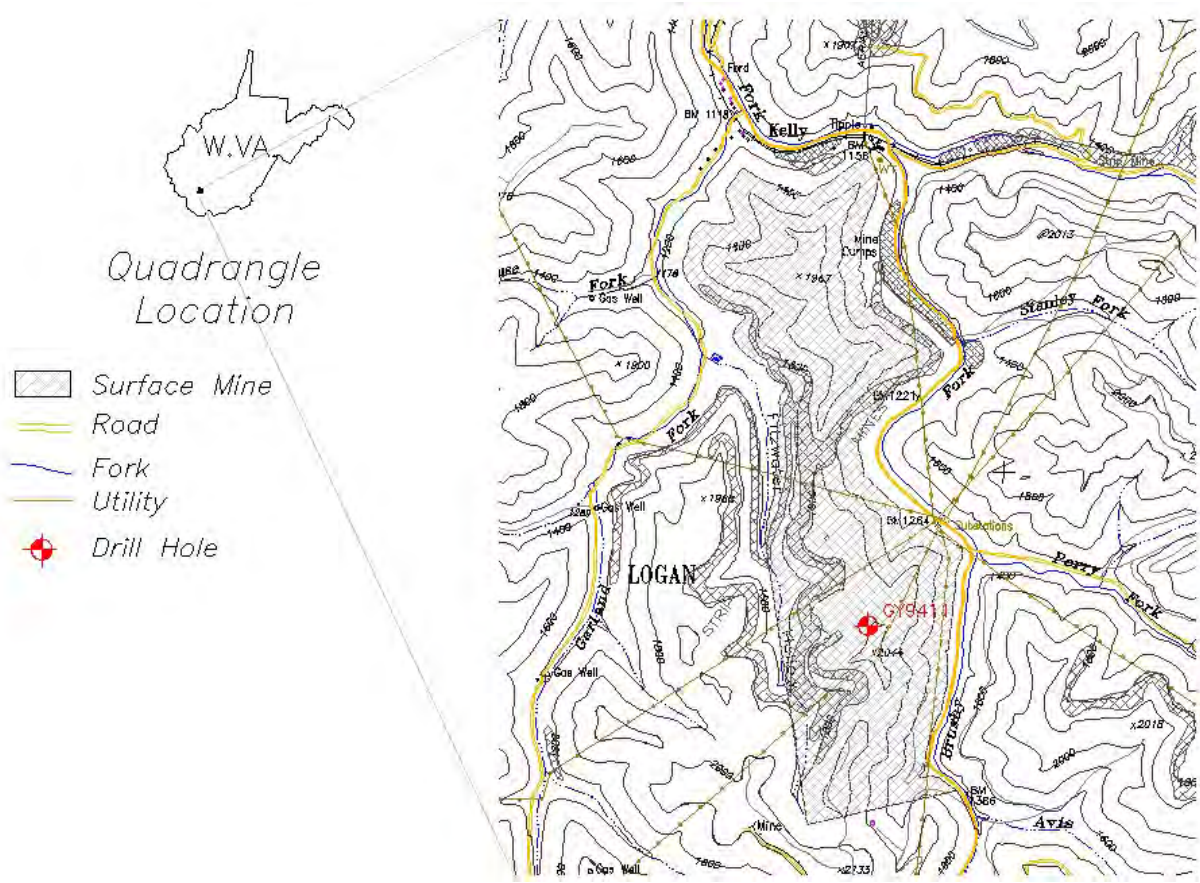

Figure 19 Location of the mine where the field experiments were conducted

Stratigraphic units present within the area include the Homewood Sandstone, multiple splits of the Stockton Coal seams, Upper Coalburg Sandstone and the Coalburg Coal seam. The overburden where the majority of blasting activity took place was the Coalburg Sandstone which is a massive sandstone and ranges in thickness from about 70 to 100 feet. Figure 20 shows the stratigraphic column in the area were the blasting activity took place during the collection of information for field experiments.

3.2.2 Instrumentation

The objective of the instrumentation was to establish the differences in ground vibrations and airblast when the delay system changes between non-electric and electronic. At the same time, the observation and analysis of shots that utilize short delays intervals (<3ms between charges) was performed.

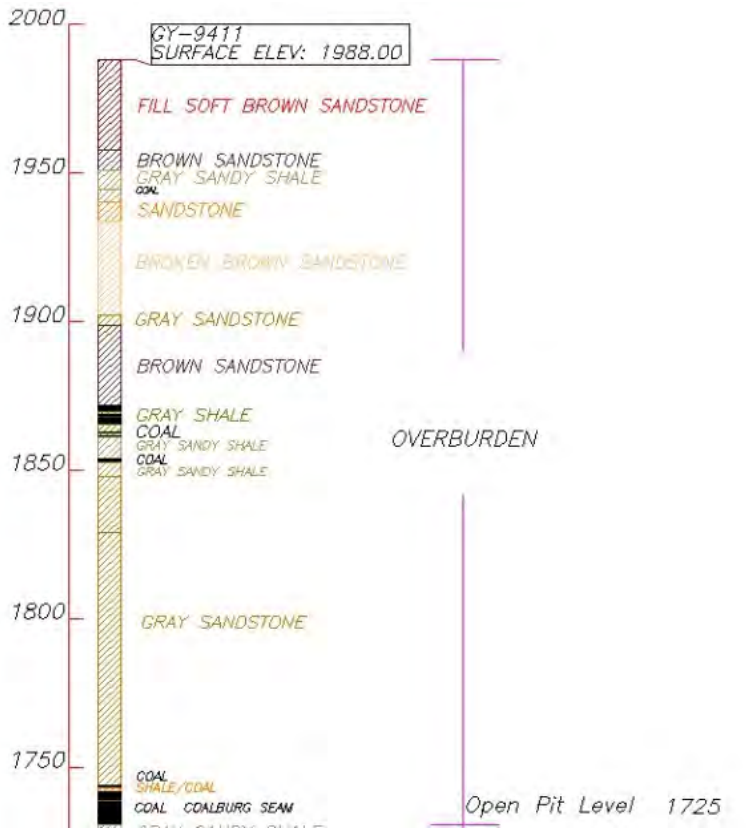

Figure 20 Drill Hole GY 9411, stratigraphic column

3.2.2.1 Instrumentation for summer and fall 2010

For the initial study period, seismograph locations were planned to follow a radial pattern centered on drillhole GY9411 (Figure 19). Several visits to the mine (three visits) were needed to verify the site conditions and install seismographs. Many modifications were required, either due to difficulties in access or because some planned locations for seismographs laid in areas outside the mine property boundary. Finally, the seismographs were installed along the three orientation lines shown in Figure 19 using drillhole GY9411, as the reference point.

During this first period of information collection, 12 seismographs were installed at the mine. Table 6 includes the description of the seismographs and the coordinates in both geodetic and state plane systems.

Table 6 Seismograph location and their characteristics

SEIS	DESCRIPTION	NAD 83		NAD 27		Owner
		E	W	X	Y	
1	MINI-SEIS II Inst# MS II 2D2G 1/4M S/N: 4763	37.827306	81.79722222	1769695.032	302194.887	UK
2	NS 5400 S/N: 2722	37.829722	81.7926667	1771018.239	303063.285	Saul's
3	NS 5400 S/N: 2242	37.829306	81.78955556	1771915.431	302904.128	Saul's
4	NS 5400 S/N: 2774	37.828472	81.78608333	1772915.656	302591.914	Saul's
5	MINI-SEIS II Inst# MS II 2D2G 1/4M S/N: 4762	37.827417	81.791	1771492.406	302219.877	UK
6	MINI-SEIS II Inst# MS II 2D2G 1/4M S/N: 3599	37.82575	81.78622222	1772867.112	301601.13	Ken - OSM
7	MINI-SEIS Inst# MS 2D2G S/N: 429	37.819056	81.79911111	1769123.556	299195.638	UK
8	MINI-SEIS Inst# MS 2D2G S/N: 2832	37.814444	81.79691667	1769742.925	297510.868	WVDEP
9	MINI-SEIS Inst# MS 2D2G S/N: 2467	37.834833	81.80225	1768266.722	304948.143	WVDEP
10	MINI-SEIS Inst# MS 2D2G S/N: 2468	37.8385	81.80044444	1768799.694	306278.84	WVDEP
11	MINI-SEIS Inst# MS 2D2G S/N: 180	37.841389	81.79933333	1769129.628	307327.998	UK
12	MINI-SEIS II Inst# MS II 2D2G 1/4M S/N: 1513	37.846167	81.79777778	1769593.786	309063.868	Dep Mines, Minerals and Energy. Big Stone GAP VA

Three seismographs (2, 3 and 4) were NOMIS® 5400 while the other nine were White Industrial MINI-SEIS series. Some of the seismographs utilized belonged to West Virginia Department (WVDEP), Office Surface of Mine (OSM), Virginia Department Mines Minerals and Energy and to the University of Kentucky (UKY). All devices conform to the ISEE Performance Specifications for Blasting Seismographs and were calibrated before any data collection activity.

In order to protect the seismographs from the environment and other factors, common plastic tool boxes were adapted to contain the seismographs. An external battery was used to extend the internal battery life of the seismograph.

An external battery was used for each seismograph allowing for each seismograph to store information for durations exceeding two weeks when the units were downloaded. This time interval was adequate to check the proper operation of the devices, clean the memory and check the battery level. During each visit some problems were detected and solved for the seismographs in the network.

Seismograph installation followed three well defined lines named according to the orientation; North, East and South. Seismographs 9, 10, 11 and 12 are the North line. The North line was planned such that all devices were to be installed at the same elevation (seismographs 9 to 12); however, access problems did not allow for installation at a constant elevation. Figure 21 show the final pattern followed to install the seismographs. Seismographs 9 and 10 were place along the ridgeline in advance of mining, Seismograph 11was mid-slope below the lowest coal being mines and Seismograph 12 was on the valley floor.

The East line has two lines of seismographs. Line one (seismographs 2, 3, 4) was at the bottom of the valley along Perry Fork. Line two (seismographs 5 and 6) was along a ridge of the adjacent valley. Seismograph 5 was just below the lowest mined coal seam in natural soils and seismograph 6 was placed in reclaimed soils.

The third line was towards the South (seismographs 7 and 8). These seismographs were placed in reclaimed areas of the mine.

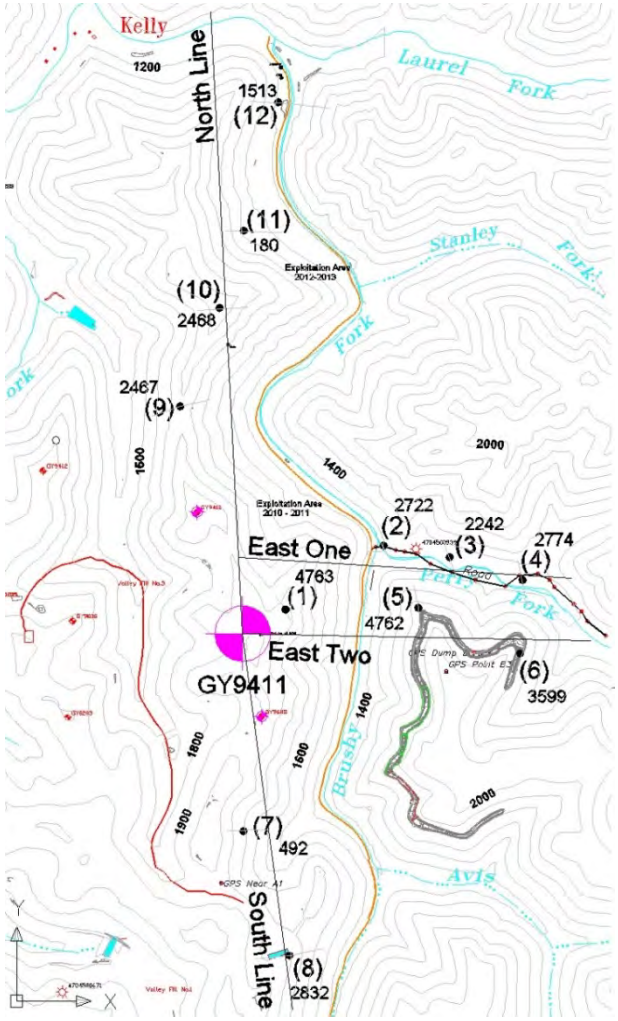

Figure 21 Seismographs location

Several tests were performed to determine seismograph trigger levels to guarantee collection of the information. Adjustment of the triggering levels were based on, proximity of the seismographs to roadways topographic conditions of the site, the distance from the source to recording point and others factors that affect the expected levels of airblast and vibrations. Despite this, data collection and analysis for seismographs 2, 3 and 4, presented little useful information. This was likely due to logging activities in the area, and road construction that interfered with monitoring equipment.

Table 7 includes the programmed seismograph trigger levels. The table includes the seismograph number, the distance from drill hole GY9411, the elevation, recording duration, sample rate and the trigger level. It should be noted that distances changed as the blasting activity progressed through data collection, so distances in Table 7 should be taken as the distance when the seismograph was installed (initial distance or distance of reference).

Table 7 Seismograph settings 2010

	Trigger parameters					
Seismograph	Distance (ft)	Elevation (ft)	Particle velocity (in/s)	Airblast (dB)	Duration (s)	Samples/second
1	667.0	1900	0.08	122	10	1024
2	2242.0	1300	0.05	118	10	1024
3	2286.8	1350	0.05	118	10	1024
4	3859.6	1355	0.05	118	10	1024
5	2404.8	1770	0.05	118	10	1024
6	3763.8	1797	0.05	118	10	1024
7	2675.4	1800	0.08	122	10	1024
8	40405.4	1900	0.08	122	10	1024
9	3191.3	1800	0.08	122	10	1024
10	4418.9	1910	0.03	120	10	1024
11	5457.1	1400	0.03	120	10	1024
12	7208.9	1200	0.03	120	10	1024

All the blasting seismographs were deployed according to the ISEE Field Practice Guidelines for Blasting Seismographs 2009 Edition. Initially it was planned to install some of the seismographs attached directly to rock, but because in most of the areas the topsoil is more than 3 feet thickness, it was not possible to fix the geophones to rock. Thus, all records collected are representative of vibration records in soil.

Despite efforts to avoid false triggers and other events that affect the collection of information, the storage (memory) capacity for some seismographs was reduced. The reduction in the capacity of storage means that continuous false triggers cause the seismograph to record only the peak vibration values instead of the vibration waveform. In addition to the non-satisfactory information collected for seismographs 2, 3 and 4, the storage of events for seismographs 1, 5 and 6 was reduced. Seismograph 1 was lost when a dozer buried it. One

unsuccessful attempt was made using a metal detector to recover the device and the recorded information. Seismograph 5 was close to wildlife areas, and continuous triggers deactivated the capacity to record the complete waveforms however the peaks were recorded. Despite the problems with seismograph 5, this unit collected the most blast events during this period of collection albeit only peak vibration values.

Even considering the problems experienced with the seismographs, a data base was generated with enough information to analyze vibrations and airblast when the delay system is non-electric or electronic.

3.2.2.1.1 Instrumentation for summer 2011

After analyzing information collected in 2010, it was decided to perform some specific blasting tests during the summer of 2011 along the same ridge of the mine.

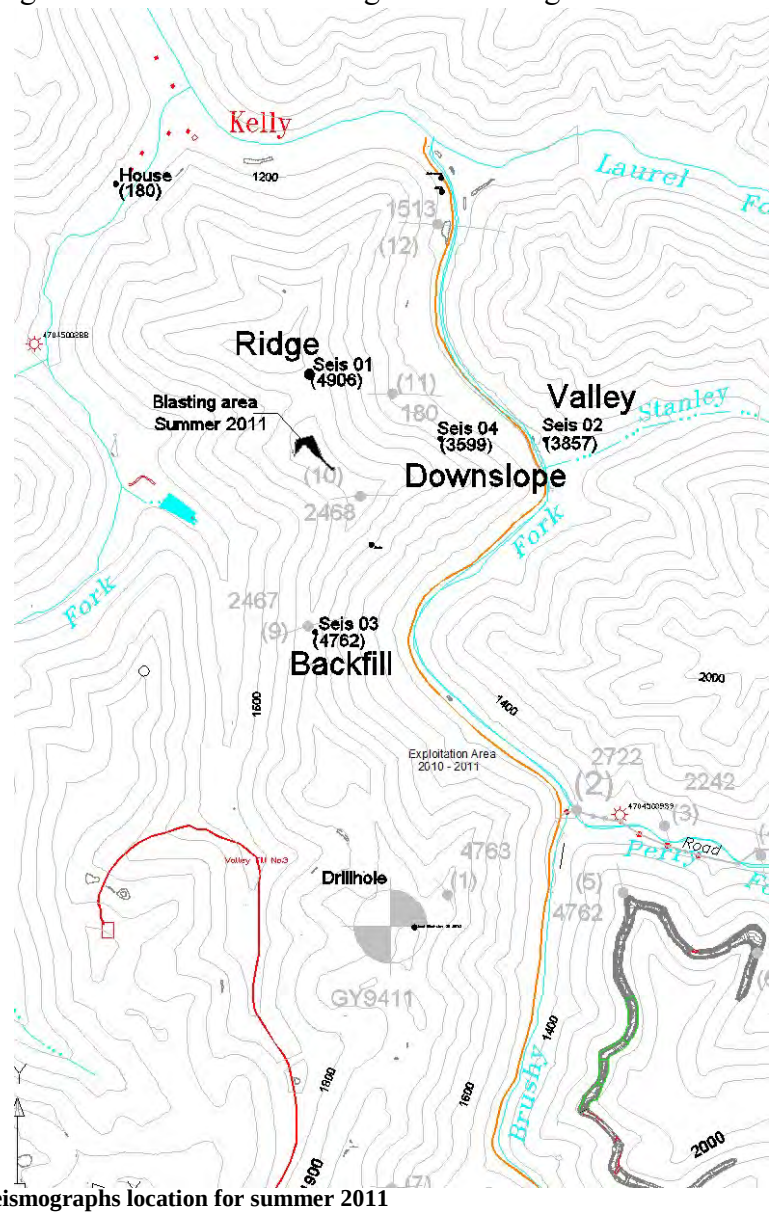

Figure 22 Seismographs location for summer 2011

The new blasting area was located 5000ft to the North of the point of reference for 2010 tests (drill hole GY9411). In this second round of tests, five (5) seismographs were used. Figure 22 shows the location of the blasting area, 2011 seismographs (Seis) , drillhole GY 9411 and some of the seismographs used during the 2010 test (locations in grey).

Two seismograph locations were kept similar during the two periods of collection of information. Seismograph 9 (2010) and Backfill (Seis 3 – 4762) (2011) were at the same location but in 2010 the area was unmined and in 2011 the area had been mined and reclaimed. The House seismograph remained in the backyard of a house owned by the mine because it was the closest structure and necessary for regulatory compliance. The house seismograph was requested by the blasting crew because some of the shot tests used delay timing below 8ms.

For the remainder of the report, seismograph information from each of the seismographs placed during 2011 data collection will be referred to by their descriptive terms of Ridge (Seis 1 – 4906), Valley (Seis 2 – 3857), Backfill (Seis 3 – 4762), Downslope (Seis 4 – 3599), and House (Seis 5 – 180). Information from seismographs in place for the 2010 data collection period will be referred to by the seismograph number to avoid confusion between the two years of separate data collection.

Ridge was located along the ridge in advance of mining and above the highest coal seam to be mined. Valley was located on the valley floor along Stanley Fork. Backfill was located south of the mining area on reclaimed or backfilled soil. Downslope was located downslope from the mine and below the lowest coal seam to be mined. House was located at the nearest structure north of the mining area. Table 8 includes seismographs settings used in the second round of test.

Table 8 Seismograph settings 2011

			Trigger parameters			
Seismograph	Distance (ft)	Elevation (ft)	Particle velocity (in/s)	Airblast (dB)	Duration (s)	Samples/second
Ridge	691.9	1850	0.01	148	12	1024
Valley	2410.1	1200	0.01	142	12	1024
Backfill	1937.8	1800	0.03	148	12	1024
Downslope	1348.1	1500	0.01	142	12	1024
House	3278.3	1200	0.01	148	12	1024

3.3 Analysis of field data

3.3.1 Storage and management of the collected information

The primary purpose of the instrumentation and information collection was to be able to compare how changes of the delay system (between non-electric and electronic), and the use of delay timing lower than 8ms affects ground vibration and airblast. The seismograph network described previously operated 24/7. The quantity of collected information was cumbersome and

required development of a database that allowed an easy way to analyze airblast and ground vibration results. After reviewing several alternatives to compile the information, including spreadsheets and other applications, a database was selected to compile the information. A brief description of the database developed in this research is included in the following section.

3.3.1.1 Database development

The information collected comprises basically two sources. The first one comes from blasting logs. The blast log information is produced and recorded by the blasting crew. Internally, the blasting crew gathers the information in a hard copy form (paper) and then produces an electronic blast log report for each shot occurring at the mine. The mine provided a copy of this information for this research. The second source of information was the seismograph readings (ground vibration and airblast data). Seismograph information comes in a digital format. Post processing was required to produce the complete waveform, peak particle velocity and the frequencies in each component of motion (longitudinal, transversal and vertical).

Figure 23 shows the information on a typical blasting log. The information recorded includes : Blast ID, blast location (state plane coordinates), distance to the nearest structure, blast time, weather conditions, closest protected structure, type of material blasted, blast type, powder factor, total explosives quantity, maximum charge weight per 8 ms delay, geometry patterns, time delay system, and a graphical hole cross section.

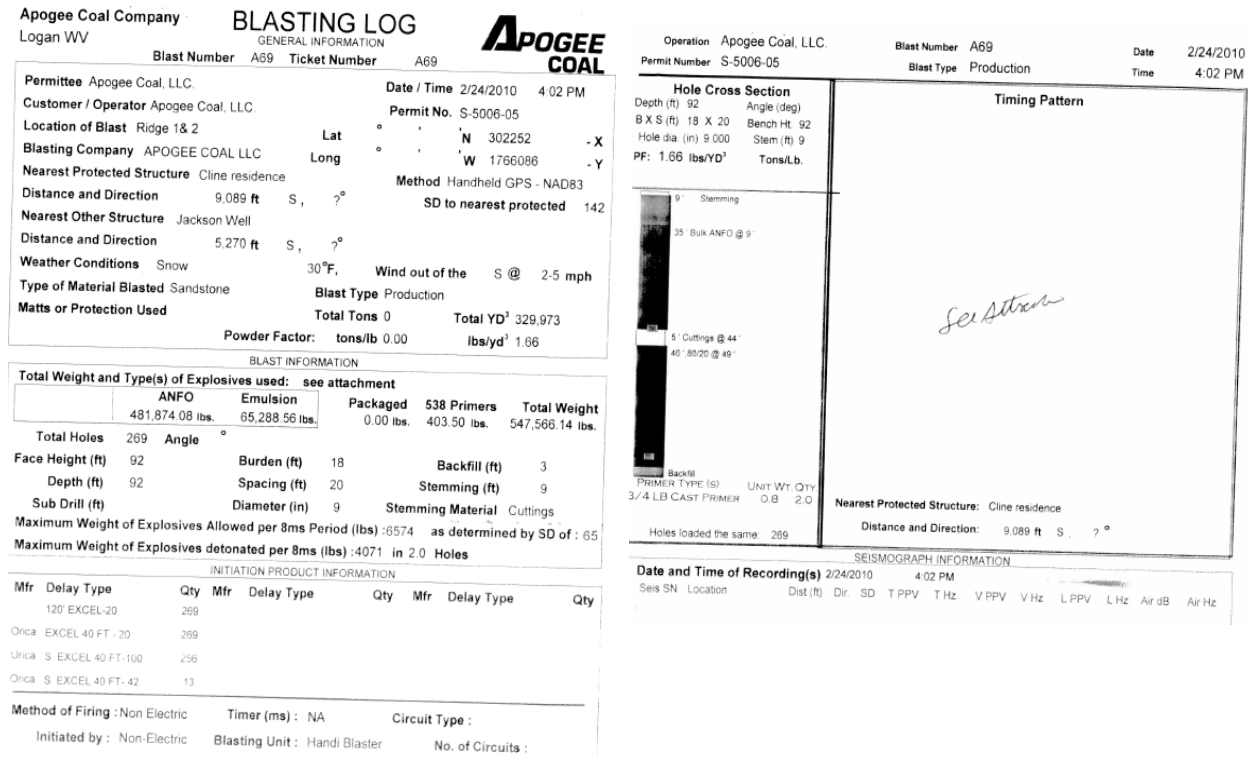

Figure 23: Typical blast report used at Guyan mine, W.V

For industry standard scaled distance analysis, accuracy of blast records can affect the outcome of the calculations. The blast records are the source for data with regard to the two

independent variables: charge weight and distance. The blast records were assumed accurate for this study; however, discrepancies in the reports may have led to some of the lower regression correlation values found during analysis as discussed in later sections. The records were spot checked for accuracy and no discrepancies were found. Overall the data supplied was deemed acceptable and thus assumed accurate. Another issue relating to blast records was the regulatory requirement for reporting charge weight within any 8 ms period. When multiple holes fired, separation in distance likely did not result in coupled energy and thus peak particle velocities may have been overestimated using scaled distance calculations. This may have resulted in skewed data plots for regression analysis. Later discussions will focus on the applicability of the 8 ms rule.

Figure 24 shows a typical reading summary for one of the events and the corresponding waveform. Seismograph information was collected using two different systems. Three of twelve seismographs were NOMIS 5400, while the other nine were White Industrial Seismology Inc. The post-processing of each required reading the peak particle velocity, the airblast peak and the dominant frequency of each. A commas delimited file (csv file) was generated and used to plot the waveforms using Dplot software.

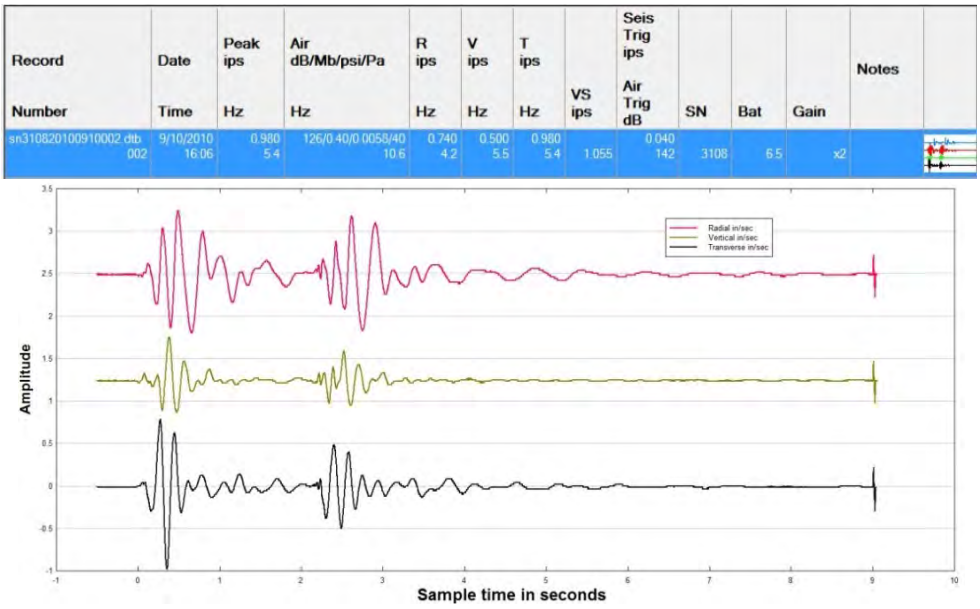

Figure 24: Summary report event and corresponding waveform

For some events, the complete waveform record was not available and only the peak values were saved. This allowed the database to be populated in the majority of the fields. During the four month 2010 monitoring period there were more than 200 shots at the mine. However for this research, only those events that triggered seismographs (have seismograph readings), were included in the database. Hence the 2010 database compiles 185 shots. Fortunately, all 45 blasts from 2011captured (triggered) data and are included in the database.

MS Access, works using tables, queries, forms reports and other objects. The information is stored in tables and using the other Access objects it is possible to produce queries and reports. In this project there are three tables where all the information was recorded. One table includes the information coming from the physical blasting report. The

second table contains the vibration and airblast readings, including the complete waveform file in most cases. Finally, a third table included the GPS coordinates of the seismograph locations. Figure 25 shows the three tables including the relationship between them (how the tables are related).

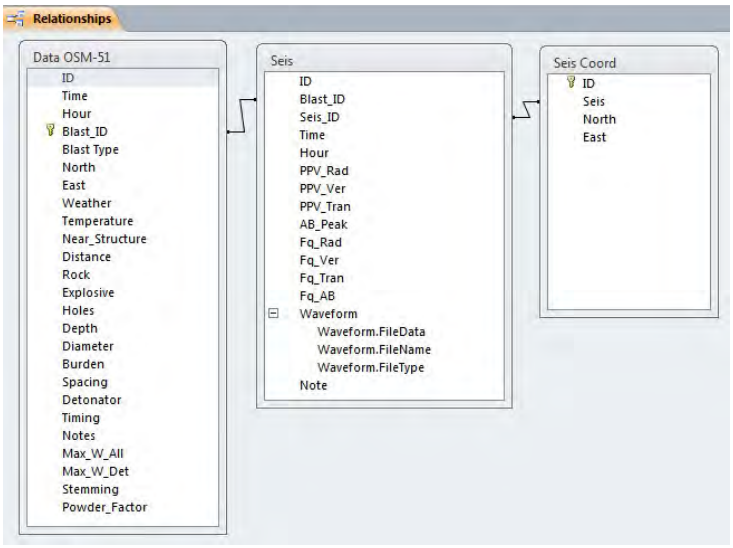

Figure 25: Main tables and relationship between them.

Forms are objects in MS Access that are useful in order to allow an easy way to interact with the software. In this project, three input forms were created to allow for intuitive input for the three main tables. In a mine setting, these databases can be populated with a clerical employee. Very limited technical proficiency is required to populate the database tables in this format, for example the blast records table was populated using the form show in Figure 26.

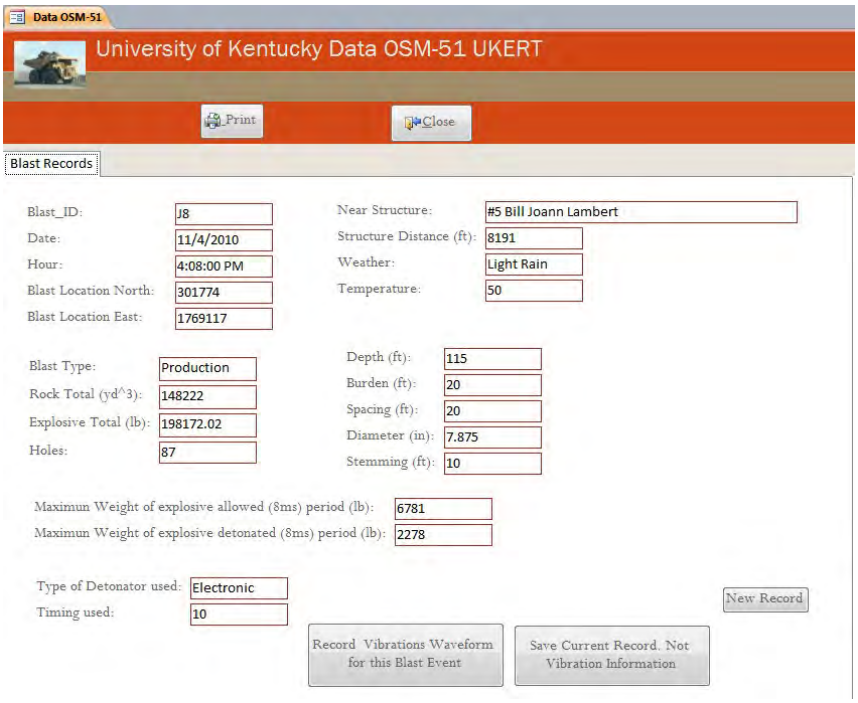

Figure 26: Input form for the blast records table.

The information entered using this form is related to blast number, date, time, location, blast type, total rock volume, number of holes, hole diameter, hole depth, burden, spacing, detonator type, timing used in the blast and the maximum weight of explosives used per dalay. The primary components used for this research are location, which permits distance calculations to seismographs, and maximum charge weight per delay. Each for are needed to calculate square-root and cube-root scaled distances for vibration propagation plots. The form used to introduce the ground vibration and airblast information is displayed as shown in Figure 27.

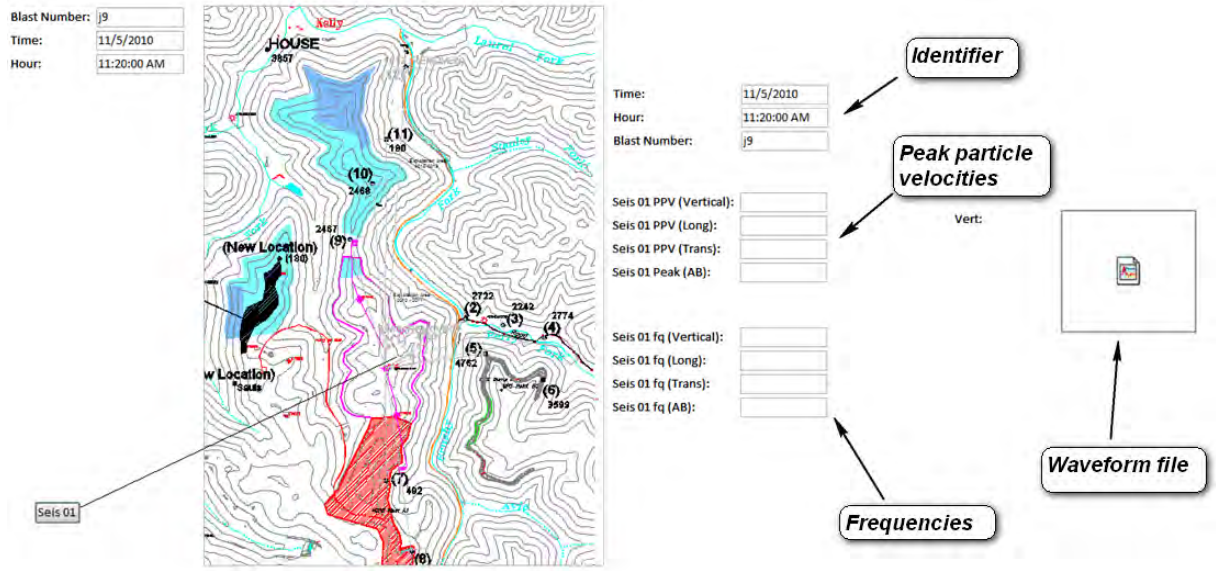

Figure 27: Input form for vibration – airblast information.

After the information is entered into the forms, tables are produced as shown in Figure 28.

Data OSM-51

ID	Time	Hour	Blast_ID	Blast Type	North	East	Weather	Temperatur	Near_Struct	Distance	Rock	Explosive
50	7/19/2010	9:28:00 AM	7	Production	292160	1773001	Sunny/Hot	88	Ball Residence	3595	28224	17786.23
3	6/19/2010	3:57:00 PM	E41	Production	300705	1768908	Sunny/Hot	90	Cline Residenc	7193	434889	572342.34
4	6/21/2010	10:20:00 AM	E42	Production	292255	1775144	Partly Cloudy	78	Dominion Well	7073	26400	30614.26
5	6/21/2010	10:21:00 AM	E43	Production	292542	1775262	Partly Cloudy	78	Dominion Well	6775	35400	55858.91
6	6/21/2010	3:58:00 AM	E44	Breakdown	302254	1769569	Sunny/Hot	95	#5 Bill Joann La	7917	12240	14925.18
7	6/22/2010	4:14:00 PM	E45	Production	301376	1769287	Partly Cloudy	90	Cline Residenc	7888	25344	30850.77
8	6/23/2010	12:07:00 PM	E46	Production	292469	1775244	Light Rain	80	Ball Residence	3817	44640	53911.22
9	6/24/2010	3:48:00 PM	E47	Production	301493	1768745	Light Rain	90	Cline Residenc	7976	331200	492013.3
10	6/25/2010	9:20:00 AM	E48	Production	292091	1775203	Partly Cloudy	75	Dominion Well	7169	15120	18022.24
11	6/25/2010	4:01:00 PM	E49	Breakdown	301154	1769565	Clear/Calm	90	Cline Residenc	7696	10800	14922.18
12	6/25/2010	4:10:00 PM	E50	Production	292015	1772957	Clear/Calm	90	Ball Residence	3475	17280	3224.86
14	6/26/2010	9:35:00 AM	E51	Production	292109	1772983	Sunny/Hot	85	Ball Residence	3553	18432	5127.78
15	6/26/2010	10:17:00 AM	E52	Production	292230	1772915	Sunny/Hot	85	Ball Residence	3690	21600	12983.19
13	6/26/2010	1:41:00 PM	E53	Production	292226	1773392	Sunny/Hot	90	Ball Residence	3543	14832	5597.7
16	6/28/2010	9:01:00 AM	E54	Production	292284	1773078	Partly Cloudy	75	Jackson Well	7965	30240	24937.79
17	6/28/2010	4:00:00 PM	E56	Production	301198	1765851	Light Rain	75	Jackson Well	4263	120213	176054.77

Figure 28a. Blasting log table

Seis

ID	Blast_ID	Seis_ID	Time	Hour	PPV_Rad	PPV_Ver	PPV_Tran	AB_Peak	Fq_Rad	Fq_Ver	Fq_Tran	Fq_AB	
	E49	1	2/25/2010	3:59:00 PM	0.22	0.11	0.12	116	9.3	9.6	17	6.4	(2)
	E41	9	6/19/2010	3:57:00 PM	0.08	0.11	0.085	137	3.3	11.3	3.9	9.6	(2)
3	E41	10	6/19/2010	3:58:00 PM	0.05	0.06	0.045	136	5.3	5.5	3.5	9.1	(2)
	E41	7	6/19/2010	3:57:00 PM	0.17	0.25	0.11	139	10	11.9	9.3	9.3	(2)
1	E41	6	6/19/2010	3:54:00 PM	0.055	0.03	0.025	129	6.4	3.2	9.1	12.1	(2)
2	E41	5	6/19/2010	3:57:00 PM	0.065	0.065	0.075	133	4	6	3	13.8	(2)
	E41	1	6/19/2010	3:58:00 PM	0.3	0.21	0.55	142	4.6	9.1	3.2	14.2	(2)
	E44	1	6/21/2010	3:56:00 PM	0.41	0.24	0.35	120	9.1	9.1	7.6	14.6	(2)
4	E45	2	6/22/2010	4:12:25 PM	0.1	0.07	0.05	112	1.1	1.5	3.1	8.53	(2)
5	E47	6	6/24/2010	3:44:00 PM	0.22	0.105	0.1	124	2.2	2.5	2.7	5.6	(2)
14	E47	12	6/24/2010	3:48:00 PM	0.02	0.025	0.04	106	8.9	2	6.4	0	(2)
9	E47	5	6/24/2010	3:47:00 PM	0.35	0.205	0.455	126	2.7	3.8	2.5	7.3	(2)
10	E47	7	6/24/2010	3:47:00 PM	0.23	0.23	0.23	133	6.8	6.2	2.3	10.6	(2)
12	E47	8	6/24/2010	3:47:00 PM	0.16	0.07	0.24	125	3.4	3.7	2.7	13.1	(2)
6	E47	9	6/24/2010	3:45:00 PM	0.005	0.005	0.005	127	0	0	0	14.2	(2)
13	E47	10	6/24/2010	3:48:00 PM	0.215	0.095	0.22	118	2.1	3.5	1.8	1.6	(2)
16	E47	11	6/24/2010	3:50:00 PM	0.115	0.08	0.1	112	6	9.4	6.2	0	(2)

Figure 28b Blasting seismograph table

Seis Coord

ID	Seis	North	East
1	1	302195	1769695
2	2	303063	1771018
3	3	302904	1771915
4	4	302597	1772904
5	5	302220	1771492
6	6	301601	1772867
7	7	299196	1769124
8	8	297511	1769743
9	9	304948	1768267
10	10	306279	1768800
11	11	307328	1769130
12	12	309064	1769594

Figure 28c Coordinates table

Figure 28: Tables containing blast information

Using the three tables shown in Figure 28, a variety of queries and reports can be generated, the information in the tables can be related through graphs, lists or another tables.

An additional field was created in the database to distinguish between the information collected in 2010 and those collected in 2011 because the information was collected in two different periods of time and the seismograph location changed between the two sets.

3.3.2 Database general description content

A general description of the data is presented, before the numerical analysis of the information. Several graphs showing the number of events, type of detonator, and quantity of records per seismograph are included. This general description was made analyzing the information through graphical representations using at the same time both types of variables qualitative and/or quantitative. This is in contrast when a spread sheet is used where generally only quantitative variables are used.

In total, the database has 230 blast events. Fifty-three percent of the shots used non-electric initiation systems and 47% of the events utilized electronic systems. This is shown in Figure 29.

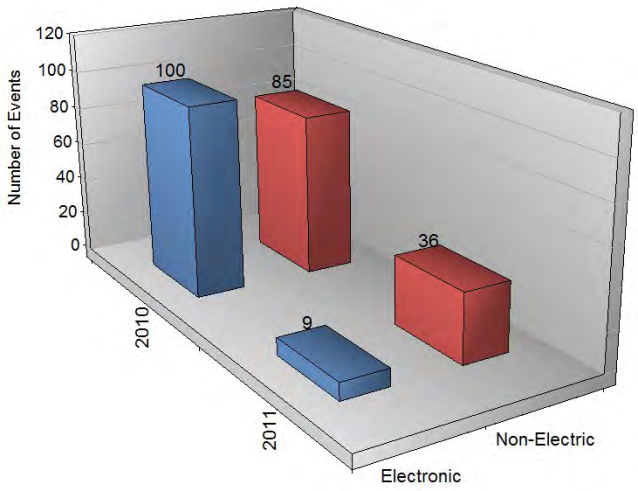

Figure 29 Number of events categorized by initiation system

Figure 29 also shows that in 2010 the number of events was 185 against 45 events for 2011. The difference is because the seismographs collected data for four (4) months in the field during 2010, and only two (2) months during 2011. In fact, during all monitoring time, (adding 2010 and 2011 periods) at the mine, there were more than 230 events but only those which triggered the seismographs were included. Figure 30 shows the result when the blast type is introduced in the graph.

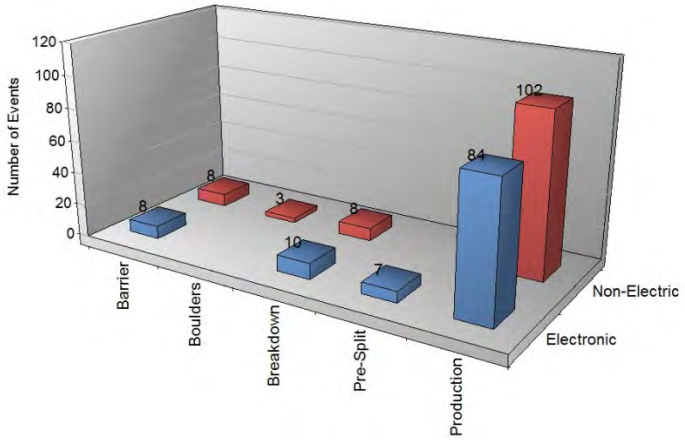

Figure 30 Detonator type usage including blast type

For production blasting, almost 55% of the cases utilized a non-electric initiation system. When specialized blasting is needed (Pre-Split blasts), it is clear that the blasting crew prefers to use electronic detonators. Regarding the initiation systems used in this particular mine, it is possible to see that the usage is almost 50% - 50% (Electronic – Non-electric).

The most active seismograph in 2010 was seismograph number 5 (despite wildlife activity). This seismograph was located on original ground very close to the reclaimed area (see Figure 21). Seismograph 5, recorded 63 of 185 blast events, 57 records include complete waveforms while in the other 6 only peak values are included. The proportion of the records triggered when using electronic versus non-electric initiation system for this seismograph was about 50-50. On the other hand, in 2011, all seismographs recorded almost 40% of the total

activity (except the House (180) seismograph due to the distance from the blast to the monitoring point). Figure 31 show the activity of the seismographs for 2010 and 2011.

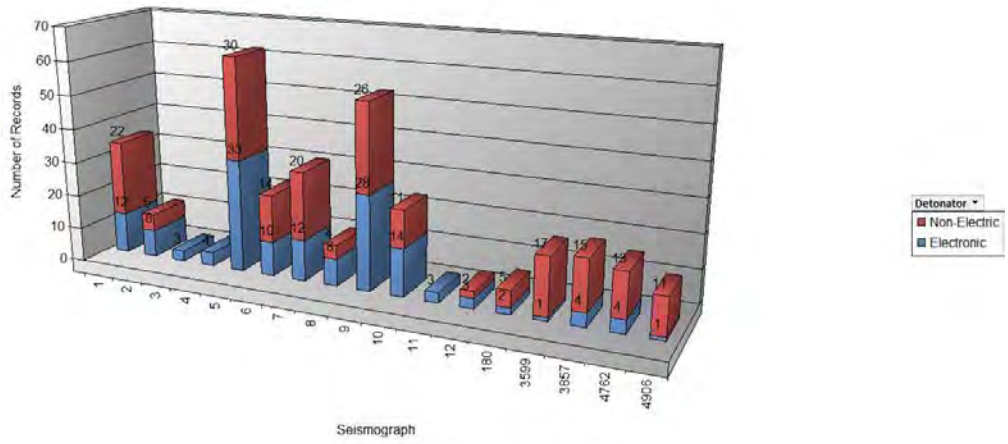

Figure 31 Seismograph activity

Almost all triggers in 2011 were related to non-electric detonators because in this year, 80% of the events used this type of initiation system.

As a further breakdown of 2010 data, Figure 32 shows that seismograph 5 has ten more production events than seismograph 9. While these two seismographs were the closest to the mining area, even they did not trigger identically. This is likely due to site conditions and the direction from the blast. Seismograph 9 was north of the blasting in undisturbed soil along the ridge, above the highest coal seam being mined, while seismograph 5 was east of the mining area across the valley in undisturbed soil.

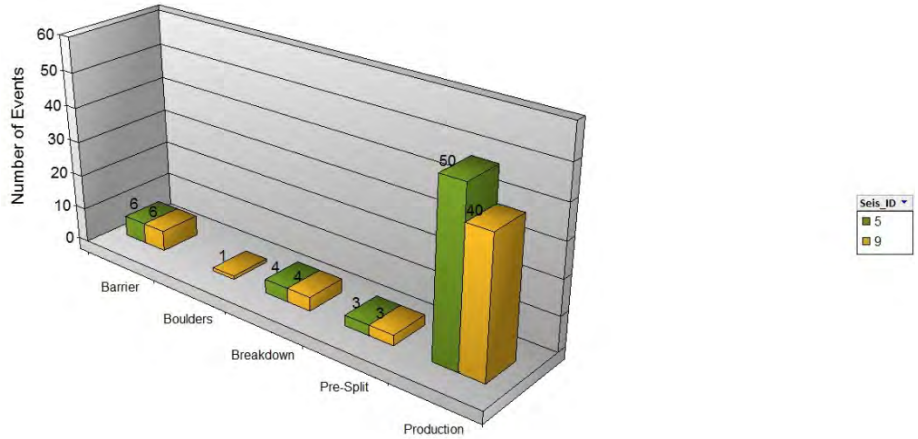

Figure 32 Event comparison between Seismographs 5 and 9 (2010)

In production blasts during the study periods, the timing configuration used most often was 100ms between rows and 42ms between holes (100/42), followed by a configuration of 42ms between rows and 17ms between holes (42/17). The total number of events for production blasts triggering a seismograph using (100/42) was 86 while the number of events using a timing configuration of (42/17) was 37 as Figure 33 shows. Others configurations where used during the period that the information was collected and their detail will be included later in this report.

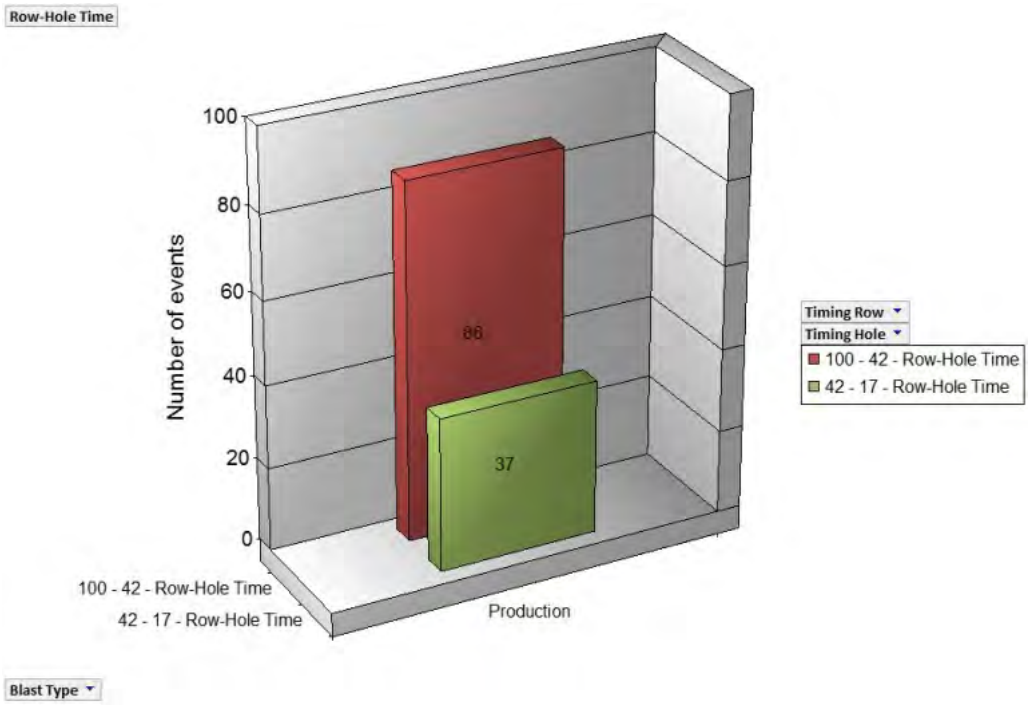

Figure 33 Production events and most used timing

Both of the most common configurations provided variable timing from one blast to another. Using (100/42) and (42/17) many specific timing combinations are possible. In many cases, multiple holes were timed to fire simultaneously (although with the measured cap scatter this likely never actually occurred) while still meeting scaled distance requirements. In general, the (100/42) timing selection resulted in a delay of 16 ms between charges or set of charges. It is important to note that when separate holes are scheduled to fire simultaneously with non-electric detonators that cap scatter will prevent this from happening while reducing the vibration and airblast effects by introducing random delay according to the distribution of timing accuracy.

When using (42/17) configurations, several cases were documented where the scheduled firing times were exactly 8 ms apart. In other cases, multiple holes were bunched to shoot together. Because of the variability in the timing designs using these products, analysis was performed separating the typical timing configurations by the products used rather than by a specific delay between charges. Later analysis utilizes scaled distance calculated from the actual scheduled delay scenarios. When multiple charges were scheduled to detonate simultaneously, scaled distance calculations included weight from multiple charges that were subject to cap scatter in actual detonation times. Due to this phenomenon, plotting scaled distance versus particle velocity resulted in low values for r^2. More detail about this will be discussed as these plots appear in this report. Refer to Appendix A for blast reports from the shots within the database. Specific timing configurations are included for each blast in the database.

Next, several analyses using scaled distance were performed. All the information regarding airblast was analyzed first, followed by the ground vibration information.

3.3.3 Analysis of airblast information

Traditional techniques of plotting cube-root scaled distance against air overpressure were employed to analyze the database for airblast. Typical linear regression exhibited limited success for correlating data due to several factors discussed throughout this section. The mine utilized typical non-electric initiation products in configurations that may have affected the r^2 values for the regression trend lines. For example, many blasts utilized timing that would have multiple holes scheduled to fire simultaneously. Variability in the accuracy of these detonators ensures that in most cases the holes did not fire simultaneously even though they were considered single charges in scaled distance calculations. For the electronic configurations, the distances between holes scheduled simultaneously could have also affected the quality of the data when assembled. Figure 34 is obtained when all information is used to visualize the behavior of airblast against scaled distance for all type of blast events and all seismographs, categorizing by delay system.

In this figure, trend lines according to the type of detonator have been included. The trend lines were included to show the trend of airblast regarding scaled distance. According to Figure 34, in general, airblast values are the same when non-electric delays or electronic are used.

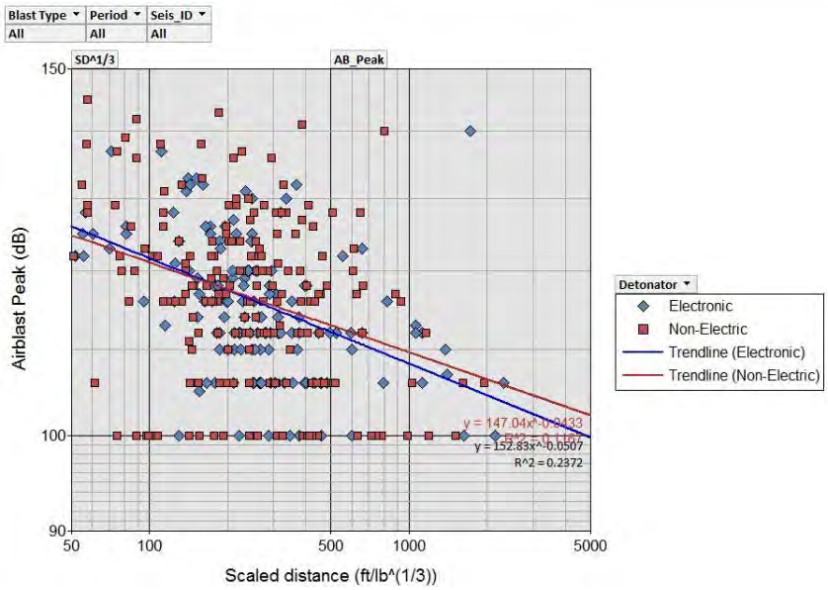

Figure 34 Airblast Vs scaled distance, all blast type and all seismographs

In Figure 34, there are around 37 events presenting an airblast value equal to 100dB (this was the threshold default level for airblast), meaning that all 37 events were likely triggered by ground vibration over airblast. Considering this, removing values equal to 100dB from Figure 34 provides Figure 35.

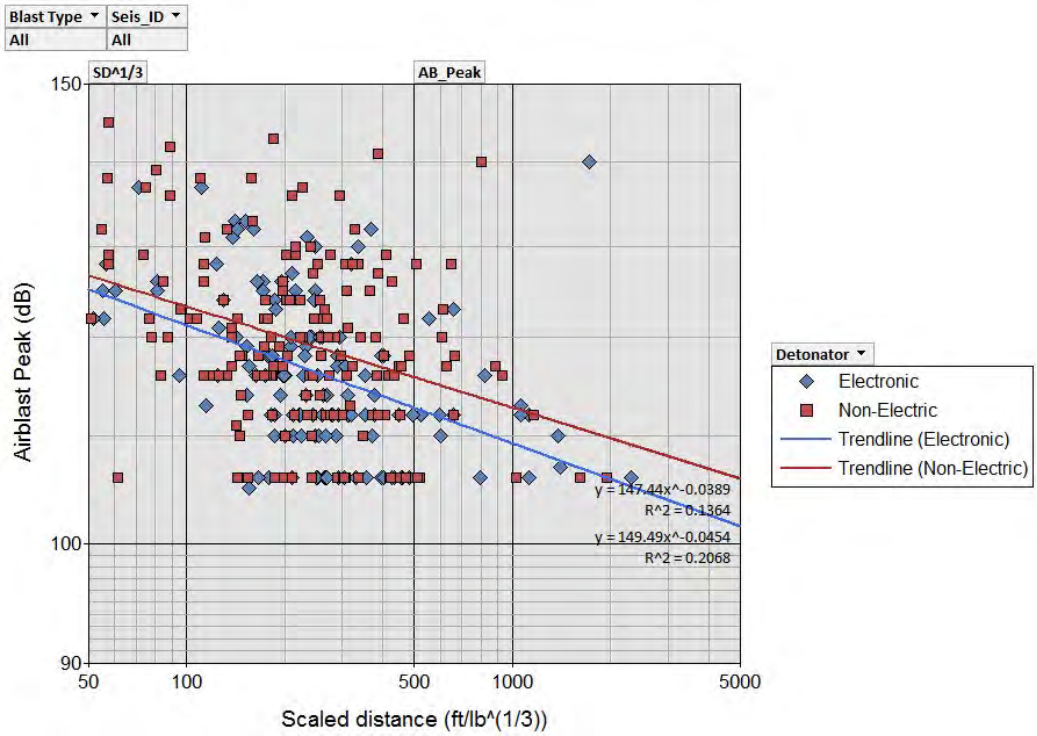

Figure 35 Airblast Vs Scaled distance excluding 100 dB airblast values

Looking at the trend line in Figure 35, non-electric detonators generate slightly higher values of airblast than electronic detonators for this data set.

To verify this slight difference between airblast production and detonator type, seismographs 5 and 9 were used, (Figure 36) In this case, the default airblast values of the threshold (100dB) were removed.

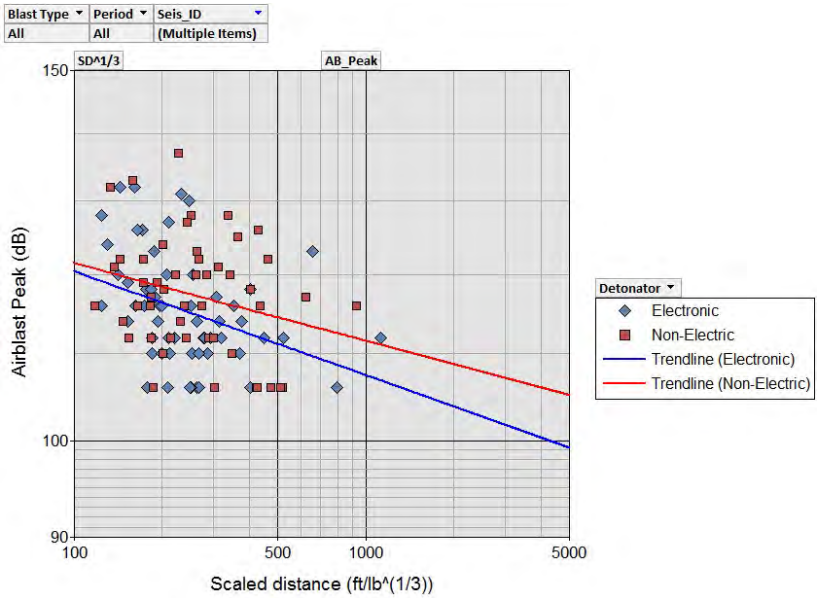

Figure 36 Airblast Vs Scaled distance, for seismographs 5 and 9

When Figure 35 and Figure 36 are compared the slight difference between the airblast produced by non-electric and electronic detonators is repeated. In conclusion, for this particular mine, the airblast value is affected slightly by the use of electronic detonators. It is not possible to generalize this conclusion for other mines because timing and environmental conditions are not included in the analysis and this conclusion should be taken just as a general trend in the current database.

As seen in previous figures most of the information falls in a range between 100 to 500 ft/lb$^{1/3}$. So when the airblast average for the production blast are compared to electronic and non-electric systems within this range, and only seismographs 5 and 9 are included, Figure 37 is obtained.

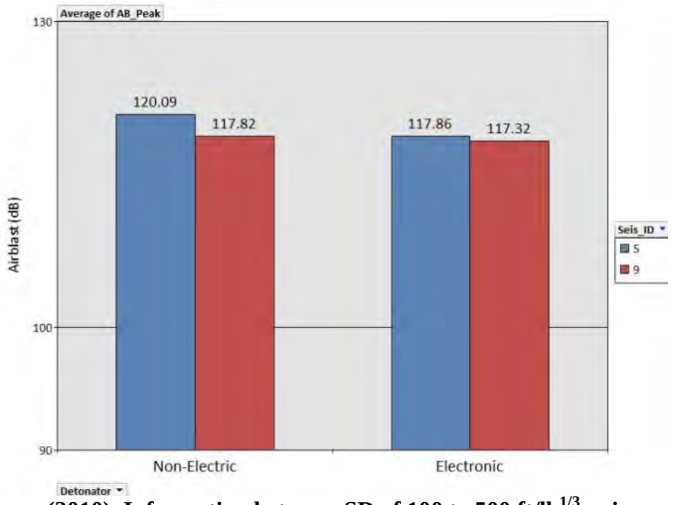

Figure 37 Airblast average (2010). Information between SD of 100 to 500 ft/lb$^{1/3}$, seismographs 5 and 9

Non-electric delay systems produced slightly higher average airblast values when compared to electronic. This is true in both seismographs (5 and 9), but is more evident in seismograph 5. The difference between seismograph 5 non-electric and electronic airblast in a production blast is around 3dB. In the case of seismograph 9, the values are closer. In both cases however, Non-electric average airblast was higher than the electronic. Those differences are significant because the measurement scale for airblast (dB) is logarithmic.

Similar behavior was observed in 2011 data between non-electric and electronic delay systems and airblast generated in production blasts (non-electric tends to produce higher airblast values). Figure 38 shows the 2011 information, including only average airblast produced by production blast for a scaled distance ranging between 100 and 500 ft/lb^3 (100dB default values were not included).

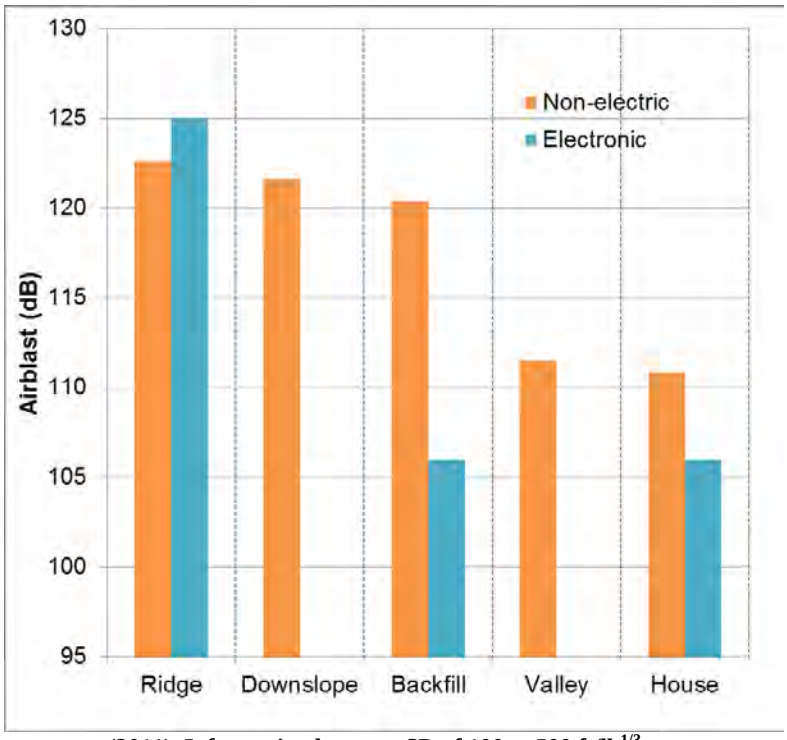

Figure 38 Airblast average (2011). Information between SD of 100 to 500 ft/lb$^{1/3}$

In some of the airblast records, it was observed that distance from the source was not the determining factor for peak airblast when multiple seismographs recorded the same blast event. This is likely due to topographical effects and blast design and orientation. In data from 2010, some of the airblast values following the ridge (north-south line) were higher than the values over the west-east line even though seismographs in the east line were closer to the blasts than seismographs in the north-south line. To illustrate this behavior, the event exhibiting maximum airblast values was chosen. This event triggered seismographs 1, 5, 6, 7, 9 and 10. Figure 39 show airblast behavior according to the approximated location in Northing and Easting coordinates.

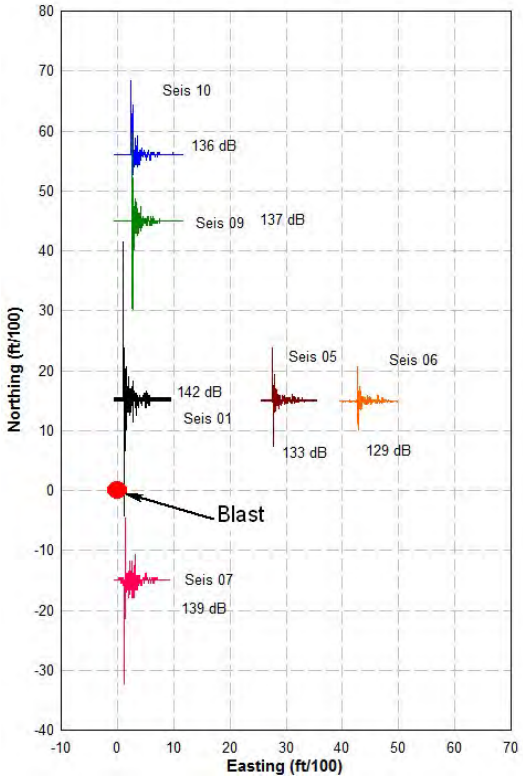

Figure 39 Airblast located in approximate North and East coordinates

There were very few events in the data base where seismographs in the North-South direction and East-West direction all triggered. There is not enough information to clearly define a correlation between these variables. Nevertheless, airblast generated by production blasts at this mine showed directionality in peak airblast.

When timing information is plotted against the airblast average for each timing configuration for production blasts recorded by seismographs 5 and 9, Figure 40 is obtained.

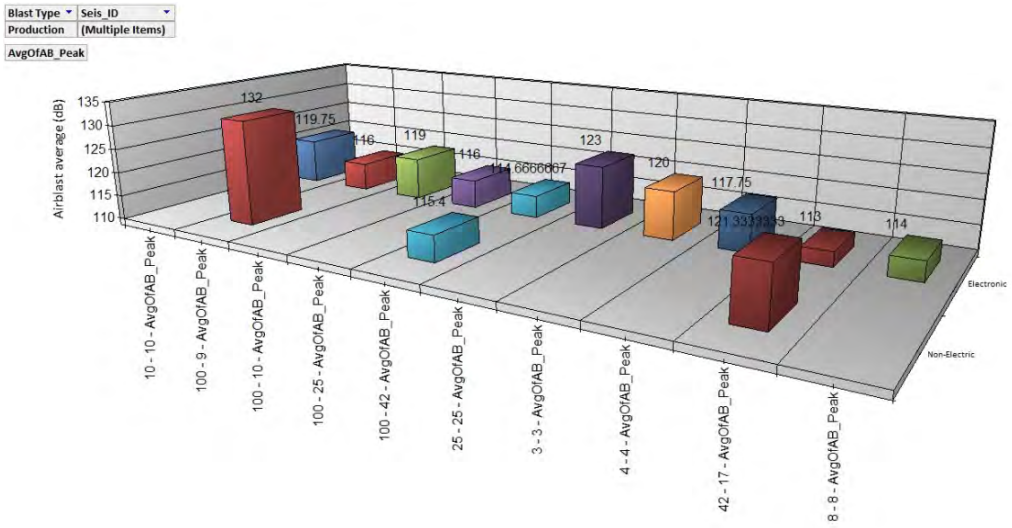

Figure 40 Timing vs average airblast, production blasts, seismographs 5 and 9

In Figure 40, the first number in the *x* axis (in front) represents the timing between rows while the second number represents the timing between holes. In this figure, for the most used timing configuration (100/42) at this particular mine, there is not a significant difference in the average airblast generated by a production blast between Non-electric and electronic delay systems (115.6dB Vs 114.67dB). It should be noted that Figure 40 is only the average value of the airblast for all production events recorded in seismographs 5 and 9 without consideration for scaled distance.

Figure 40 also shows how a long timing (100/42 usually resulting in 16 ms between charges or groups of charges) generates lower average airblast values (115.4 dB) when compared to shorter timing arrangement (42/17 usually resulting in 8 ms between charges or groups of charges) (121.33dB). When (100/42) and (42/17) electronic delays are used, the airblast peaks ranged between (114.67 and 113dB) respectively. In Figure 41, scaled distance is introduced to the analysis to verify the behavior of the average values.

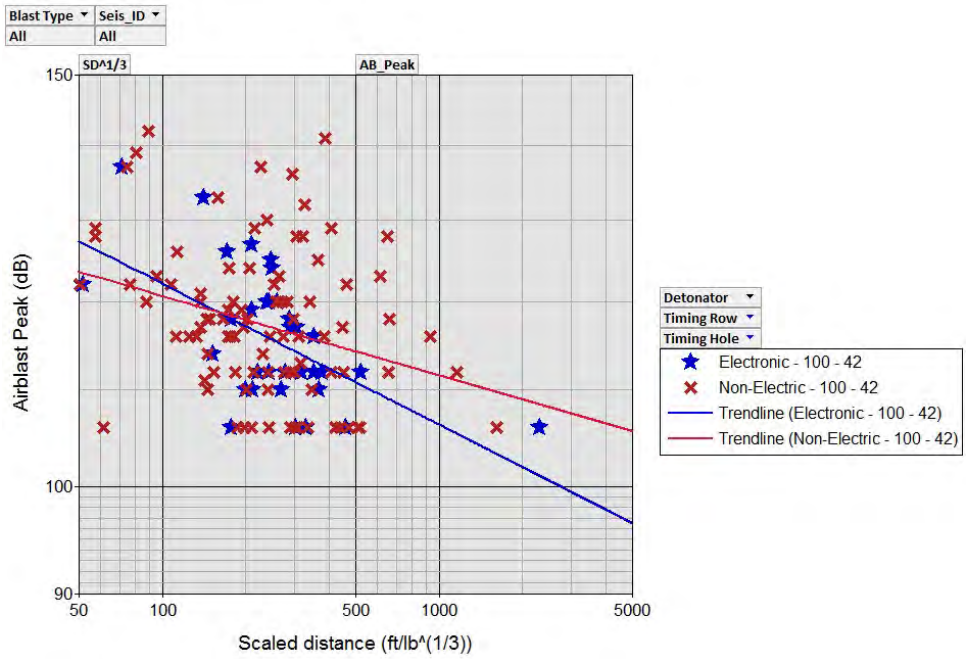

Figure 41 Airblast for Non-electric and electronic delay system (100/42) arrangement

Figure 41 shows trend lines for both initiation systems (100/42) using all the airblast information in the database (100 dB default values were removed from the analysis). Figure 41 is used here to illustrate the difficulty in assessing airblast performance between the two systems due to the issues previously discussed. The trend lines are included only as a reference and are not meant to show correlation.

To compare 100/42 timing arrangement against 42/17 Figure 42 was prepared. In this figure, only 100/42 trend line (not the data) has been included for reference.

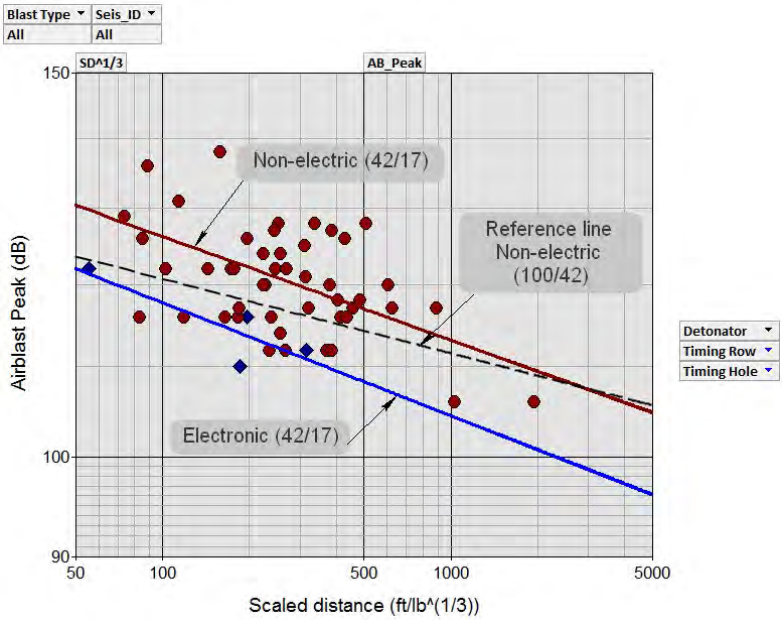

Figure 42 Airblast timing comparisons 42/17 Non-electric and electronic

Figure 42 illustrates that airblast values for non-electric blasts trend higher when the timing arrangement is changed from 100/42 to 42/17 (all types of blasts are included). This is more applicable for scaled distance values lower than 1500 ft/lb$^{1/3}$. On the other hand, the trend line for electronic arrangement of 42/17 always produces lower airblast values than the non-electric system. It is necessary to be cautious about this trend because there are only four data points for electronic devices. Figure 43 is generated for only production shots when previous figures are compared, the trend is the same.

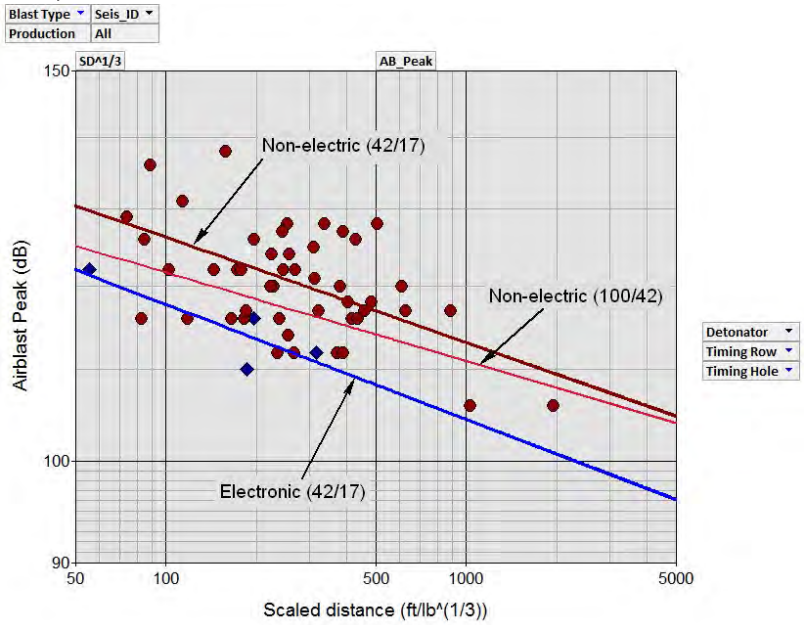

Figure 43 Airblast timing comparisons 100/42 vs 42/17 Non-electric and electronic only production blast type

Using Figure 42 and Figure 43, it is possible to reach a conclusion about the non-electric systems. When the timing arrangement is changed from long delays, in this case 100/42

(16 ms between charges), to short delays 42/17 (8 ms beween charges) the average value of airblast is higher. Regarding electronic systems, it is necessary to collect more information using the 42/17 arrangement to form a solid conclusion. In Figures 42 and 43, the trend line for non-electric (100/42) is about the same (for all blast type and only production shots), however in both cases the electronic system caused more favorable levels of airblast (lower levels of airblast).

In the database there are several timing combinations row/hole, especially when the electronic delay systems are used. Figure 44 was made to see the behavior of airblast when short delays are used.

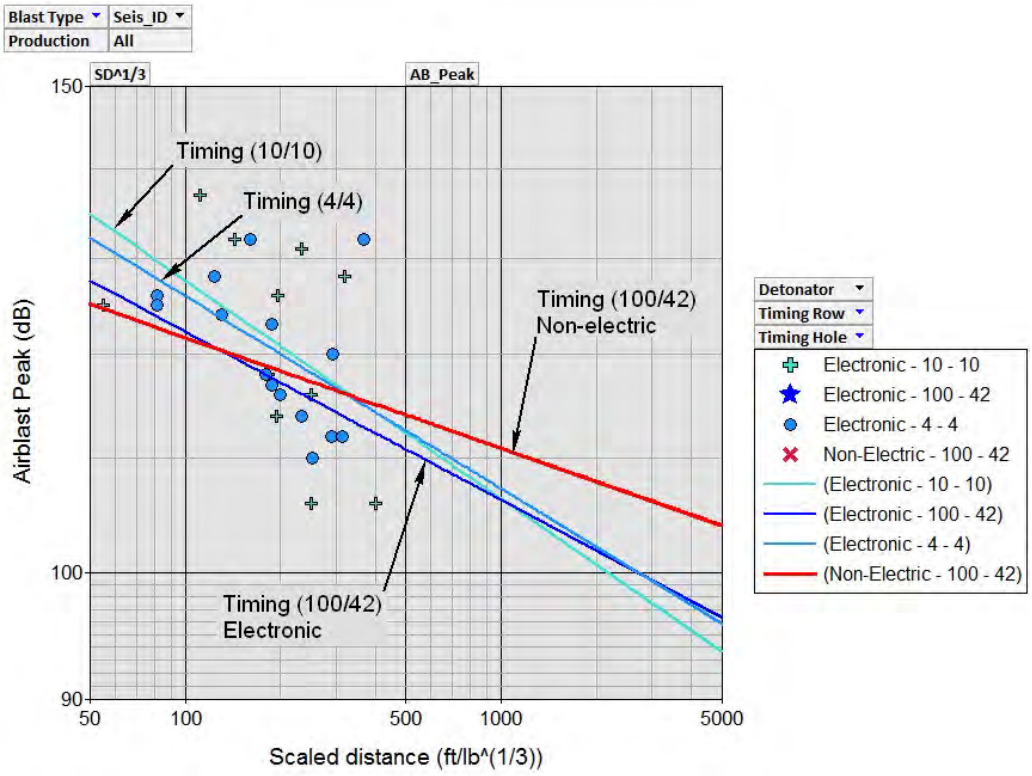

Figure 44 Airblast vs Scaled distance for short delay timing

The trends for non-electric and electronic delay systems using (100/42) are included for reference. According to this figure, there is almost no difference in airblast generated when electronic delay system is used applying timing arrangement of (10/10) and (4/4). However when those two timing arrangements are compared against non-electric (100/42), the electronic delay system tends to present higher values of airblast for scaled distances below 350ft/lb$^{1/3}$. This may be due to the accuracy of the detonators. When multiple holes are programmed to fire simultaneously, the electronic systems allow for this to actually occur while the non-electric system most likely reduces airblast values due to cap scatter introducing delay between "simultaneous" charges. No data is available for scaled distances beyond 500 ft/lb$^{1/3}$, thus trend lines in this region has no merit.

Figure 45 was made using all production blasts (2010 and 2011) and including all seismographs. Much of the data was collected with weather sunny to calm, and wind speed below 5 MPH. It is expected for airblast that the frequency response at the measurement point

exhibits some characteristics of the source (lower frequencies at the source). This observation is based on the assumption that no interference in the traveling airblast waves due to the weather conditions occurs.

Regarding frequency content, several figures involving timing arrangement, detonator type and frequency of the airblast were compared. Figure 45 shows for the frequency interval between 0 and 5 Hz how the frequency content of the airblast wave tends to be lower when delay periods are shorter (green line).

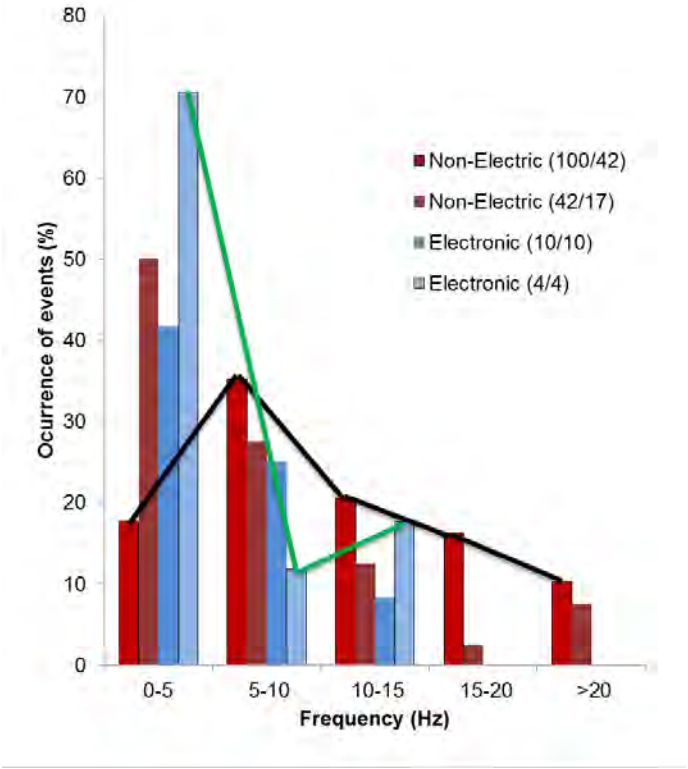

Figure 45 Histogram comparing frequency differences for (100/42) and (42/17) timing arrangement

A summary of observations regarding analysis of airblast data, initiation systems and timing follow:

- Trend lines were included in the graphs to generally compare the behavior of the airblast against initiation system and timing. It is difficult to propose any equation due to the scatter of the data and the low values of the correlation coefficient (r^2 lower than 0.5). Likely detonator inaccuracies and distance separations of charges contribute to poor statistical correlations.
- In airblast generated by production blasts in this particular research, directionality was observed. Airblast waves tend to attenuate less in the direction of the ridge than across the valley. This is illustrated in Figure 39.

- In general, non-electric initiation systems tend to generate airblast values higher than electronic. This trend can be observed in several figures.
- Regarding timing, it is difficult to combine airblast information, timing and the scaled distance concept, however the general trends indicate that shorter delay times produce higher average values of airblast in this dataset.

3.3.4 Ground vibration information

The database contains a total of 360 records with ground vibration data (2010 and 2011). When all records are used to plot a graph of maximum peak particle velocity vs square-root scaled distance Figure 46 is obtained.

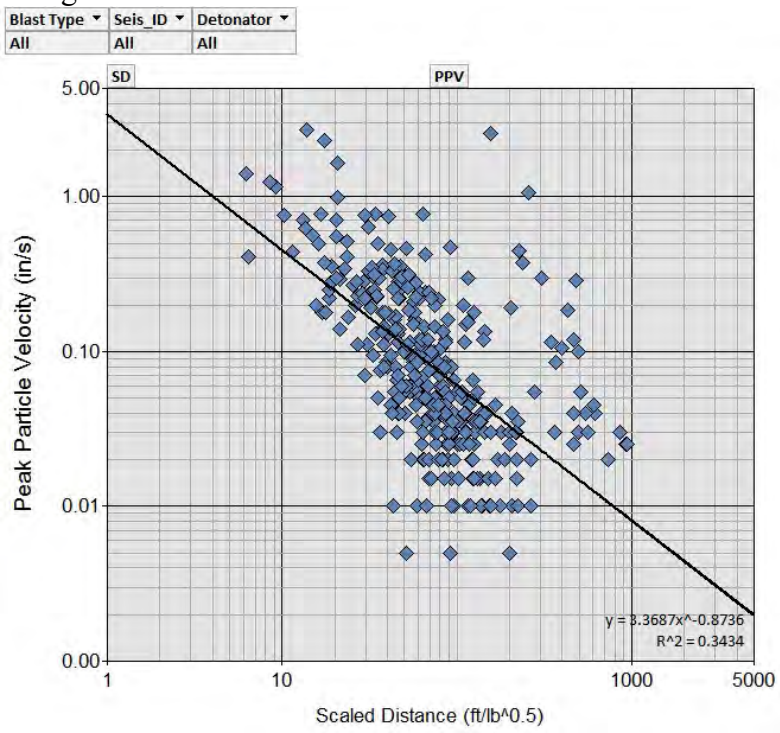

Figure 46 Peak particle velocity Vs Scaled distance

Scaled distance was calculated using the 8ms delay between charges. If the information is categorized by detonator type between non-electric and electronic some differences start to emerge. Figure 47 shows all the maximum peak particle velocity values categorized by detonator type. This figure shows that the trend line has different slopes between the two types of detonators. The electronic trend line exhibits a steeper slope when compared against non-electric (similar behavior was observed in airblast trend lines). The trend lines are introduced to show the behavior of the variables and are not intended to produce a regression equation. The correlation coefficients are better in this particular mine when electronic initiation systems are compared to non-electric (r^2=0.47 Vs r^2=0.27). This is likely attributed to the accuracy of the electronic detonators.

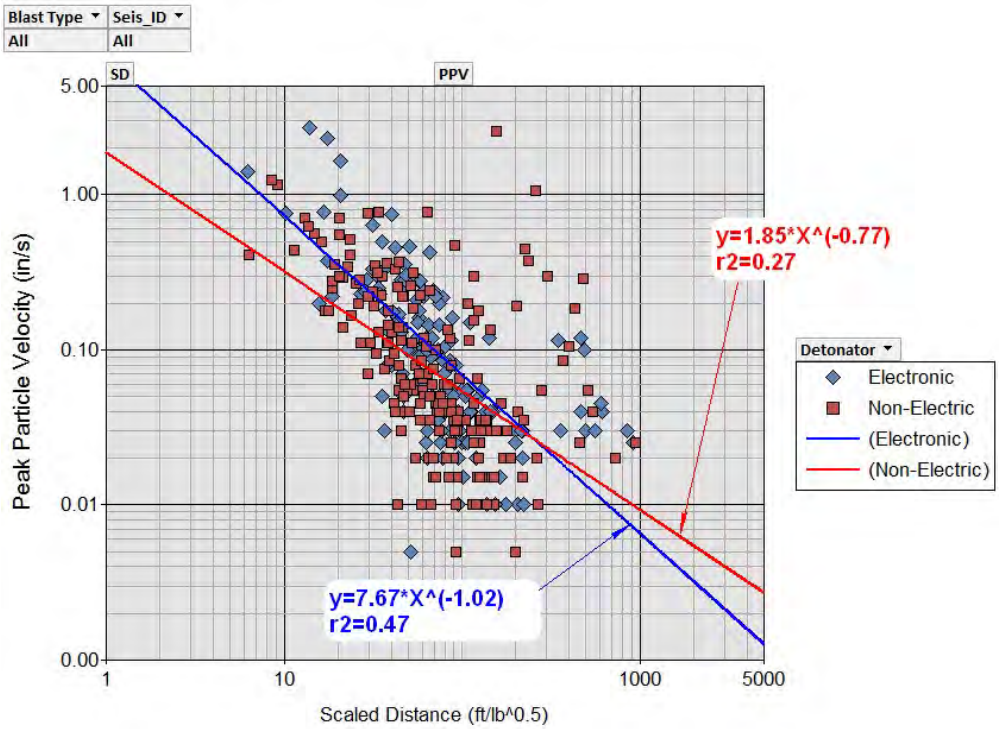

Figure 47 PPV vs Scaled distance (electronic Vs non-electric)

The differences are more evident between the two initiation systems if only production blasts are compared as shown in Figure 48.

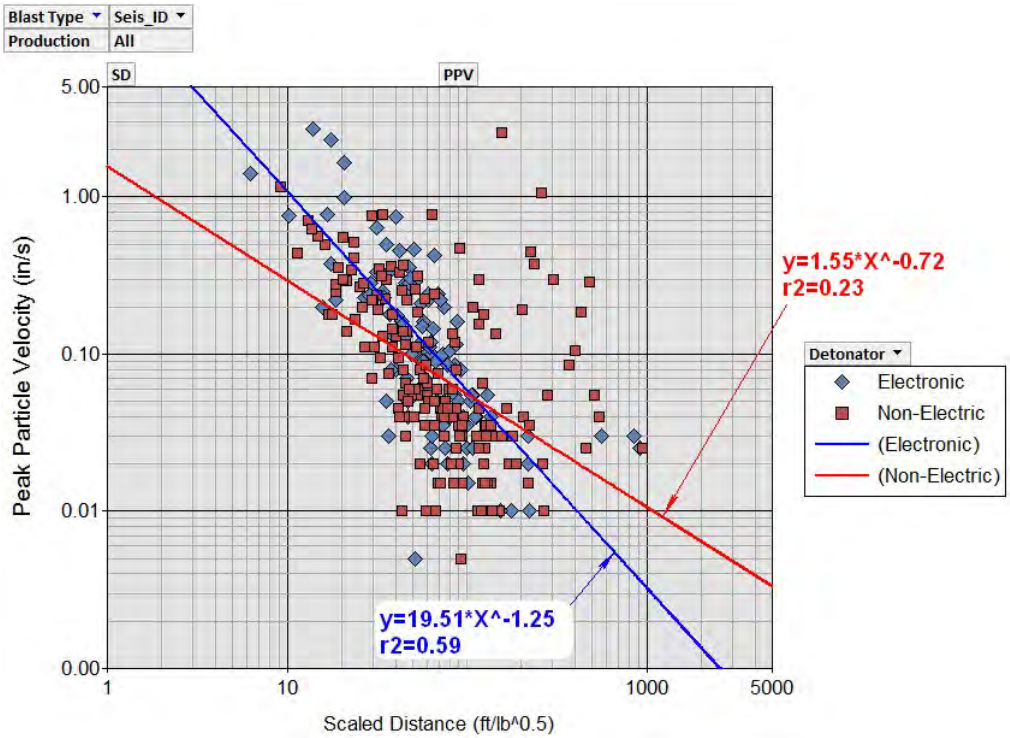

Figure 48 PPV vs Scaled distance only production blasts (electronic Vs non-electric)

Those general trends are corroborated if only production blast and seismographs 5 and 9 are used (5 and 9 are the most active seismographs in 2010) see Figure 49.

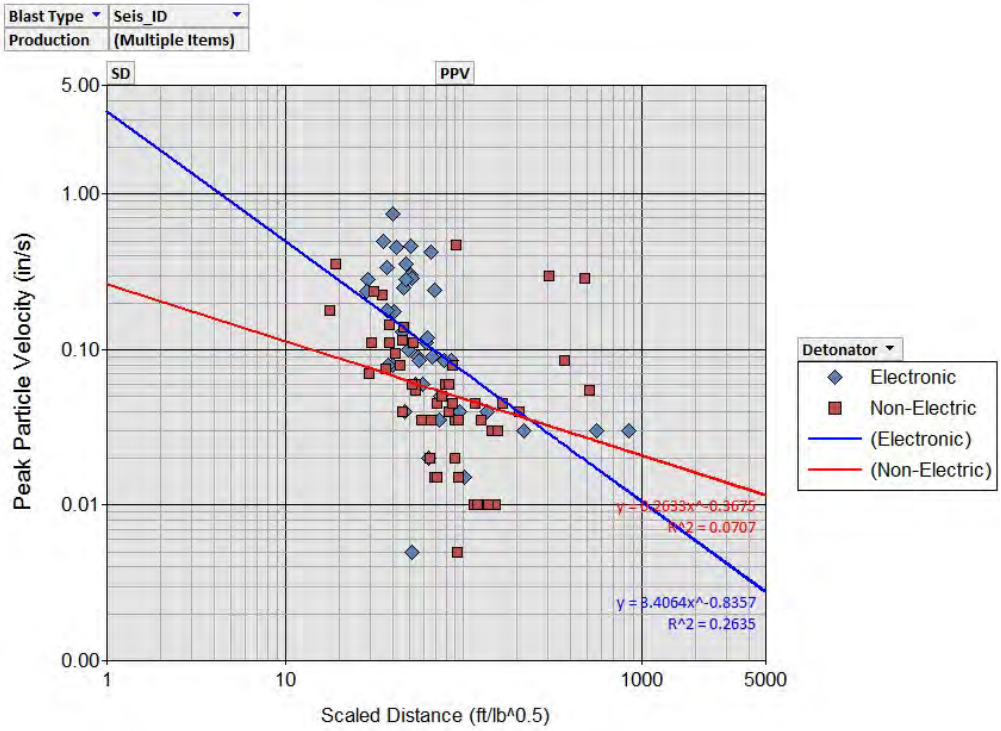

Figure 49 Peak particle velocity for seismographs 5 and 9 production blast

In order to analyze the different axis of measurement in the seismograph, Figure 50 was created including only non-electric initiation system. It simply shows that the three axis exhibited similar trends.

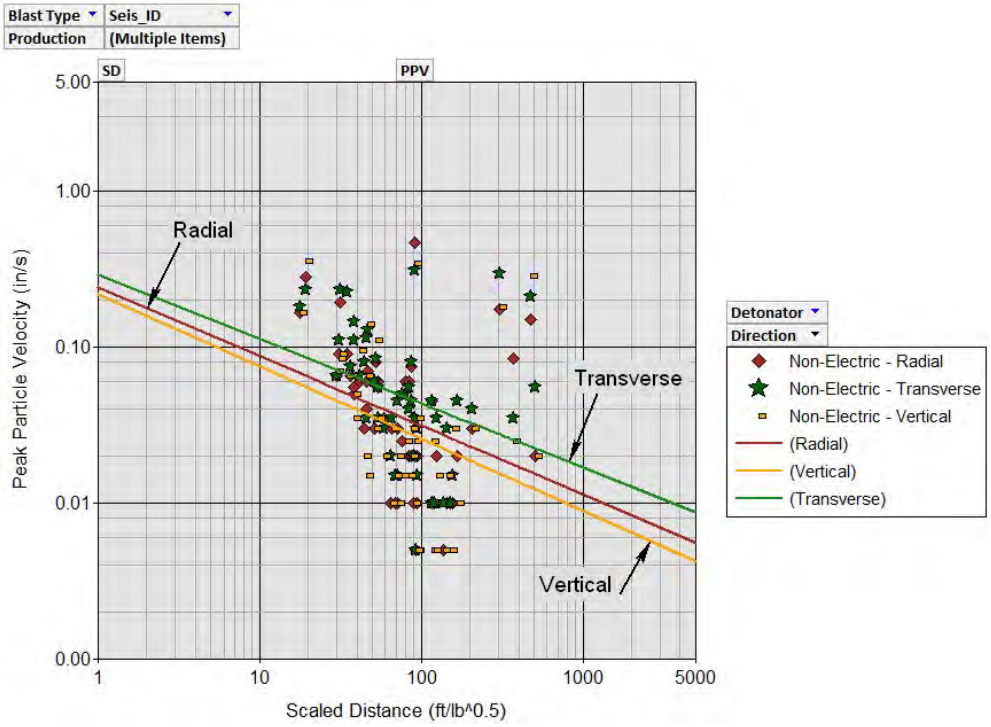

Figure 50 PPV vs SD Non-electric delay system, seismographs 5 and 9 production blast

Figure 50 was made using only production blasts and seismographs 5 and 9. The slopes in the trend lines are almost parallel. The trend lines are included only to see the trend of the data and not to produce a regression equation. In the interval of analysis the transverse vibration direction is higher than the other two directions. The same graph was made including only electronic detonators and the results are included in Figure 51.

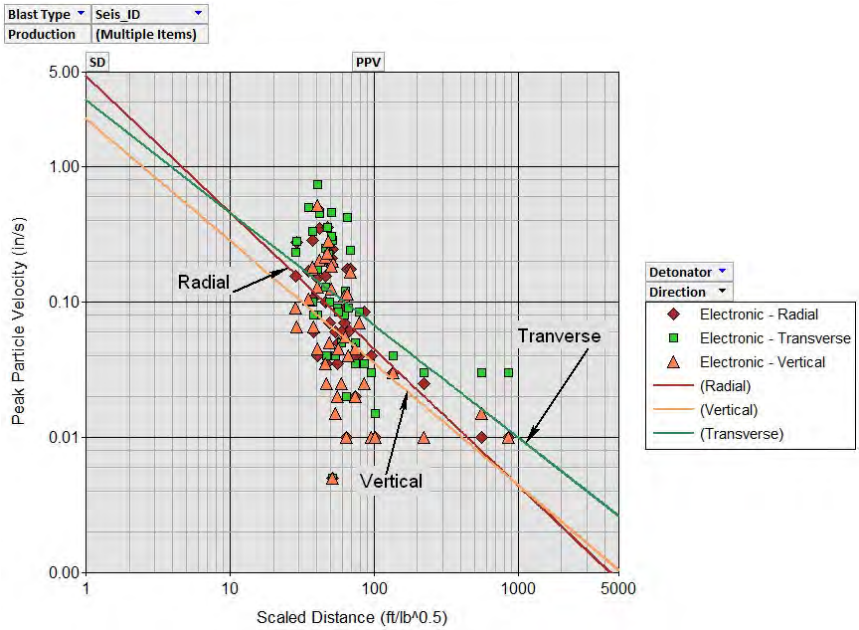

Figure 51 PPV vs SD electronic delay system, seismographs 5 and 9 production blast

In this case, the trend is the same as non-electric, transverse direction presents higher values of particle velocity than the other two directions. Thus, for comparison between two delay systems, transverse direction was chosen.

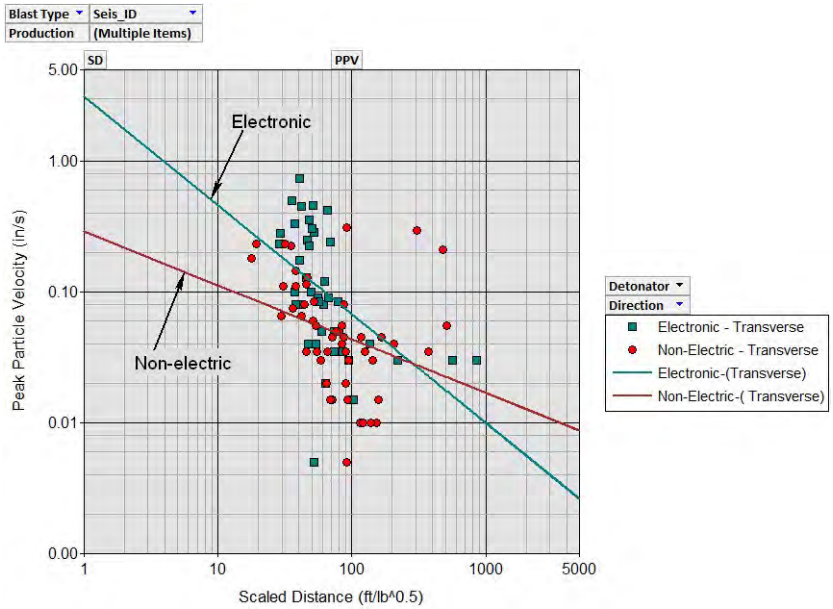

Figure 52 PPV vs SD delay system comparison, seismographs 5 and 9, production blast and transverse direction

As observed in previous figure, electronic delay system tends to generate higher particle velocity than non-electric system. This observation should be taken with caution because timing is not involved in the analysis. In Figure 52, only the type of initiation system was included. This phenomenon is one of the inherent problems with scaled distance analysis when considering electronic detonator systems with infinite timing options.

When timing is introduced in the analysis, Figure 53 is obtained. Figure 53 was prepared including the two most common timing arrangements, used in this particular mine, (100/42) and (42/17). Only non-electric delay system blasts were used for Figure 53.

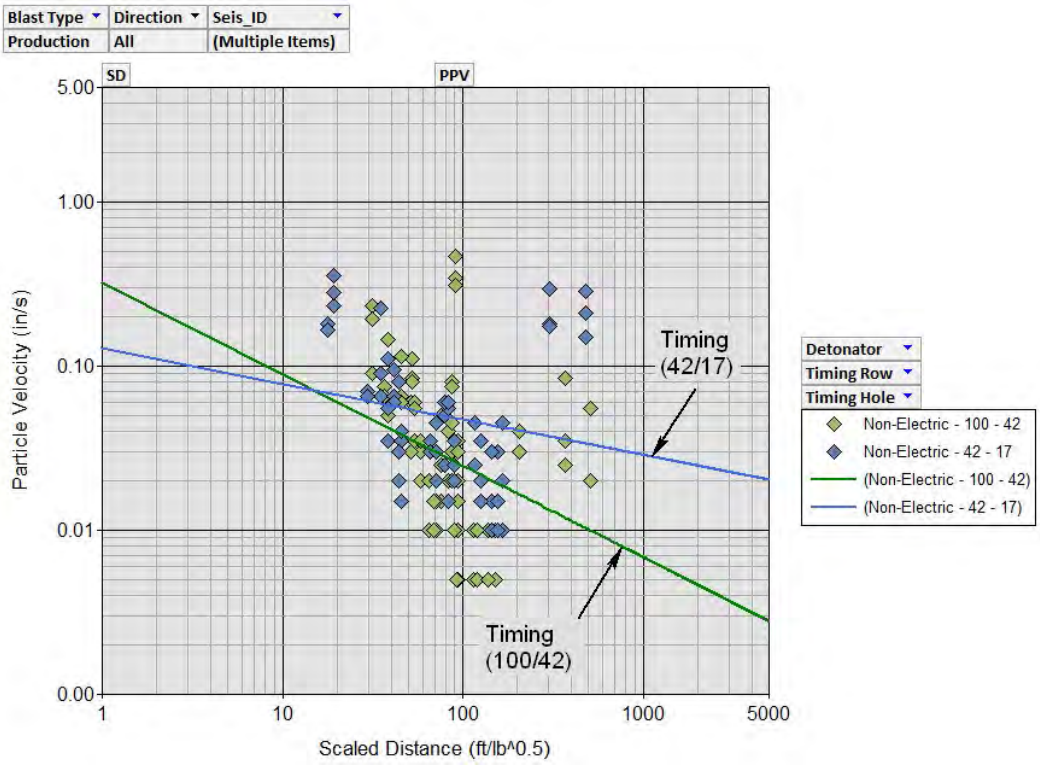

Figure 53 PPV vs SD Non-electric delay and timing of (100/42) and (42/17), production blast and seismographs 5 and 9

Figure 53 shows that shorter delay intervals result in an increase in the peak particle velocity when 100/42 are compared against 42/17. This behavior is similar to that observed in the case of airblast. The difference in particle velocity between both timing arrangements becomes larger as scaled distance increases and is more evident for seismographs 5 and 9.

In order to verify the increase in the particle velocity when short timing is used, Figure 54 was created. In this figure, timings of (10/10) and (4/4) were included. These delay configurations were only possible with the electronic delay system. Figure 54 shows as the delay timing is shorter, the peak particle velocity increases.

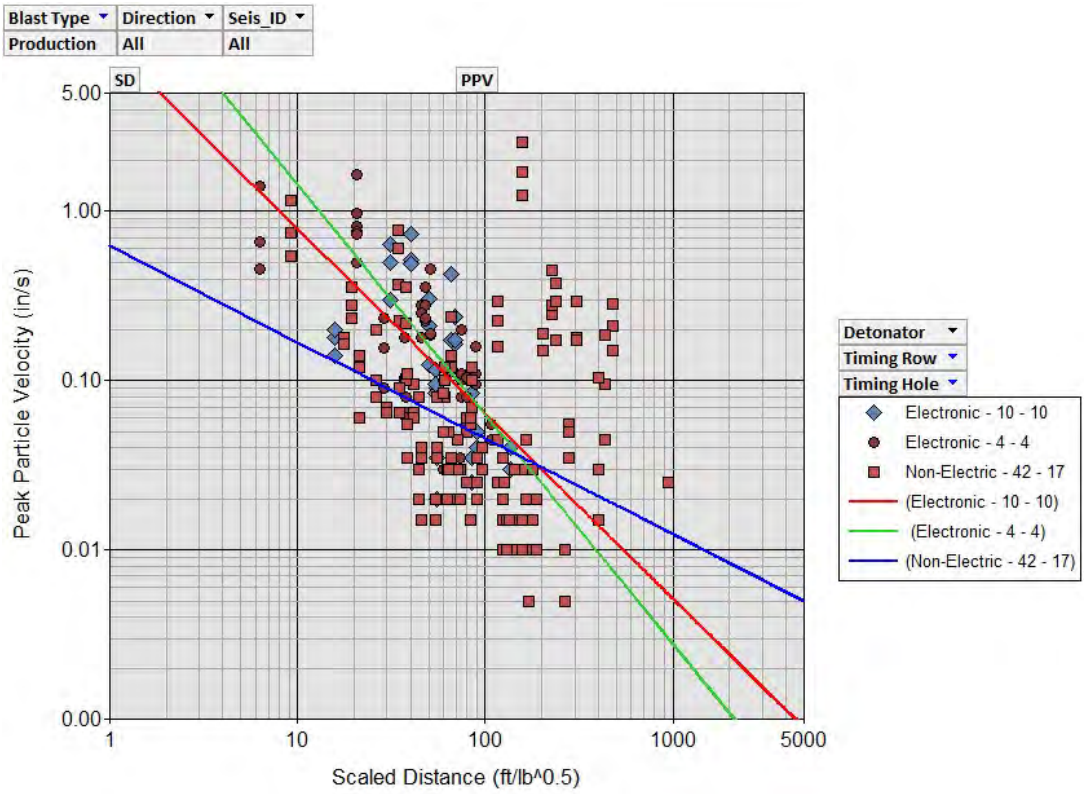

Figure 54 PPV vs SD long and short timing, production blast and all seismographs

Next some preliminary observations and conclusion regarding ground vibrations, initiation systems and timing are included:

- Trend lines were included to understand the behavior of the ground vibration regarding initiation system and timing. It is difficult to propose any equation due to the scatter of the data and the low values of the correlation coefficient (r^2 lower than 0.5) in most of the cases. Likely detonators inaccuracies and distance separation of the charges contribute to poor statistical correlations.
- Despite low regression coefficients, the data collected when using electronic detonators shows less scatter than non-electric system (r^2 values are bigger in the trend lines for electronic system, see figures 47, 48 and 49).
- For this particular data set, electronic initiation systems tend to generate ground vibration levels higher than electronic. Most of the electronic blasts in the data set mimicked timing expected from non-electric systems. More detailed analysis would be required to draw conclusions about choice of delay.
- Shorter delays (<8 ms) tend to generate higher peak particle velocity than long delays.
- The variability in the data illustrates a weakness in the application of scaled distance and linear regression when making decisions about timing configurations. The technology available with electronic detonators prompts the use of more probabilistic methods for predicting ground vibration and airblast.

Prompted by the final observation, and in order to analyze in more detail the collected information, it was necessary to develop a mathematical model. The mathematical model was calibrated using some of the blast tests. After calibration, other case scenarios for timing combinations where analyzed. Also the differences between electronic and non-electric initiation system was included in those analyses. In addition the model was able to simulate timing scenarios in order to more clearly define the term "delay". A brief description of the model is included in the following section

3.4 Model Development

There are several methodologies and approaches to model airblast and ground vibrations. These methods include; scaled distance methodologies, numerical modeling and signature hole analysis. In this research signature hole analysis was selected to develop a model to study the variables that are involved in the blast vibration problem. Signature hole analysis was chosen for the relative ease of implementation. In addition, this methodology considers the main variables in the problem such as the delay used hole to hole and row to row, the traveling time between the area where the blast is taking place and the monitoring or recording point, and the vibration characteristics of the monitoring point. In general through this methodology it is possible to introduce random behavior of the variables mentioned above to account for scatter experienced in the collected data.

The model described in this report is a modified signature hole technique. The technique has four distinct steps:

1. Synthesis of signals (one unique signal for each charge or hole in the blast) from signature hole data using the Silva-Lusk equation. The signals are created with random variability in amplitude and frequency within a reasonable range to account for energy output variation from hole to hole detonations.
2. Prediction of complete blast time history utilizing unique synthetic hole output signal for each hole or charge in a blast sequence. The blast is simulated considering variations in wave travel time, initiation system accuracy, and nominal timing.
3. Monte Carlo iteration of complete blast vibration output. The number of iterations is determined based on convergence of data. Typical blasts have required less than 100 iterations for a normal distribution of peak particle velocities.
4. Creation of a peak particle velocity histogram. The histogram allows for determination of maximum and minimum expected particle velocities.

Utilizing the Silva-Lusk modified signature hole technique, timing scenarios can be adjusted in the model to investigate the effects on blast vibration output. This procedure allows for assessment and definition of a "delay" and also allows for optimizing timing for minimizing vibration output. Each step in the technique is described in detail in the next sections.

3.4.1 Signature hole technique

This technique is based on signals and system theories. In a blast event, a structure's response is a function of the amplitude and frequency content of the ground vibration signal reaching the structure (Siskind et al., 1980b). Past research has shown the benefits of the use of

wave interference to reduce the ground vibration levels in a blast event (Lusk et al., 2006). This concept was introduced in 1980 with information about the potential for wave interference (Crenwelge, 1980). The basic concept behind the signature hole technique is similar to the principles applied in signals and systems theory. In signal and system theories, a system is defined as an entity with a unique relationship between the excitation or input and the response or output (cause and effect) Figure 55 shows this similarity for continuous (signals that are defined for every instance) and discrete (signals that are defined only for some specific values) signals.

There are many types of systems. From an Input - Output point of view, they can be:
SI-SO: Single Input – Single Output
MI-MO: Multiple Input Multiple Output

or combinations:
MI-SO: Multiple Input – Single Output
SI-MO: Single Input – Multiple Output

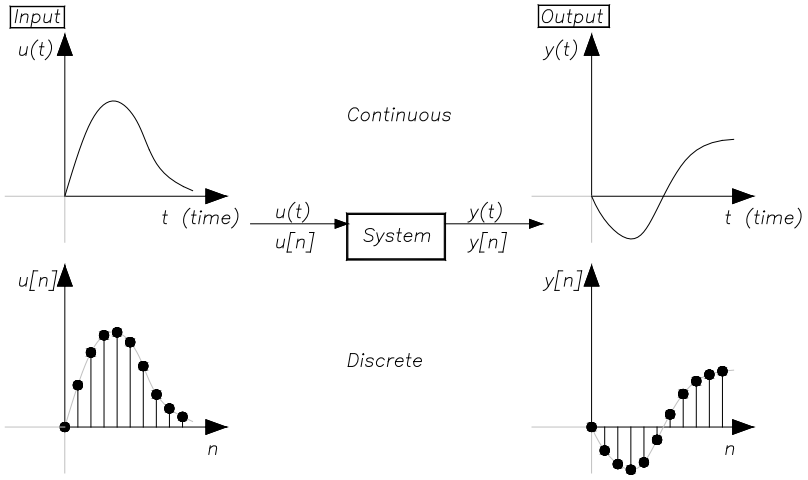

Figure 55 Sketch of a system with continuous and with discrete signals.

The systems can also be classified according to the characteristics in causal or non-causal, lumped or distributed, linear or nonlinear and finally as time invariant or time varying.

Single-Input, causal, linear and time invariant systems are very useful in the "real world" because many physical phenomena can be modeled using the system theory applicable to that type of systems. Figure 56 shows the basic concepts of the SI-SO, and time invariant systems.

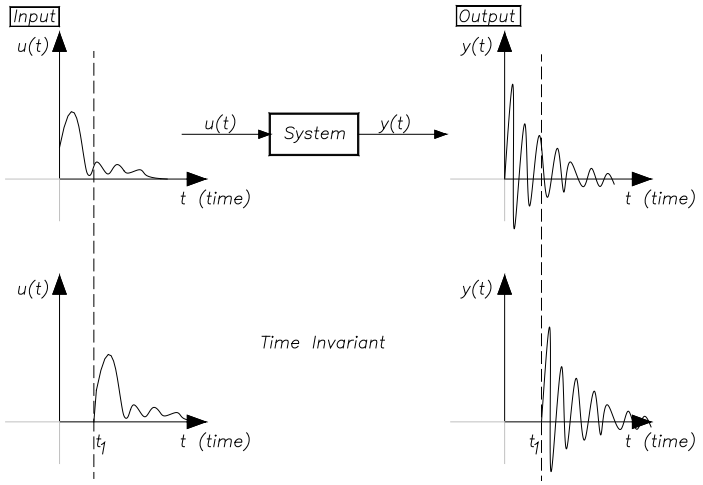

Figure 56 Time Invariant systems single input - single output (Adapted from "Signal and Systems" 3th edition)

Causality is related to the relationship between the Input-Output and the time. One system is causal if the current output is only related to the current input (the current response is not related to past or future inputs). On the other hand, linearity in the systems theory is related to the linear superposition of different actions to produce a response. Finally, if the system does not change over time, this means that the system is time invariant, i.e., an input in current time, produces the same output that an input given to the system in the future.

All these concepts mean that if the system is Continuous (**C**) Linear (**L**) and Time Invariant (**TI**), by knowing a pair Input – Output signals, it is possible to predict the outputs for whatever Input signal. Figure 57 shows this concept in more detail.

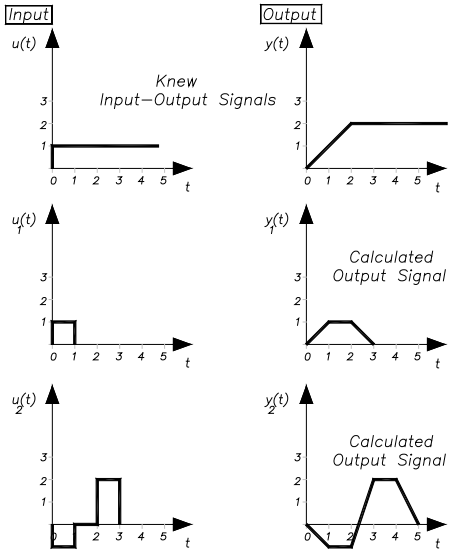

Figure 57 SI-SO, C, L, TI systems (Adapted from "Signal and Systems" 3th edition)

In blasting, the signature hole technique assumes that the vibrations generated as energy released in a blast, and transformed into elastic waves travelling within the rock, are a physical phenomenon developed in an SI-SO, C, L, TI system.

In such case, the system is the entity that wraps the site specific geological conditions between the event site and the point under study (joints, faults, lithology etc.,), and the path of the vibration waves, including reflections and refractions of waves propagating away from the event site. Figure 58 shows this concept.

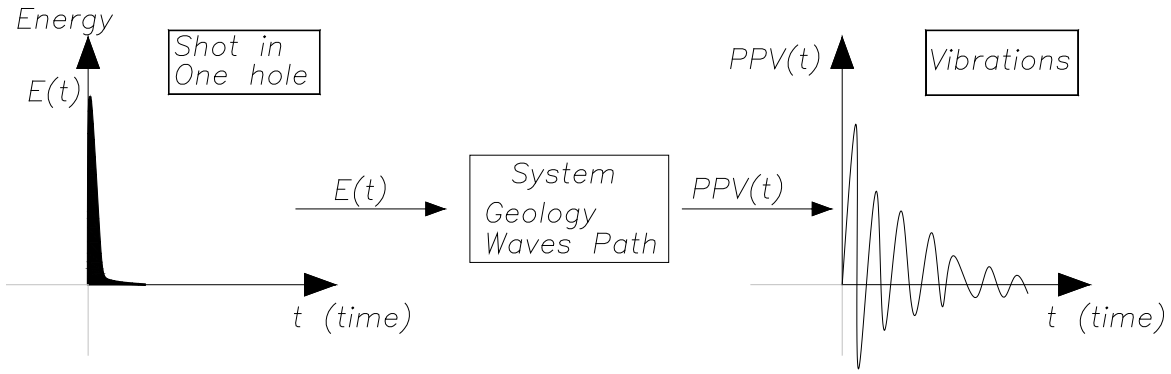

Figure 58 Systems Theory and Signature Hole Technique similarity.

Other assumptions to the signature hole technique are (after Anderson 2008):

- There is a need to control the vibrations in a specific location.
- All holes are detonated at the same location, so that the path traveled by the waves is identical.
- All holes have the same explosive charge type and weight. In others word, the quantity of energy converted into elastic waves each time a hole is blasted is the same.
- The phenomenon occurs in a system ideally SI-SO, C, L, and TI, so that all holes have the same explosive-rock interaction. That means that the source pulse (detonation) always generates the same response in the site under study (signature wave).

In the signature hole technique, assuming that all the assumptions are fulfilled, the signature wave recorded in a specific site (the signal recorded when a single hole is blasted) can be expressed as a finite impulse response (FIR). This means an impulse response with finite nonzero entries, which can be expressed in a discrete form as:

$$h[n] \neq 0 \;\; for\; n = 0,1,2, \dots, N-1$$

Equation 1

with

$$h[N-1] \neq 0$$

Equation 2

and

$$h[n] = 0 \; for \; n \geq N$$

Equation 3

Graphically, the impulse response concept in blasting is represented in Figure 59.

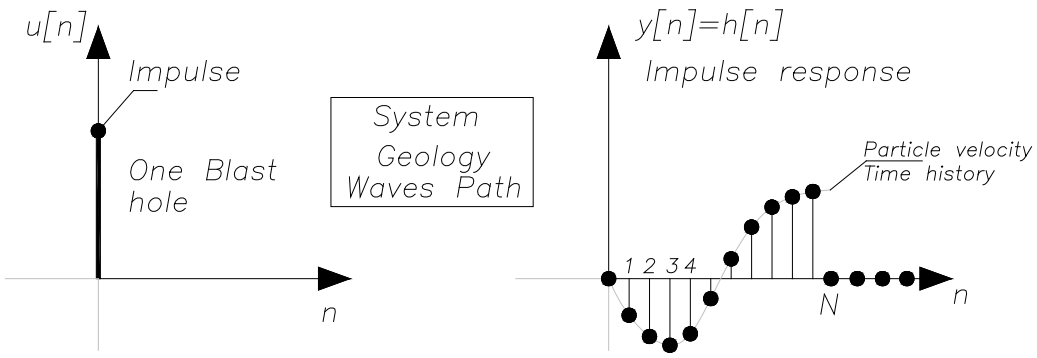

Figure 59 Finite impulse response from one hole blasted

When the input signal is the impulse, (one blasted hole at n=0), it can be expressed as:

$$u[n] = A_i\delta[n] \quad or$$

Equation 4

$$u[0] = A_i\delta[0]$$

Equation 5

In previous equations:

$u[n]$:	Impulse
$\delta[n]$:	Delta Dirac function
n:	Integer number given by: $n = \frac{t-t_o}{\Delta t}$
t_o:	Time of reference
t:	Time when the explosion occurs
Δt:	Time interval
A_i:	Relative energy of the explosion (usually assumed as 1)

Equation 4 expressed in a more general form is given by:

$$u[k] = A_i * \delta\left[\frac{t - t_o}{\Delta t}\right]$$

Equation 6

And the complete blasting initiation sequence is given by:

$$u[n] = \sum_{k=0}^{\infty} u[k]\delta[n-k]$$

Equation 7

Assuming the system is linear and time-invariant, and using the shifting, homogeneity and additive properties of signals, the output *y[n]* excited by the input *u[n]*, for n≥0, can be given by:

$$y[n] = \sum_{k=0}^{n} h[n-k]u[k]$$

Equation 8

Or in a general form:

$$y[n] = \sum_{k=-\infty}^{\infty} h[n-k]u[k] := h[n] * u[n]$$

Equation 9

Where:

$y[n]$: Discrete predicted vibration waveform
$h[n]$: Discrete signature waveform (signal recorded for one hole blast)
$u[n]$: Discrete initiation sequence (timing sequence of the holes in the blast)

This algebraic equation is called a "discrete convolution." This equation relates the input and output of a system. Due to this relation, the convolution is also sometimes called input-output description of the system. In this case, the description of the system (calculation of the output given an input) is developed without using any physical properties of the system and is based on signal-system properties as linearity, time invariance and causality.

Predicting vibration levels of a production blast at the same monitoring point that a signature wave was recorded allows for the recorded signature wave to be used directly to calculate the blast vibration waveform. On the other hand, if signature waveforms are not available at a place where it is required to predict vibrations levels, some authors combine scaled distance estimations and transfer functions to get the signature waveform at the point of interest (Spathis, 2010).

In the signature hole technique, the main variables involved in the problem are:

- Signature waveform
- Timing initiation sequence
- Wave traveling time

A description of the variables involved in the model is included in the next section.

3.4.1.1 Signature Waveform

Most current methodologies using the signature waveform technique assume that the signature wave does not change from hole to hole. In this model, waveform variability was introduced into the signature hole technique. There are at least two reasons why the signature waveform hole to hole changes.

The first phenomenon that affects the waveform hole to hole is related to the damage in the surrounding rock by previous holes (confinement). When a hole is detonated, it changes the rock properties around the hole in a specific area. The extension of such area is a function of the initial conditions of the rock (i.e. rock joint system before detonation) as well as the geometry of the hole and the efficiency of how the chemical energy is transferred from the explosive to the rock. According to this, if the separation between holes S is enough to have no interference, the signature waveform from hole (i) will be equal to the signature waveform from hole (j) as show in Figure 60.

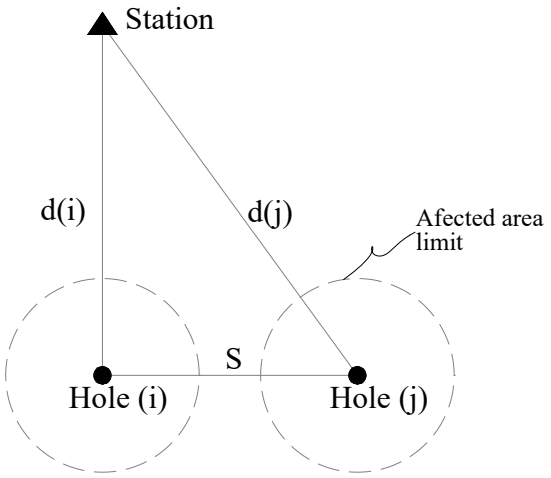

Figure 60 Signature hole reproducibility (adapted from Blair 1993)

On the other hand, if the affected area from hole (i) over lay or interfere with the affected area from hole (j), (i.e. the separation between holes S is such that affected areas interfere), there is a need to find a relationship to describe the nonlinear variation of the signature waveform hole to hole in a production blast event.

In this research, a methodology for varying the signature waveform hole to hole was developed. This approach takes in to account the change in both main parameters of the seed waveform amplitude and frequency. Current methodologies only modify amplitude in the waveform hole to hole. The methodology is based on the main characteristics of any recorded signature waveform and utilizes Fourier series to create an equation that produces different waveforms for each hole in the vibration prediction process. Involving both the change in amplitude and frequency, it is expected that changes in the surrounding material to the detonated hole and the changes in the path from hole to monitoring point be involved in the prediction process.

The equation developed (Silva-Lusk) equation, based on Fourier series to approach the signature waveform has the general form:

$$\mathrm{f(t)} \approx \left[\mathrm{c_o} + \sum_{\mathrm{n=1}}^{\mathrm{m}} \mathrm{ASF}_n * \{\mathrm{A}_n * \sin(2\pi * \mathrm{frequency}_n * \mathrm{t} + \emptyset_n)\}\right] * e^{+rise\ factor * t}_{-\ decay\ factor * t}$$

Equation 10

where:

$f(t)$:	synthetic signature waveform for hole (i)
ASF_n:	amplification scale factor for frequency m.
c_o:	first term in the Fourier series
m:	number of frequencies chosen to simulate the measured signature waveform.
A_n:	amplitude coefficient for frequency m in the Fourier series

$frequency_n$:	one of the main frequencies (frequency m) chosen to simulate the measured signature waveform.
t:	time
$\emptyset_n$:	phase for frequency m
$decay\ factor$:	factor related to the attenuation energy in that particular point.

These parameters are explained using the following figures. Assuming that Figure 61a represents the signature waveform recorded in a specific point, the frequency content of that signal is giving in Figure 61b.

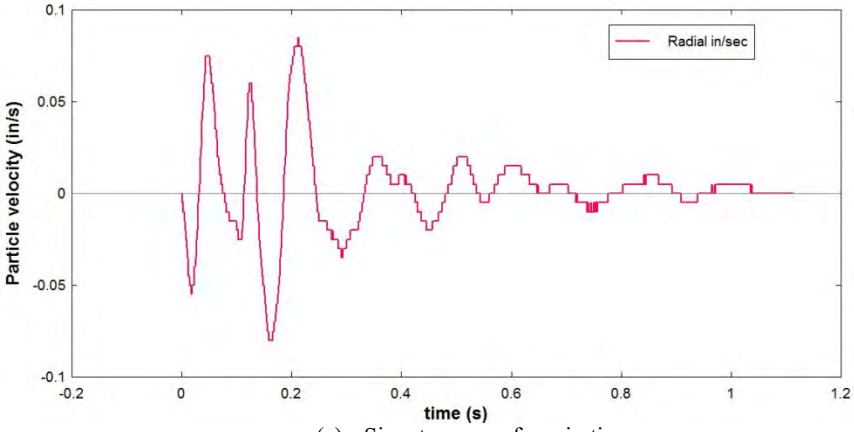

(a) Signature waveform in time

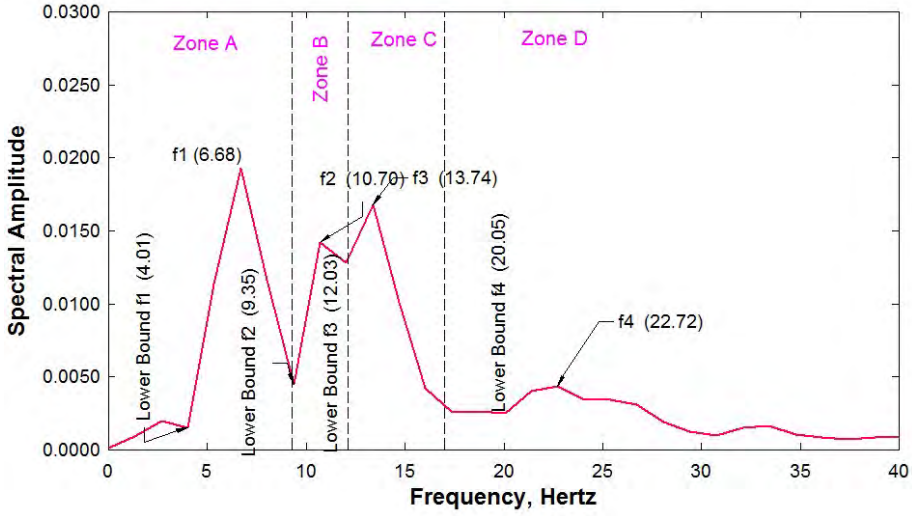

(b) Signature waveform frequency content

Figure 61 Signature waveform

Using the four main frequencies of the signal (6.68, 10.70, 13.74 and 22.72 Hz), when applying Fourier series, the terms inside the brackets in Equation 10 are given by:

$$terms\ in\ brackets = [0.002353 + 0.01625 * \sin(2\pi * 6.68 * t - 0.4495\pi) + 0.01140 * \sin(2\pi * 10.70 * t - 0.27924\pi) + 0.01196 * \sin(2\pi * 13.74 * t + 0.9513\pi) + 0.003033 * \sin(2\pi * 22.72 * t + 0.5429\pi)]$$

Equation 11

When this equation is plotted against the signature waveform, Figure 62 is obtained.

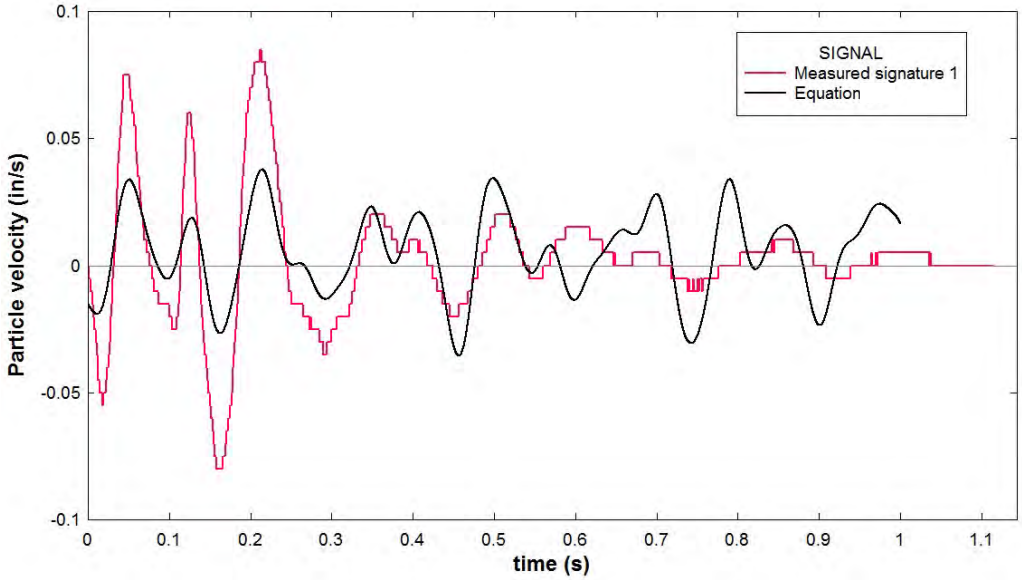

Figure 62 Signature waveform and equation 11

The decay factor is calculated using an exponential decay envelop from the measured signature signal as included in Figure 63

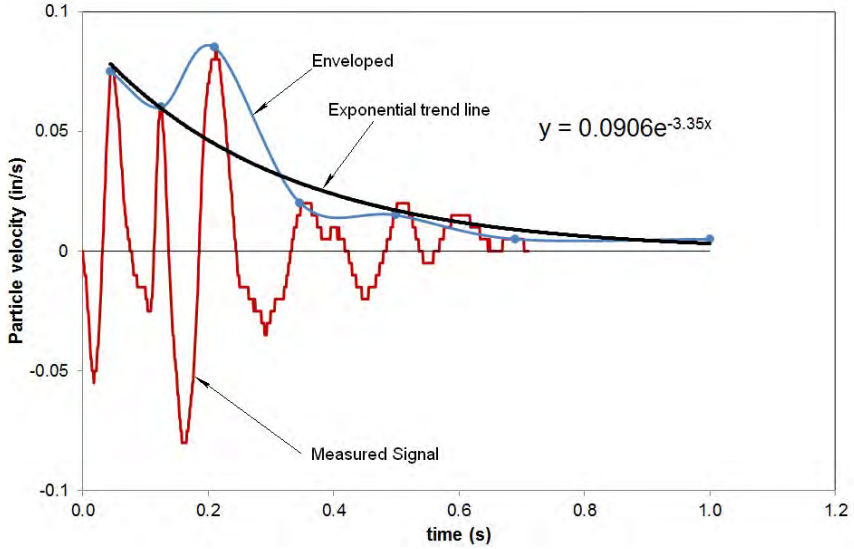

Figure 63 Decay factor calculation.

Figure 64 is obtained when decay factor is included in the Equation 11.

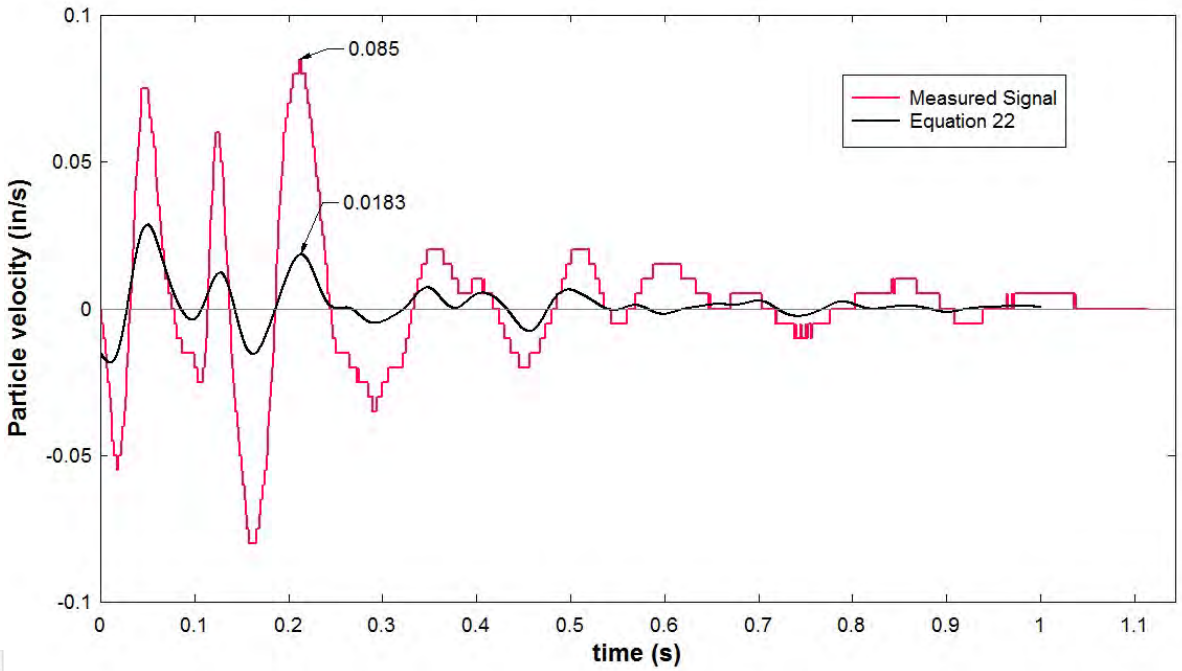

Figure 64 Measured signal Vs base equation including exponential decay factor

Then amplitude factor is calculated at the PPV as:

$$ASF = \frac{0.085}{0.0183} = 4.64$$

Equation 12

Following this procedure, the numerical values of Equation 10 are given by:

$$f(t) = \mathbf{4.64} * (0.002353 + 0.01625 * \sin(2\pi * 6.68 * t - 0.4495\pi) + 0.01140 * \sin(2\pi * 10.70 * \mathrm{t} - 0.27924\pi) + 0.01196 * \sin(2\pi * 13.74 * \mathrm{t} + 0.9513\pi) + 0.003033 * \sin(2\pi * 22.72 * \mathrm{t} + 0.5429\pi)) * \boldsymbol{e^{-3.35 * t}}$$

Equation 13

Figure 65 is obtained when the synthetic signature waveform signal and the measured signature waveform are plotted in the same plot.

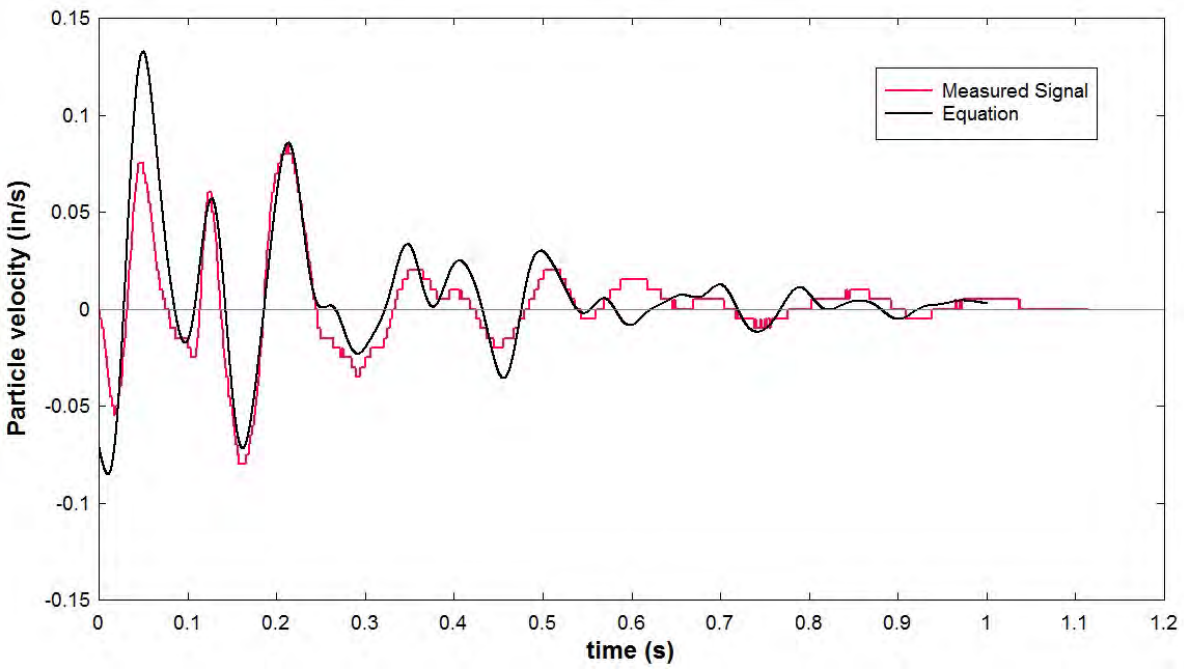

Figure 65 Measured signal Vs final approach

To introduce the variability hole to hole in the signature waveform, there are three parameters where a random normal distribution behavior was assumed; they are the amplification scale factor, the frequency content of the signal and the decay factor. The formulation is as follows:

$$ASF_m = \overline{ASF} + randn * Std(ASF)$$

$$Frequency_m = \overline{Frequency} + randn * Std(Frequency)$$

$$Dec_{fact} = \overline{Dec_{fact}} + randn * Std(Dec_{fact})$$

Equation 14

Where:

$\overline{ASF}, \overline{Frequency}, \overline{Dec_{fact}}$: mean values for the parameters in Equation 10

$Std(ASF), Std(Frequency), Std(Dec_{fact})$: standard deviation for the parameters in Equation 10

$randn$: pseudorandom values drawn from the standard normal distribution

Using Equation 10 and Equation 14 a random signature waveform is generated for each hole in the modeling process of the complete waveform from a specific production blast.

3.4.1.2 Timing initiation sequence

The blasting sequence depends of the initiation device used to initiate the explosives. As observed in the lab experiments, the statistical parameters to use in the model to predict vibrations from blast depend on the accuracy of the two initiation systems tested. In total 674 detonators were tested. Each system (electronic and non-electric) was tested over the viable ranges of delays available.

In this research, the statistics for the initiation systems were included in the model assuming a random normal distribution, and using the laboratory measured parameters of mean and standard deviation for both initiation systems.

The general equation used in the Monte Carlo scheme to predict vibrations levels from mining blast and regarding to delay timing between holes is given by:

$$\Delta dt_{ji} = \overline{dt} + randn * (\sigma_t)$$

Equation 15

Where:

Δdt_{ji}:	time interval between detonation hole (i) and hole (j).
$\overline{dt}$:	average delay timing, measured or assumed
σ_t:	standard deviation of the normal distribution of the average delay timing, assumed or measured
$randn$:	pseudorandom values drawn from the standard normal distribution

3.4.1.2.1 Wave traveling time

If two holes are blasted as showed in Figure 66, the vibration signal from hole (i) is going to be recorded at the station or monitoring point at time $\mathrm{dt_{is}}$. This time includes the time that the vibration wave takes to travel form hole (i) to the monitoring point. If after detonation of hole (i), the second hole (hole (j)) is detonated, at time $\mathrm{dt_{ji}}$. The total time, having the detonation of hole (i) as a reference, that the vibration from hole (j) is going to be recorded at the station will be $\mathrm{dt_{ji}} + \mathrm{dt_{js}}$.

In this research, the traveling time of the waves from the source to the monitoring point, are introduced in the model through the compressional or shear wave propagation velocity according to the vibration component that is going to be modeled. If the blast vibration component to model is the longitudinal component, the wave propagation velocity to use is the *p-wave velocity*, on the other hand if any other component of the vibration is needed (vertical or transverse), *s-wave velocity* should be used.

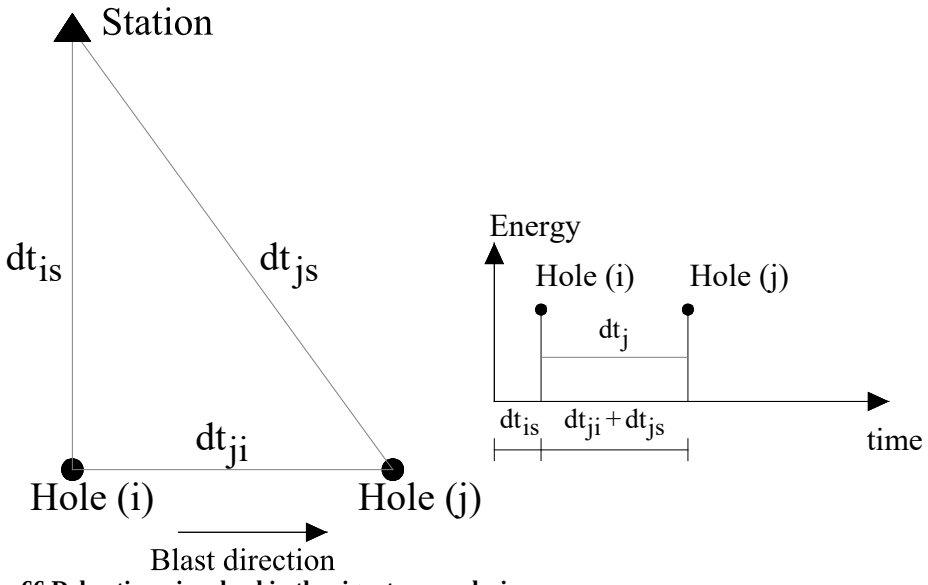

Figure 66 Delay times involved in the signature analysis

In Figure 66:

dt_{is} vibration travel time between hole *i* and station *S*.
dt_{ji} delay time between hole *j* and hole *i*.
dt_{js} vibration travel time between hole *j* and station *S*.
dt_{j} total delay time between holes in the sequence for the hole *j*

The best practice to assess the numerical value of the wave propagation velocity is through field tests similar to those used in earthquake engineering to measure the dynamic properties of the rock and soil. There are different methods including:

- Seismic reflection
- Seismic refraction

Those methods are based on the basic physics equation for velocity:

$$v = \frac{x}{t}$$

Equation 16

Where:
x: distance source receiver
t: arrival time

Measurement of the actual wave velocities was outside of the scope of this project; therefore, literature values for wave velocity in typical rock strata were used in the model. Table 9 contains typical rock velocities for some of the rocks existing in the Appalachian region.

Table 9 Typical rock velocities (from Bourbié, Coussy, and Zinszner, Acoustics of Porous Media)

Type of formation	P wave velocity (m/s)	S wave velocity (m/s)	Density (g/cm^3)
Scree, vegetal soil	300-700	100-300	1.7-2.4
Dry sands	400-1200	100-500	1.5-1.7
Wet sands	1500-2000	400-600	1.9-2.1
Saturated shales and clays	1100-2500	200-800	2.0-2.4
Marls	2000-3000	750-1500	2.1-2.6
Saturated shale and sand sections	1500-2200	500-750	2.1-2.4
Porous and saturated sandstones	2000-3500	800-1800	2.1-2.4
Limestones	3500-6000	2000-3300	2.4-2.7
Chalk	2300-2600	1100-1300	1.8-3.1
Salt	4500-5500	2500-3100	2.1-2.3
Anhydrite	4000-5500	2200-3100	2.9-3.0
Dolomite	3500-6500	1900-3600	2.5-2.9
Granite	4500-6000	2500-3300	2.5-2.7
Basalt	5000-6000	2800-3400	2.7-3.1
Gneiss	4400-5200	2700-3200	2.5-2.7
Coal	2200-2700	1000-1400	1.3-1.8
Water	1450-1500	-	1.0
Ice	3400-3800	1700-1900	0.9
Oil	1200-1250	-	0.6-0.9

A normal distribution was assumed for the wave velocity and 10% of the main value as standard deviation in order to calculate the traveling time between the hole and the station or monitoring point. The statistical parameter for the wave velocity is given by:

$$v = \bar{v} + randn\ (0.1 * \bar{v})$$

Equation 17

In order to estimate the traveling time, using Equation 16 and Equation 17, it is obtained for the time:

$$dt_{ns} = \frac{x}{\bar{v} + randn\ (0.1 * \bar{v})}$$

Equation 18

Where:

dt_{ns}: traveling time between hole n and station or measuring point s
x: distance between hole hole n and station or measuring point s
$\bar{v}$: wave velocity, assumed or measured
$randn$: pseudorandom values drawn from the standard normal distribution

In the situation that field measurements for wave velocity are performed, it is not needed to assume any parameters and the statistical parameters for the field measurements can be used in Equation 17 and Equation 18.

The time used to perform the linear superposition is given by the time of the arrival of the vibration wave plus the time interval between detonation holes. For example and using Figure 66, the time of hole (j), using hole (i) as time reference is giving by:

$$t_j = \Delta dt_{ji} + dt_{js}$$

Equation 19

Where:

t_j: time for hole (j) reference to hole (i)

Δdt_{ji}: time interval between detonation hole (i) and hole (j).Equation 15

dt_{js}: traveling time between hole (j) and station or measuring point (s). Equation 18

4. RESULTS AND DISCUSSION

The complete database of vibrations collected during this project is composed by 230 waveform events. In chapter 3, a detailed analysis of the recorded information was done through the conventional analysis base on scaled distance. In this chapter, only those tests containing at least one signature hole are described. This is because for those events, it is possible to use the proposed signature methodology to compare the results of the predicted vibrations levels versus the recorded vibration waveform. Using the proposed signature hole technique it is also possible to analyze different case scenarios regarding initiation timing. Table 10 summarizes the tests and the main characteristics of the tests like number of holes, depth, diameter, etc.

In total, 15 field tests were used to analyze the influence of the timing in the vibration levels. Some of the tests were set up using short delays (less than 8ms) to meet the requirements of the current research. Analysis of test No.14 and 15 is of special interest because the main difference between those tests was the type of initiation system used between electronic and non-electric.

Appendix A contains the blasting log report from the mine. The location of the holes in the last six tests (performed in 2011) were controlled using topographic survey of precision. The plan layout of those tests and the vibration records are included in Appendix B.

Table 10 Tests including signature hole

Test	Date	Holes	Depth (ft)	B (ft)	S (ft)	Detonator	Total explosive	Main Delay	Signature
1	09/10/2010								
2	09/11/2010	29	95	9	9	Electronic	2,125.57	1ms	Three hole@same time (Pre-split)
3	09/11/2010	66	30	18	18	Electronic	21,160.37	80ms	
4	09/15/2010	194	90	20	20	Electronic	342,763.93	4ms	One hole
5	09/16/2010	69	44	20	20	Electronic	55,050.03	4ms	Four Holes@same time
6	09/17/2010	41	30	18	18	Electronic	11,069.31	100/42 ms	One hole
7	09/18/2010	96	95	18	18	Electronic	181,778.14	4ms	Two holes@same time
8	09/22/2010	67	75	20	20	Electronic	86,719.03	4ms	Two holes@ same time
9	10/01/2010	176	95	20	20	Electronic	298,139.26	17ms	One hole
10	06/22/2011	11	45	18	18	Electronic	5,928.63	5ms	Three signatures
11	06/23/2011	26	30	18	18	Electronic	22,090.28	100/5ms	Two signatures
12	06/24/2011	29	45	18	18	Electronic	24,271.73	5ms	Two signatures
13	06/29/2011	32	45	18	18	Electronic	26,039.31	3ms	One hole signature
14	06/29/2011	35	45	18	18	Non-electric	30,106.45	42/100 ms	NO-Signature
15	06/29/2011	40	45	18	18	Electronic	33,478.25	42/100 ms	NO-Signature

As an example of the performed tests, Figure 67 shows the plan layout for the test 06/29/2011 (test No.13). In this figure, red indicates the detonation order of the hole, and black indicates the nominal delay used in milliseconds. In this test, one signature hole was recorded at 3800ms. This test is divided in two different timing arrangements. The first part was detonated using a nominal timing delay of 8ms hole to hole and 100ms between rows. In the second part of the test, a timing of 3ms between holes and 100ms between rows was used. In total, this test accounted for 32 holes blasted. The order of the number of holes as shown in Figure 67 is nineteen (19) holes, one (1) signature and twelve (12) holes. The recording of the vibrations in the three components radial, vertical and transverse are included in Figure 68 for the Ridge seismograph which was the closest.

The maximum peak particle velocity recorded (0.68in/s) was for the radial component when a timing arrangement of 3/100ms was used. This result was expected and shows the influence of the initiation timing in the vibration levels for a blast event. This test will be analyzed later in detail. Figure 69 shows the attenuation of the radial component with distance from the source for test No.13.

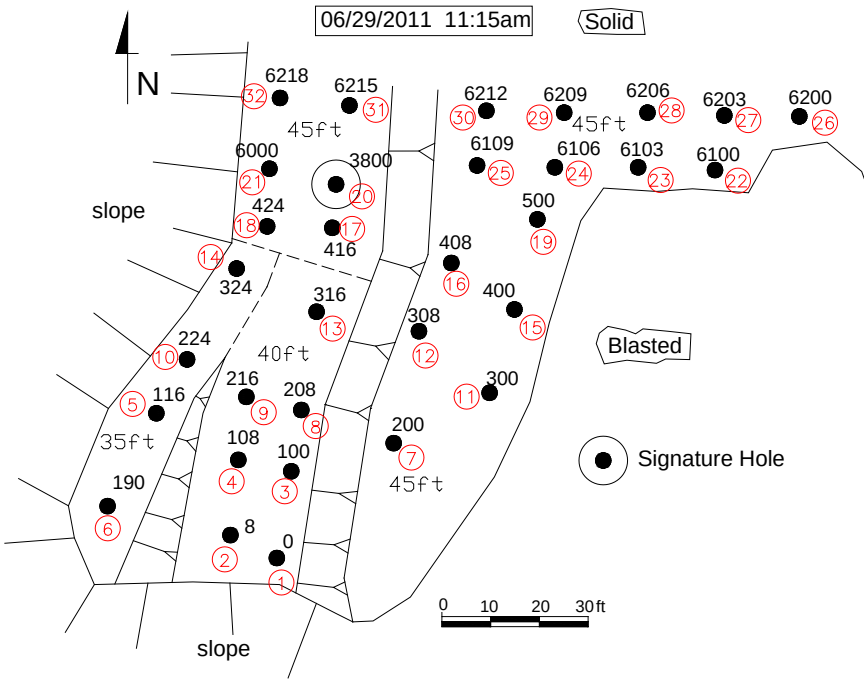

Figure 67 Plan layout test Number 13

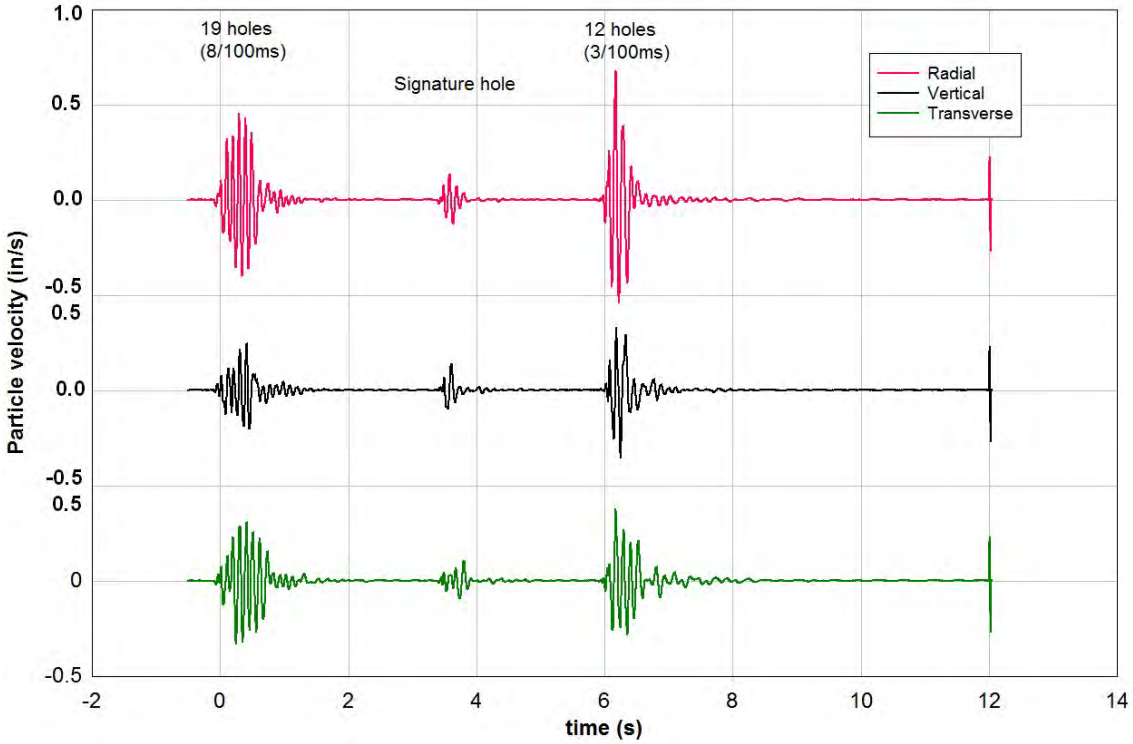

Figure 68 Vibration record for test No.13, Ridge seismograph (approx. 836ft from source)

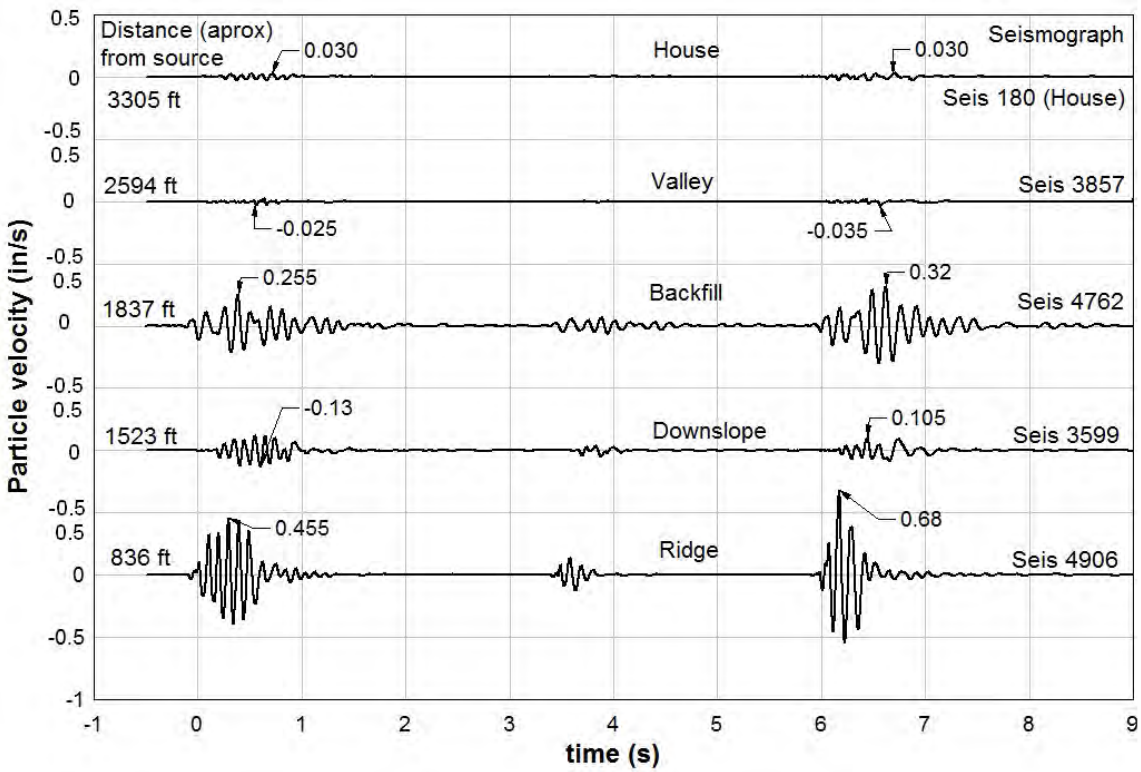

Figure 69 Radial vibration components for test No.13 and all the seismographs in summer 2011

In Figure 69, the Downslope seismograph is closer than the Backfill seismograph. Vibration levels are lower for the closest seismograph. This situation is likely due to the topographic influence on blast vibrations, or the change in elevation between the source and the monitoring point. Ridge seismograph, Backfill seismograph and the source are more or less at the same elevation (1825ft) when compared to the Downslope seismograph that is approximately 300ft below the source of the blast vibration (1500ft). The different behavior could be a consequence of different particular site conditions of the places where the seismographs were installed. The Backfill seismograph was placed in a reclaimed backfill and thus was not buried in undisturbed soil. This is evidenced by the low frequency components of the waveform that are common with thick unconsolidated soils.

The difference between the two timing arrangements reflected in the values of the peak particle velocity is more evident for seismographs close to the explosion source. This fact emerges when the peak values between the two sets of blasted holes (19 holes and then 12 holes) are compared. However, as in the case of downslope seismograph 3599 the first sequence gives peak particle velocity values higher than the second sequence, indicating again a high dependence of the specific site conditions. For seismographs farther than 2500ft, in this specific test, there is little or no difference between the peak values from both timing sequences (8ms and 3ms between holes).

When signature signals are isolated from the complete record, it can be seen that it is not possible to assess, in this case, a signature for the points located at 2594ft (Valley seismograph) and 3305ft (House seismograph) away from the source. In those cases, it is not possible to use the signature hole technique because no signature is available to calculate a prediction using this methodology.

Appendix B includes the vibration records for six 2011 tests included in Table 10.

Test No. 13 was used to calibrate and validate the **Silva-Lusk modified signature hole technique** with the Ridge, downslope and backfill seismographs. After calibration and verification of the reliability of the technique, the model was then used to analyze different timing sequences. Model validation and timing analysis is described in the following sections.

4.1 Signature hole technique calibration, test No.13

4.1.1 Ridge seismograph (North)

Using the modified signature hole methodology, the predicted values for the first set of holes blasted using 8ms are included in Figure 70 and Figure 71.

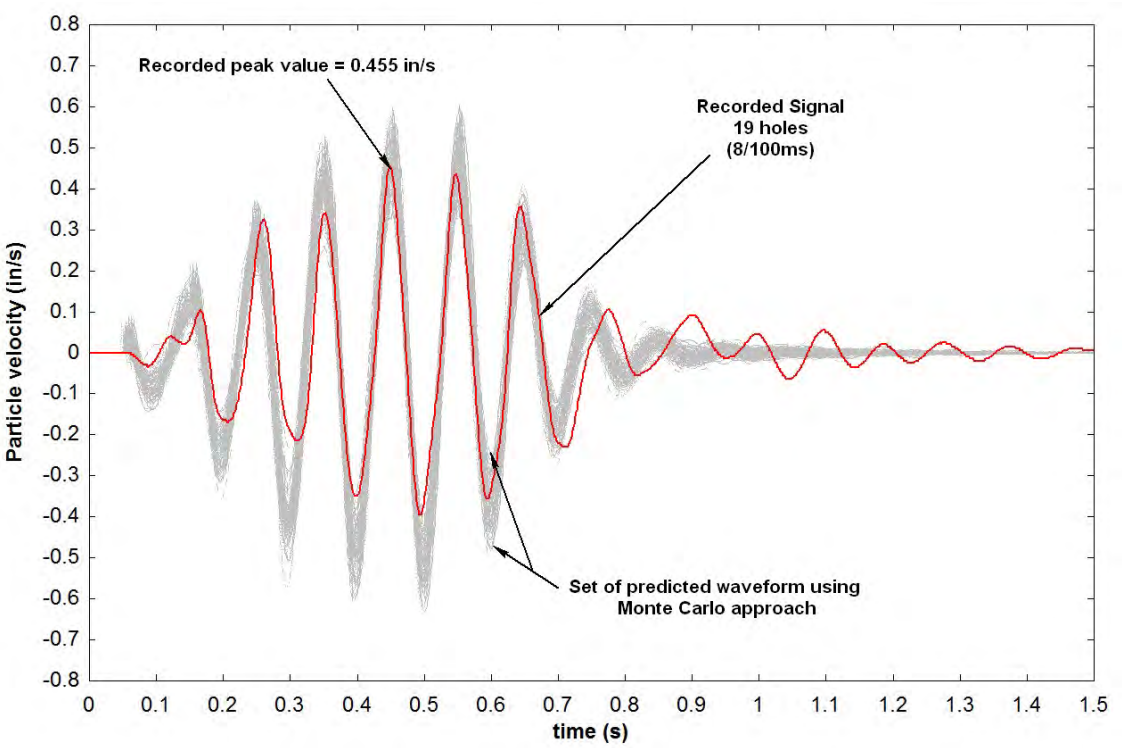

Figure 70 Waveform envelop using Silva-Lusk modified signature hole technique vs recorded signal Test 13, ridge seismograph (19 holes).

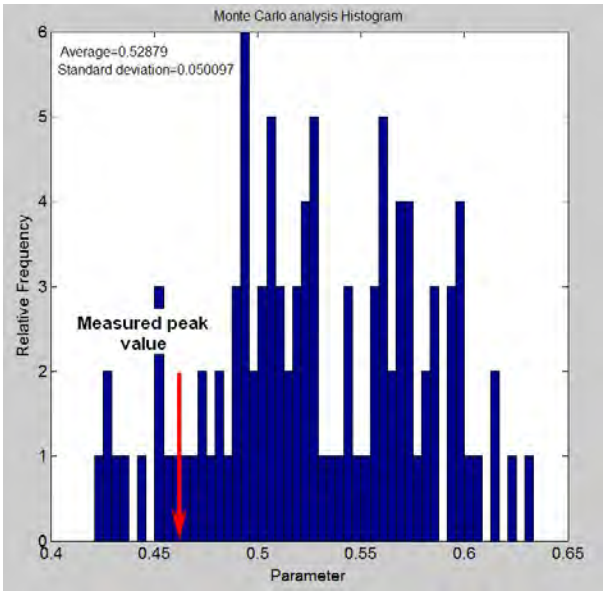

Figure 71 Monte Carlo analysis histogram predicted results test No.13, ridge seismograph (19 holes)

Figure 70 and Figure 71 show a good correspondence between the results of the developed methodology and the recorded signal in test No. 13. The average predicted value is 0.529in/s with a standard deviation of 0.05 (Figure 71). When those values are compared against the recorded peak value (0.455in/s), it can be concluded that using the developed methodology the recorded peak value falls at 1.5 standard deviations of the predicted mean value.

Using the same methodology, the second set of holes was modeled and the results are included in Figure 72 and Figure 73.

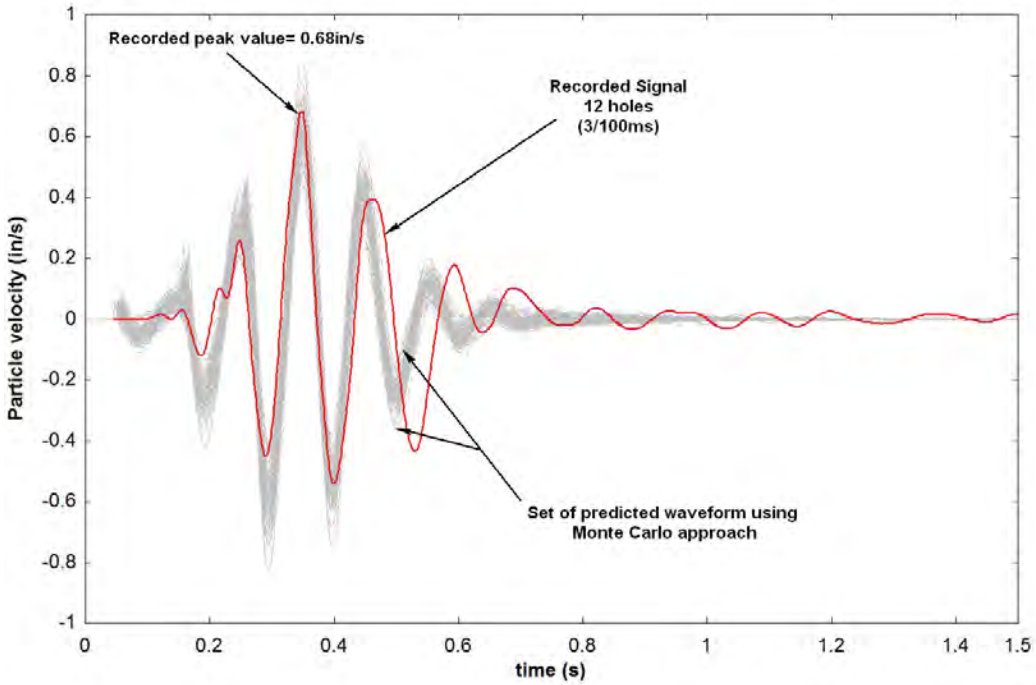

Figure 72 Waveform envelop using Silva-Lusk modified signature hole technique vs recorded signal Test 13, ridge seismograph (12 holes)

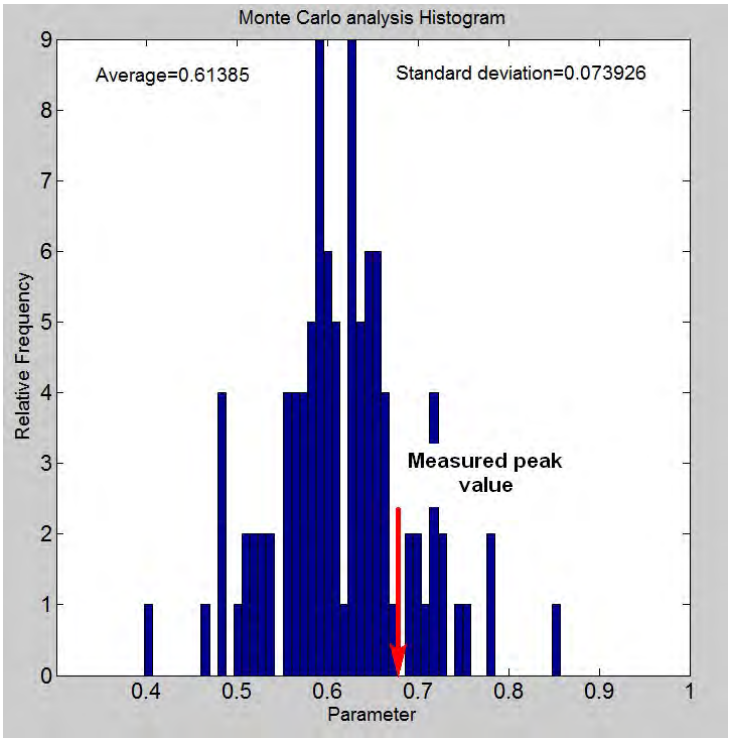

Figure 73 Monte Carlo analysis histogram predicted results test No.13, ridge seismograph (12 holes)

For the ridge seismograph and the second set of detonated holes (12 holes), the model was successful in predicting wave shape and peak particle velocity. The histogram in Figure 73 shows a possible range of velocities between ~ 0.4 in/s and 0.85 in/s. This information is useful because it would allow a mine operator to understand the possibility of a particle velocity reaching almost 0.9 inches per second with this type of layout and timing for the second set of detonated holes. The measured value was 0.68 in/s for this particular seismograph, but the histogram provides confidence in design to keep particle velocities below 0.85 in/s (three standard deviations). If 0.85 in/s would not be acceptable, design changes would be necessary to shift the histogram lower.

4.1.2 Downslope seismograph (East)

For downslope seismograph and the first set of 19 holes, the comparison between the actual recorded signal and the envelope of simulated signals is included in Figure 74. The greater spread in waveform shapes when compared to the simulations shown in Figures 70 and 72 can be partially attributed to the greater distance from the blast to the Downslope

seismograph. The deviations used in the model to allow for random fluctuations in wave velocity and phase are amplified with distance.

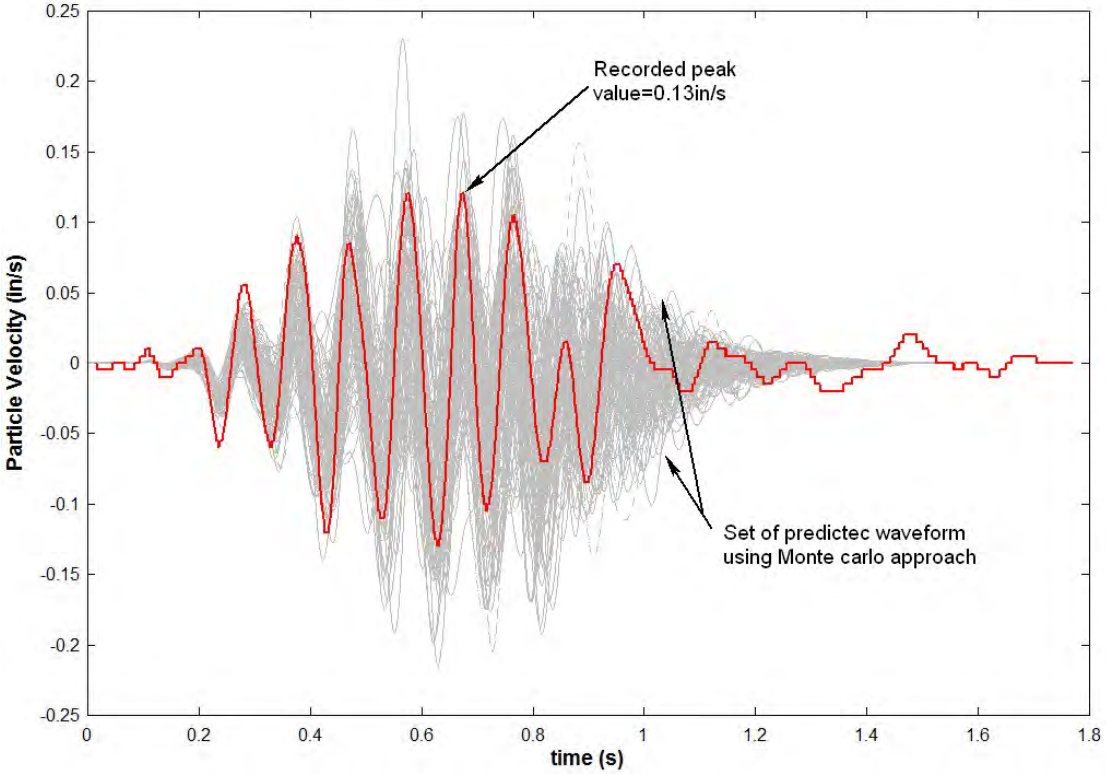

Figure 74 Waveform envelop using Silva-Lusk modified signature hole technique vs recorded signal Test 13, downslope seismograph (19 holes)

The histogram of the peak values is included in Figure 75.

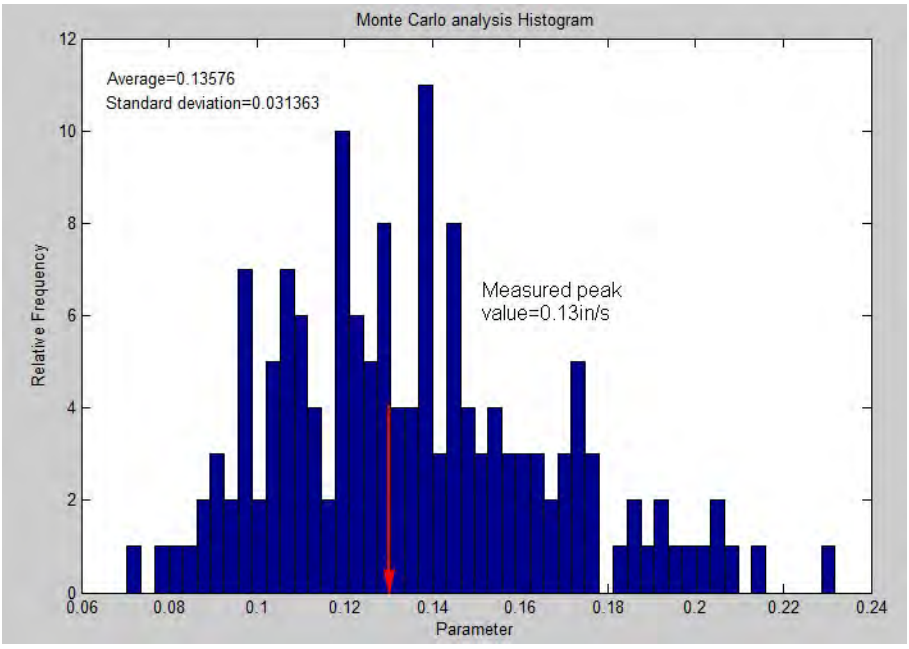

Figure 75 Monte Carlo analysis histogram predicted results test No.13, downslope seismograph (19 holes)

For this seismograph, the histogram shows a possible range of velocities between 0.08 in/s and 0.22 in/s. The average value is 0.135 in/s and the measured peak was 0.13in/s.

4.1.3 Backfill seismograph (South)

Figure 76 includes the envelop using modified signature versus the actual reading for backfill seismograph. The greater variance in waveforms can again be attributed to the greater distance when compared to the ridge seismograph simulations. Other factors may have also contributed; however, distance is the most likely reason.

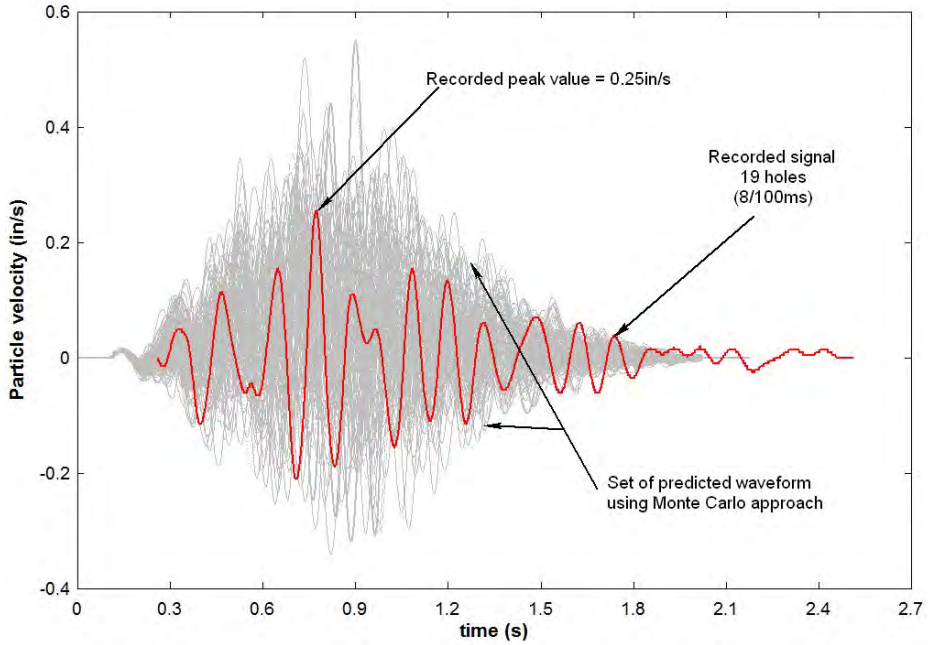

Figure 76 Waveform envelop using Silva-Lusk modified signature hole technique vs recorded signal Test 13, backfill seismograph (19 holes)

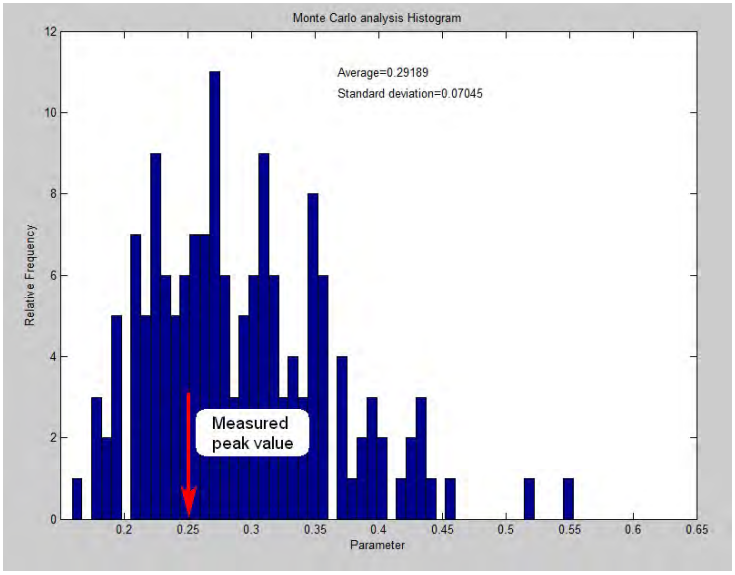

Figure 77 Monte Carlo analysis histogram predicted results test No.13, backfill seismograph (19 holes)

In this case, for this seismograph, the histogram shows a possible range of velocities between 0.10 in/s and 0.45 in/s. The average value is 0.29 in/s and the measured peak was 0.25in/s.

4.1.4 Findings

All previous models mimic conditions often experienced in the mining field. Blasting may proceed for extended periods of time without excessive vibration measurements. In some cases, higher particle velocities are measured unexpectedly when no design or timing changes are made. The histograms for the three seismographs have the ability to predict this behavior.

Several important conclusions can be deducted from the previous results:

- Silva-Lusk Modified signature hole technique (using Monte Carlo approach) is an accurate tool to simulate blast vibrations at sites where a signature waveform is available.
- The predicted particle velocity amplitude from the Silva-Lusk Modified signature hole technique can be presented as a histogram. The average value in the histogram could be termed as the prediction. In each case, the measured value varied slightly from the average predicted value, but generally falls within 2 standard deviations of the average.
- The Monte Carlo produced histogram provides the ability to determine highest expected particle velocity. With this information, mine operators can be confident that designs would not produce particle velocities beyond the distribution of the histogram. For example, as shown in Figure 73, the modeled layout and timing would not produce particle velocities beyond approximately 0.85 in/s at the ridge, 0.23 in/s at the downslope and 0.55 in/s at the backfill.
- The ability to create accurate predictions is still dependent upon the ability to collect signature hole information at the monitoring point of interest and in approximately the same distance and direction as the blast for which prediction is needed. Several other researchers are also working on the ability to transfer signature hole information by location and distance, but this concept is new and under development.

4.1.5 Frequency content for test No.13

In this particular test, two different initiation timing scenarios were used. As mentioned before, the first set of holes (19) were detonated using a timing of 8/100ms and the second set was detonated using a set of 3/100ms. Power spectra of the signal was used to analyze the characteristics of the waveforms in frequency domain. Power spectra allows for understanding how the strength of a signal is distributed in the frequency domain.

By definition, the energy of a signal contained in the frequency range $[\omega_1, \omega_2]$, with $\omega_1 < \omega_2$, is given by: (Signal and Systems page 141).

$$E = \frac{1}{2\pi}\int_{\omega_1}^{\omega_2} |X(\omega)|^2 d\omega$$

Equation 20

Where:
E= power spectra
$X(\omega)$: is the CT Fourier transform of $x(t)$
$x(t)$: signal

The following figures show the power spectra for test No. 13 at the different locations (ridge, downslope and backfill).

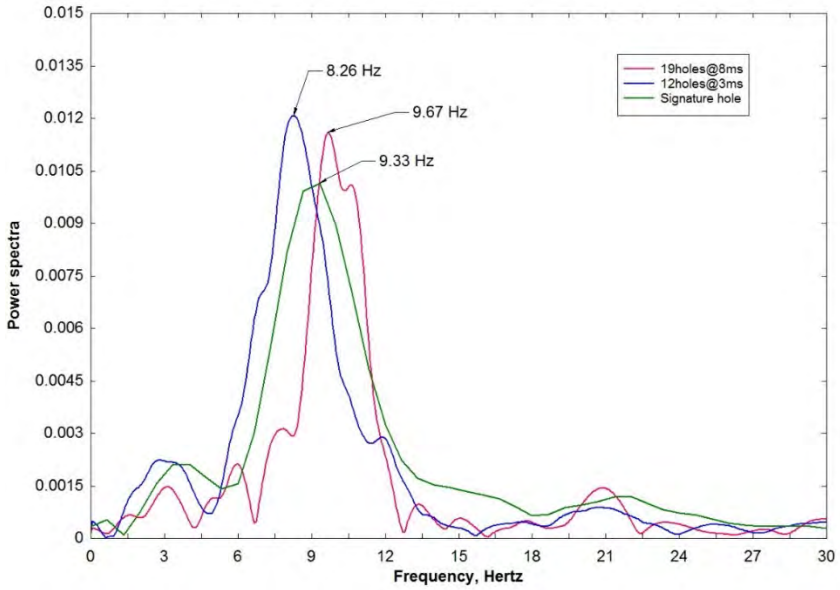

Figure 78 Power spectra of the signals, test No. 13, ridge seismograph

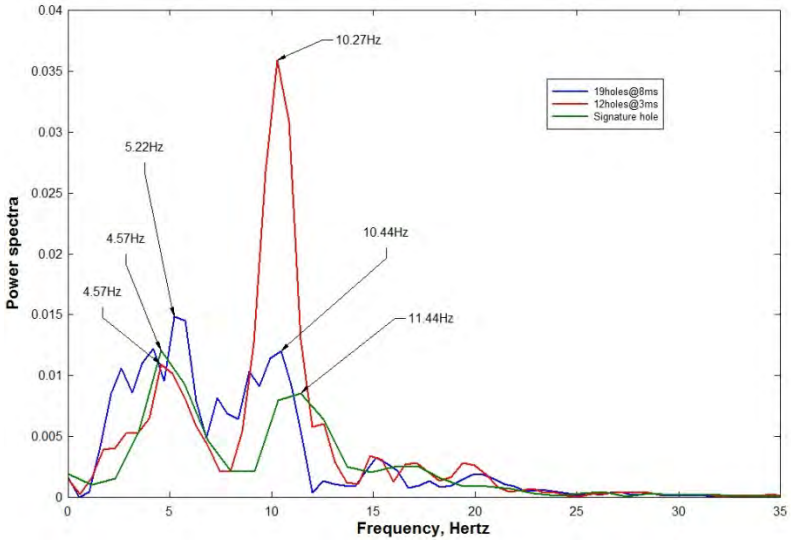

Figure 79 Power spectra of the signals, test No. 13, downslope seismograph

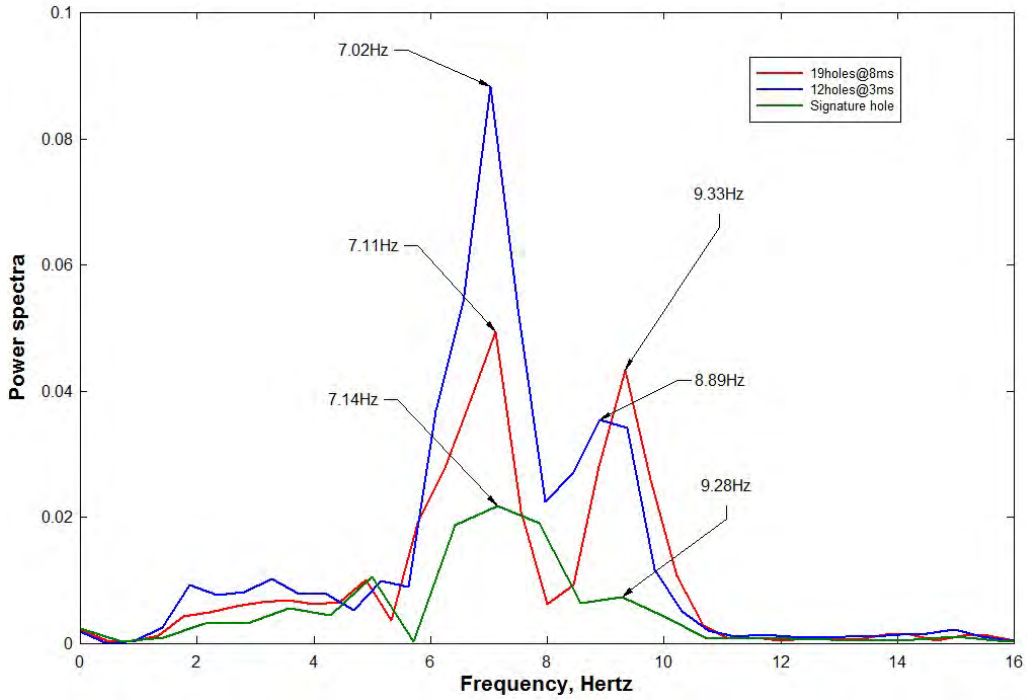

Figure 80 Power spectra of the signals test No. 13 backfill seismograph

Field results are not conclusive about the control of the frequency through initiation timing, however some conclusions can be deducted when Figure 78 to Figure 80 are analyzed:

- The general shape of the frequency content of the signature signal (green line in previous figures) is similar to the shape of the signals for 19 and 12 holes. In other words, the frequency content of the signature waveform is similar to the frequency content of the blast signal waveform for 19 or 12 blast holes.
- Contrary to common belief, the change in timing sequence in a mine blast doesn't change the frequency content of the produced waveform.
- The timing in a mining blast event determines which of the frequencies becomes the main frequency for a produced waveform. In other words, the frequency content of the signal is the same for a single detonated hole (signature waveform) but according to the timing used in the blast one of the frequencies becomes the dominant frequency for the production waveform.
- Underground mines below the ridge unit and thick soils under the backfill unit appear to affect ground vibration frequencies and support the conclusions of USBM RI 9078.

This topic is discussed later in more detail using different models and the Silva-Lusk modified signature hole technique.

4.2 Study of different timing scenarios using modified signature hole technique.

Having confidence in the methodology through field validation, several timing scenarios were studied using the model. The sequence comprised by the last 12 holes in test No. 13 was chosen to study the different results when there are variations in initiation time for ridge No. 4906 (836ft), backfill No. 4762 (1837ft) and downslope No. 3599 (1523ft) seismographs. In order to compare the modeled results against the field result, sequence of detonation was held constant. Variation in the time between holes and the time between rows was incorporated into the model.

4.2.1 Ridge seismograph

Results of peak particle velocity for different timing configurations are presented in Table 11 and Figure 81.

Table 11 Simulation results using different timing configurations (Mean Peak particle velocity) ridge seismograph 4906 (836ft)

	Row time (ms)					
Hole to hole time (ms)	3	8	17	25	42	100
3	0.580	0.480	0.336	0.269	0.340	0.613
8	0.233	0.217	0.258	0.310	0.380	0.288
17	0.190	0.187	0.178	0.165	0.198	0.173
25	0.159	0.156	0.140	0.146	0.158	0.152
42	0.1536	0.147	0.1439	0.140	**0.133**	0.139
50	0.145	0.152	0.139	0.135	0.138	0.141
100	0.210	0.200	0.200	0.199	0.192	0.198

Figure 81 shows (as expected) that keeping delay timing between rows constant, the peak particle velocity is higher while shorter delay timing between holes are used.

Also it is possible to see in this particular test that for any given time between rows, changing the time between holes after 20ms has little effect on peak particle velocity. In other words, a timing configuration of 100/42 will produce similar or equal peak particle velocity to a 100/25 configuration. This is likely because waveform interaction becomes important for delays below 20ms. This time (20ms) is certainly related to the response characteristics of this specific site and the geometry and characteristics of the blast (hole size, depth, burden, spacing, etc.) for ridge seismograph location.

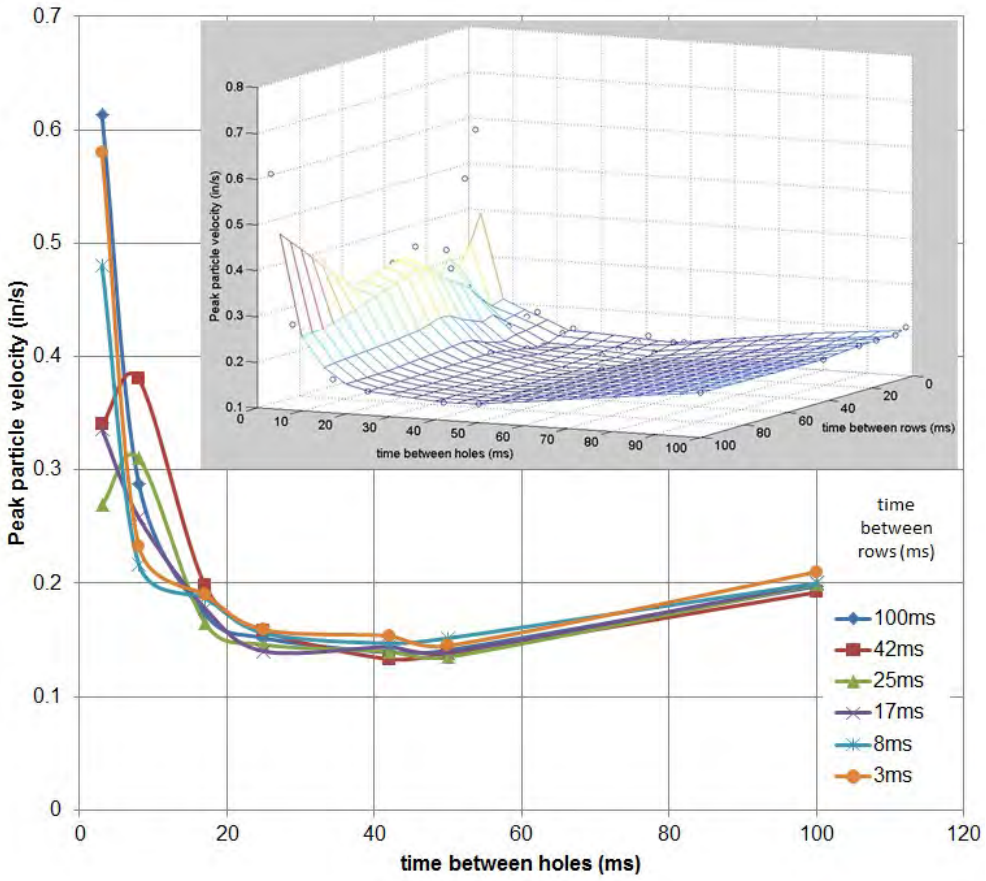

Figure 81 Simulation of timing configuration for 12 holes test No. 13 peak particle velocity seis 4906 (ridge seismograph)

In order to analyze the effect of the initiation timing in the frequency content of the production waveform, the average of the waveforms after applying Monte Carlo approach was used. Figure 82 shows the Monte Carlo result, the average waveform, and its comparison against the measured waveform in test No.13 for 12 holes.

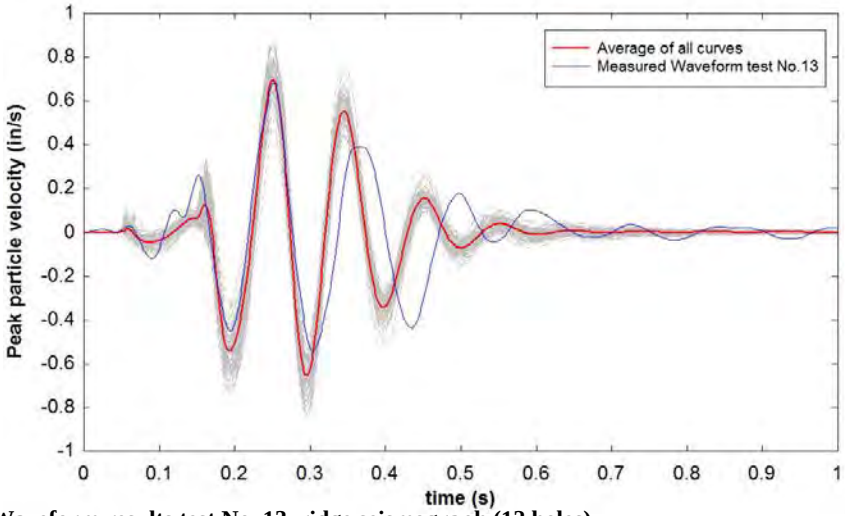

Figure 82 Waveform results test No. 13, ridge seismograph (12 holes)

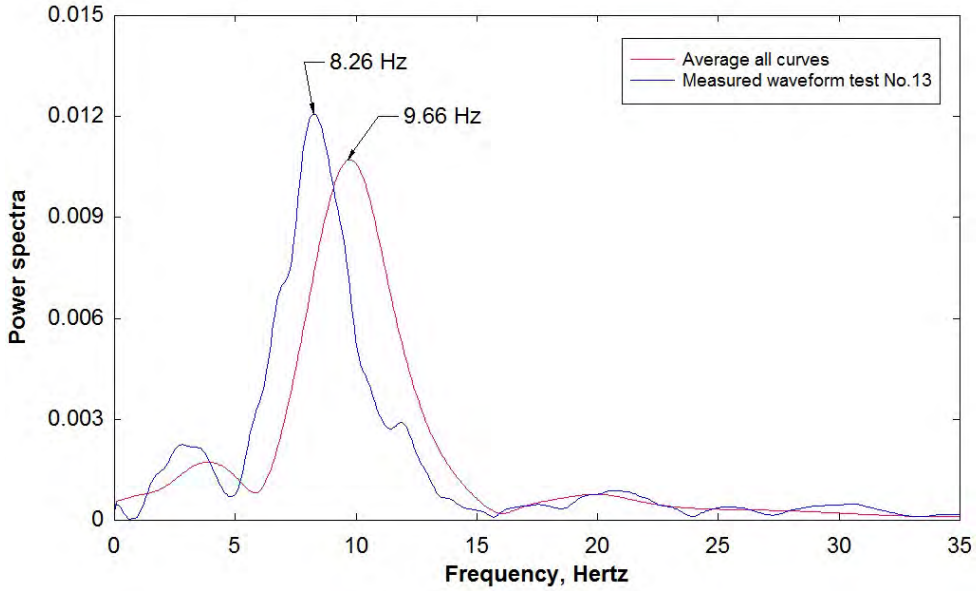

Figure 83 Frequency content comparison average all curves vs measured waveform test No. 13, ridge seismograph (12 holes)

Table 12 was created using different initiation timing configurations as indicated in Figure 83.

Table 12 Simulation results using different timing configurations (Frequency)

	Row time (ms)					
Hole to hole time (ms)	3	8	17	25	42	100
3	9.66	9.52	9.19	8.99	10.19	9.66
8	8.12	10.99	10.39	10.05	9.86	8.46
17	8.39	8.26	7.99	7.79	9.86	8.92
25	9.12	8.79	8.52	10.39	9.46	9.39
42	9.59	9.52	9.32	8.99	8.52	9.86
50	9.93	9.72	9.52	10.99	10.32	9.92
100	9.99	9.86	9.72	9.66	9.46	9.99

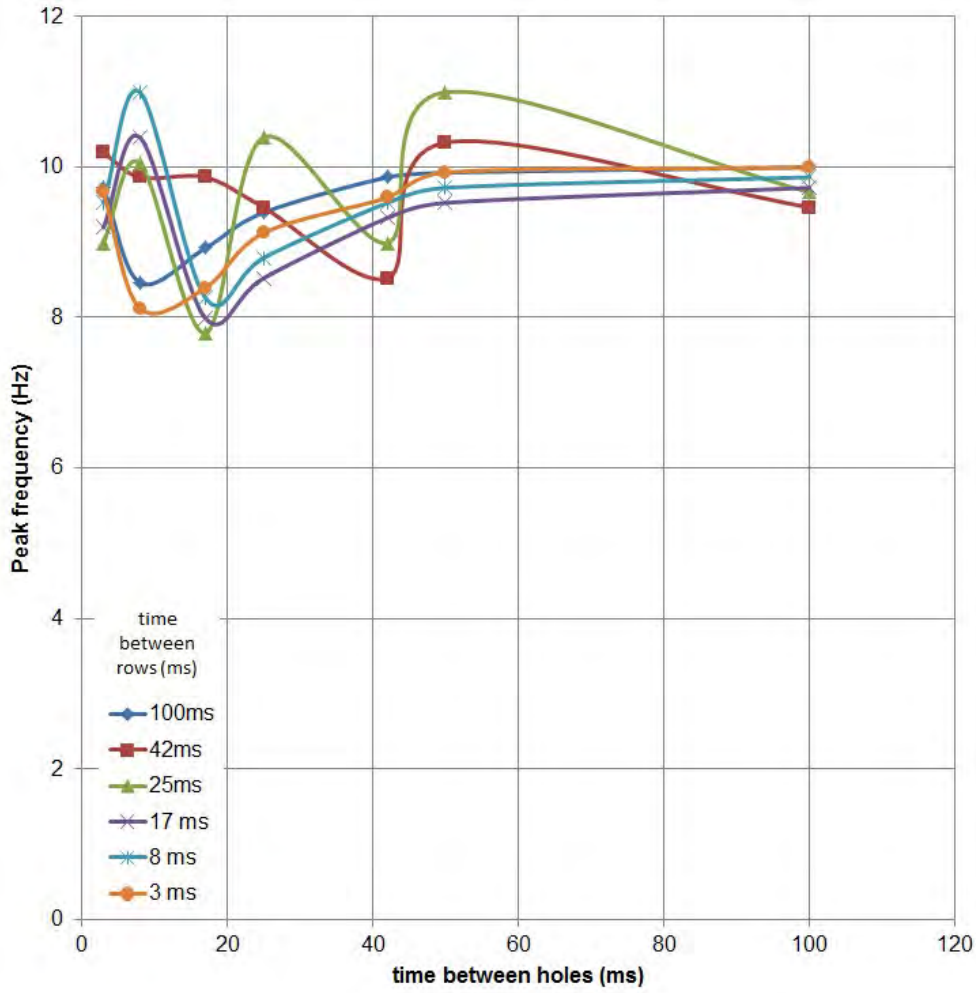

Figure 84 Frequency Simulation of timing configuration for test No. 13 12 holes

When Figure 84 is analyzed, there is not a clear tendency regarding the main frequency of the signal and its relationship with hole timing. In other words for this test, there is no influence of the initiation timing in the frequency content of the production vibration waveform signal when different initiation timing is used. Based on analysis of test No. 13, ridge seismograph and 12 detonated holes, it is not possible to control the frequency content of the produced vibration waveform signal through the manipulation of the initiation timing.

This finding is consistent with the results observed in Figure 78. In that figure, the range between the maximum main frequency (9.67Hz for 19 holes @8ms) and the minimum frequency (8.26Hz for 12 holes @3ms) is less than 2 Hz.

Figure 85 shows the frequency content of the average signal for different timing between holes while keeping the timing between rows at 100ms (last column Table 12) for ridge seismograph and 12 holes.

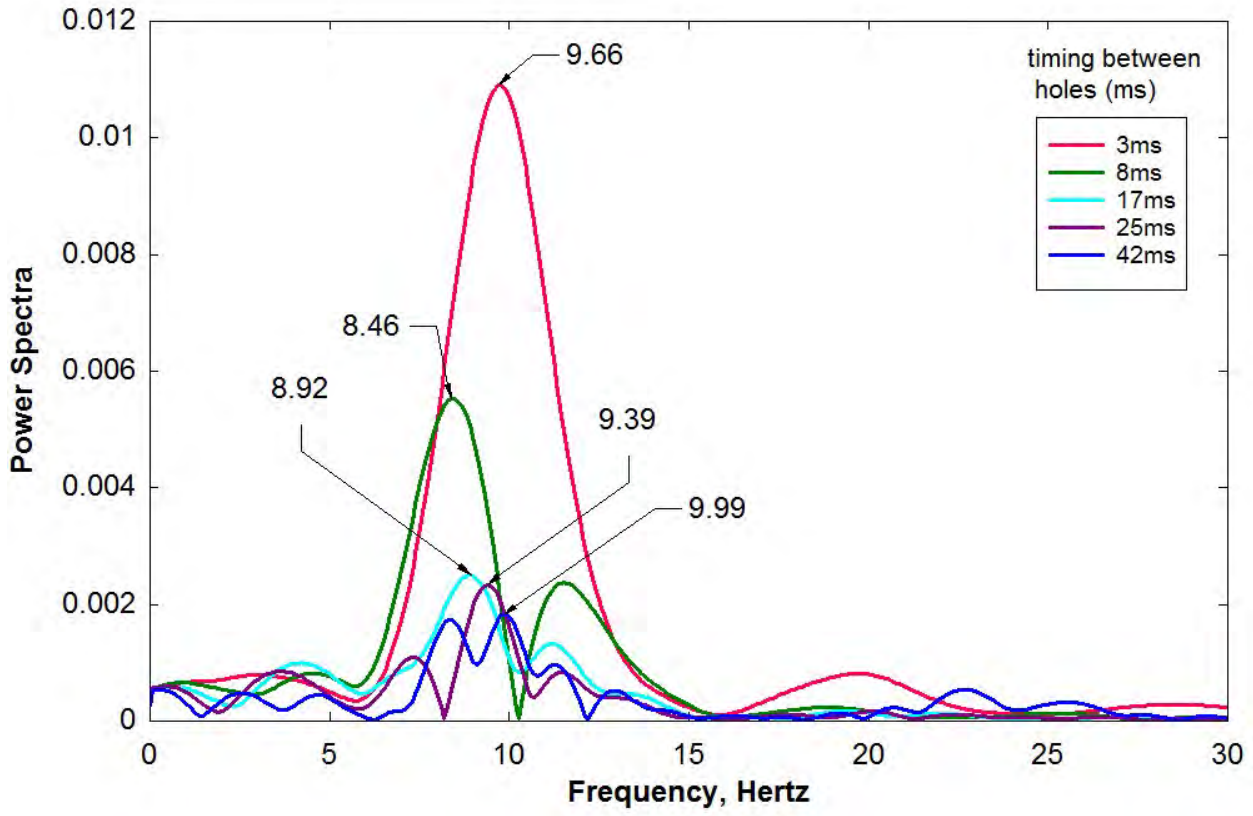

Figure 85 Spectrum vs frequency for 100ms between rows and different timing between holes test No. 13, 19 holes.

Figure 85 shows that for different configuration timing the main frequency ranges between 8 and 10 Hz, in other words for this particular test (12 holes and ridge seismograph) configuration timing doesn't change substantially the main frequency.

Now if the concept of the total energy of a signal is introduced (the energy carried by the signal) and given by:

$$E = \int_{-\infty}^{\infty} |x(t)|^2 dt$$

Equation 21

If this concept is applied to the signals used to produce the power spectra of Figure 85, it will be possible to see the effect of the initiation timing in the vibration energy that reaches the seismograph in the ridge for the 12 holes. Using this concept, Figure 86 was produced.

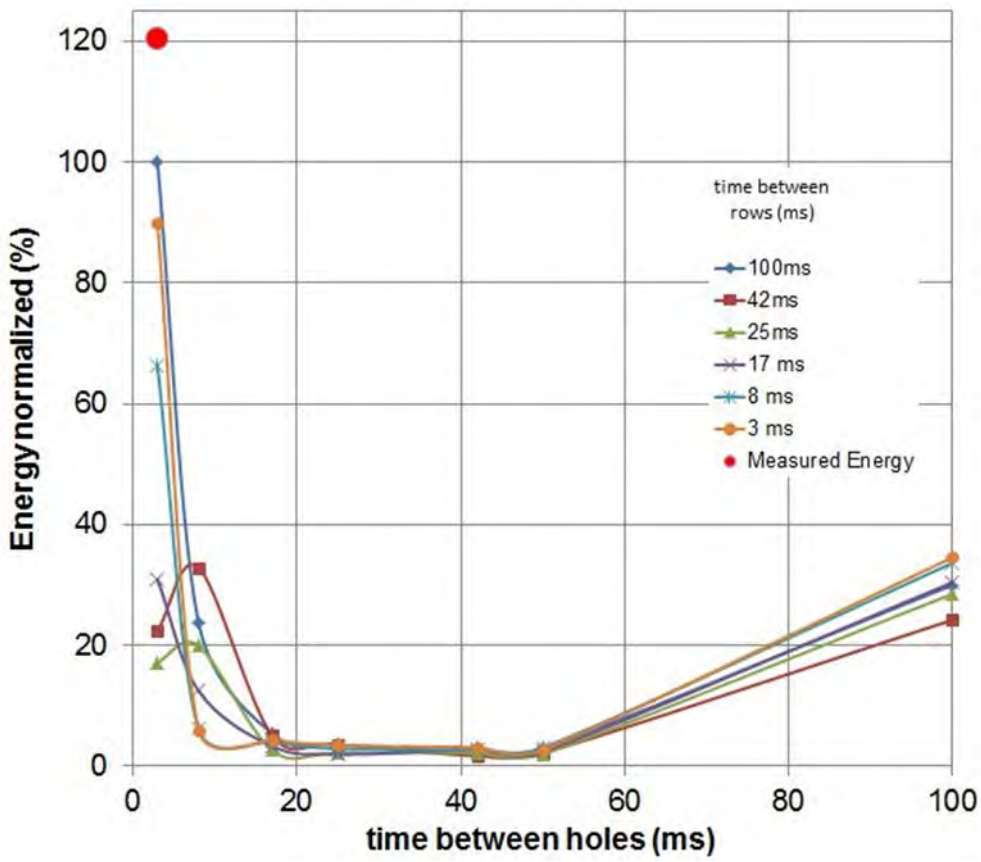

Figure 86 Total energy of the signals for simulation of test No .13

The energy value for a simulated timing configuration of 100ms between rows and 3ms between holes was chosen to normalize the energy of the other simulations. Using this timing configuration, the maximum energy value was obtained for the simulations. However, the energy measured in the test was 21% higher than the simulated; this is the explanation of the location of the red dot at 120% in Figure 86.

Figure 86 shows for this particular case how an interval between 17ms and 50ms (hole to hole) results in similar energy arriving at the monitoring point (ridge seismograph) regardless of timing configuration between rows or between holes. Finally and as expected, Figure 81 and Figure 86 keep a similar shape or tendency. The reason for this similar behavior is that levels of peak particle velocity are related directly to the energy that reaches some specific point in a blast vibration waveform.

Finally, two extreme scenarios were analyzed using the modeling tool. One scenario where the delay between holes was 1ms and the other where the delay between holes was chosen to avoid any wave interference (the total length of the signature was 500ms) so the delay used between holes was approximately 600ms. In both cases according to test No. 13 for 12 holes, 100ms where used between rows. Figure 87 is the Silva Lusk modified signature hole technique for 1 and 600 ms and Figure 88 is the power spectra for the two waveforms.

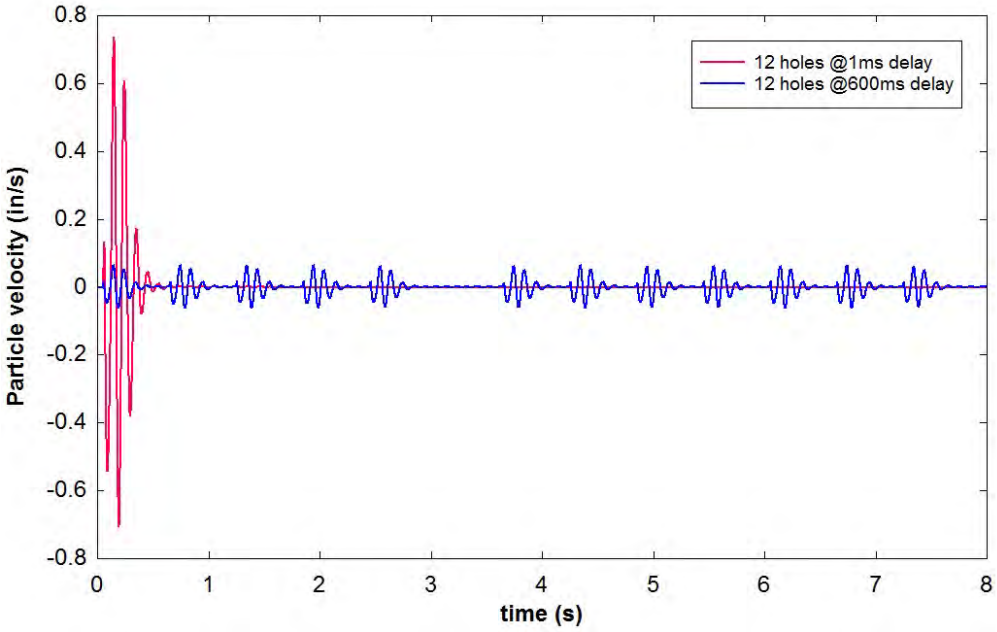

Figure 87 Extreme scenarios analyzed, 1ms and 600ms delay base on test No. 13, 12 holes (time domain)

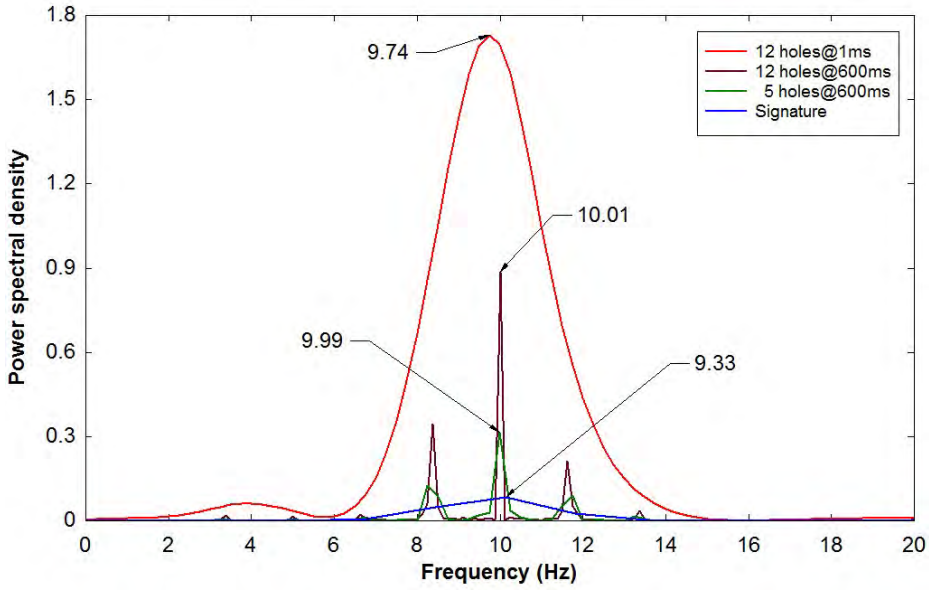

Figure 88 Extreme scenarios analyzed, 1ms and 600ms delay base on test No. 13 (frequency domain)

Some interesting conclusions can be drawn from Figure 87 and Figure 88. Most importantly the main frequency does not change when different initiation timing configurations are used; however, the changes in the energy content of the signals are very sensitive to the timing.

4.2.2 Backfill seismograph

Similar analyses were performed for the backfill seismograph 4762 (1837ft), test No. 13, 12 holes. This was performed to see if the trend of Figure 81 is similar for a seismograph in

unconsolidated material (backfill material). Results of peak particle velocity for different timing configurations are presented in Table 13 and Figure 89.

Table 13 Simulation results using different timing configurations (Mean Peak particle velocity) Backfill seismograph 4762 (1837ft)

	Row time (ms)					
Hole to hole time (ms)	3	8	17	25	42	100
3	0.429	0.418	0.396	0.368	0.290	0.25
8	0.376	0.367	0.348	0.315	0.257	0.242
17	0.287	0.279	0.267	0.241	0.229	0.206
25	0.229	0.243	0.215	0.224	0.203	0.197
42	0.207	0.206	0.193	0.198	0.197	0.195
50	0.199	0.203	0.196	0.190	0.192	0.188
100	0.183	0.182	0.187	0.184	0.182	**0.173**

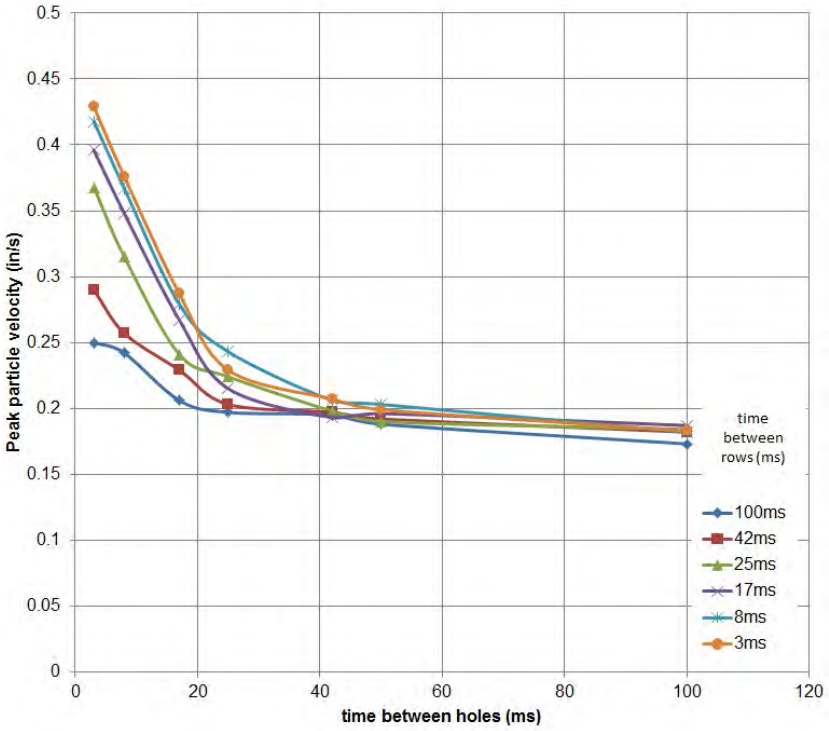

Figure 89 Simulation of timing configuration for 12 holes test No. 13 peak particle velocity Backfill seismograph.

4.2.3 Downslope seismograph

Analyses were performed for the downslope seismograph 3599 (1523ft), test No. 13, 12 holes. Results of peak particle velocity for different timing configurations are presented in Table 14 and Figure 90.

Table 14 Simulation results using different timing configurations (Mean Peak particle velocity) Downslope seismograph 3599 (1523ft)

	Row time (ms)					
Hole to hole time (ms)	3	8	17	25	42	100
3	0.17	0.14	0.11	0.10	0.11	0.11
8	0.09	0.09	0.08	0.08	0.08	0.07
17	0.07	0.06	0.06	0.06	0.06	0.07
25	0.06	0.06	0.06	0.06	0.05	0.06
42	0.05	0.05	0.05	0.05	0.05	0.05
50	0.06	0.06	0.06	0.05	0.05	0.05
100	0.06	0.06	0.05	0.05	0.05	0.05

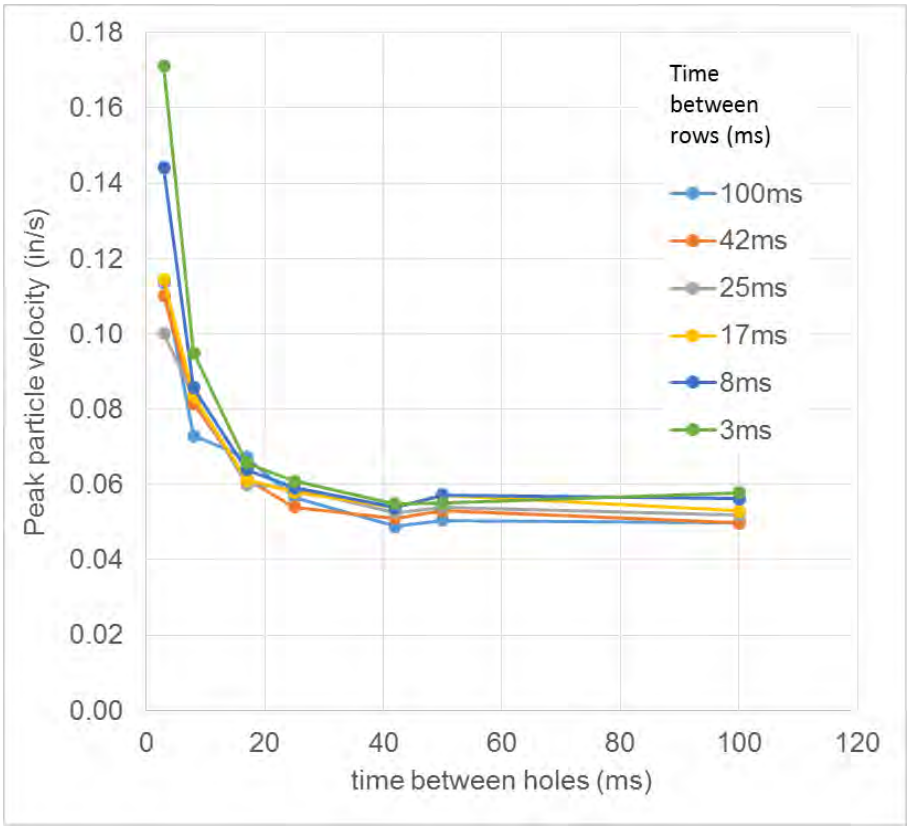

Figure 90 Simulation of timing configuration for 12 holes test No. 13 peak particle velocity Downslope seismograph.

Figure 91 is obtained when the trend of Figures 81, 89 and 90 (Ridge, backfill and downslope seismographs) are compared.

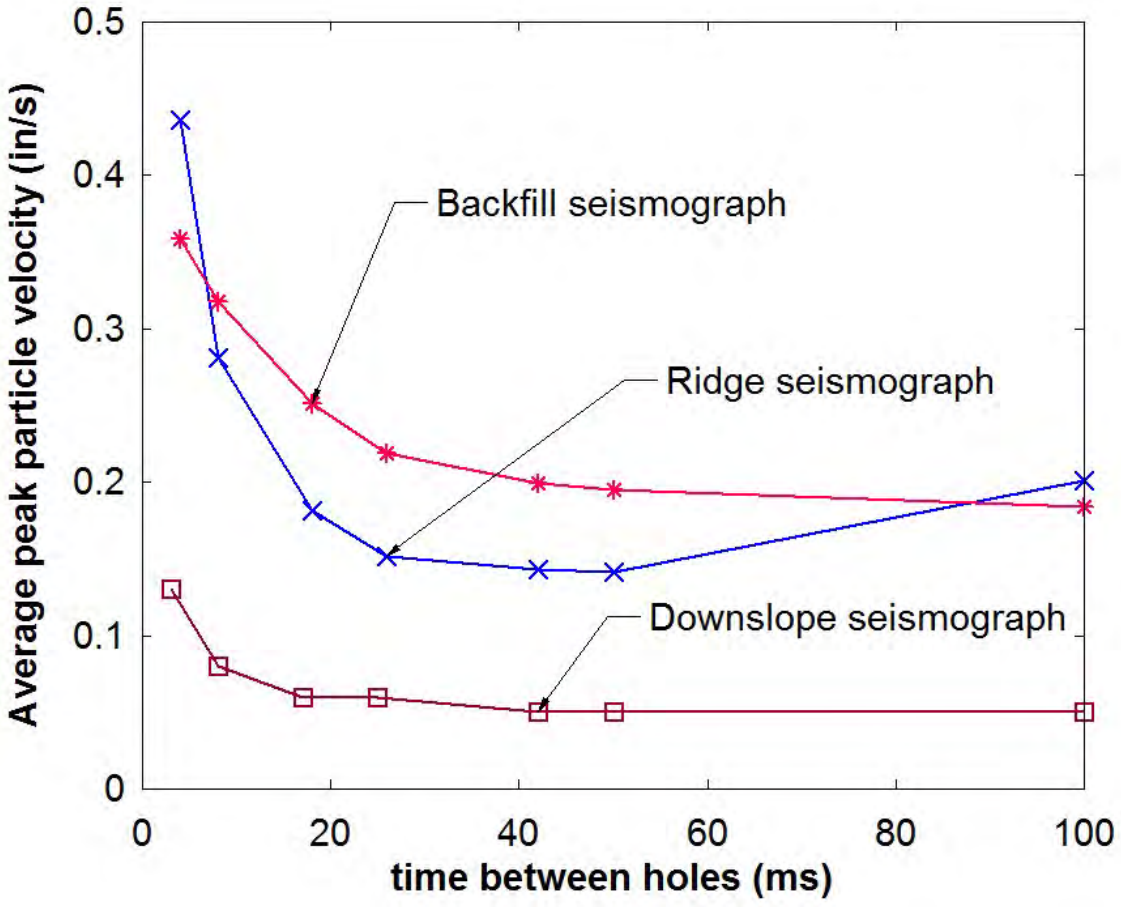

Figure 91 Timing trend behavior comparison between ridge, backfill and downslope eismographs

According to Figure 91, to control vibrations levels in a mine blast, the initiation timing of the blast is more crucial in the ridge than for the backfill and downslope places. This is represented by the high slope of the curve for ridge curve when compared to backfill and downslope curves (slope of the curves in the interval 0 and 20 millisecond). The general trend for the three places of vibration measurement is the same; high particle velocity when lower delays are used. For all three locations, there is an optimum delay that produces low vibration levels (point of maximum curvature). While the backfill seismograph was located at a greater distance than the other two, the difference in behavior exhibited in Figure 91 cannot be attributed only to differences in distance nor solely to the type of material in which the geophone was placed. It is likely a combination of both factors.

A discussion about the definition of a delay is presented next according to the findings in the current research study.

4.3 Definition of Delay: Optimum Delay Times

In order to define what a delay in a production blast is, several outcomes are needed to be addressed. In a mining blast the outcomes are; vibrations, airblast, fragmentation, rock movement, and efficiency of the blast. The main variable measured under the current research was the ground vibration. The following discussion about what a delay is comes from the point of view of the vibration generated as a consequence of a mining blast.

Tests No. 10 and 12 are examples of why the delay between rows and the delay between holes are important. Figure 92 shows the plan layout for both tests.

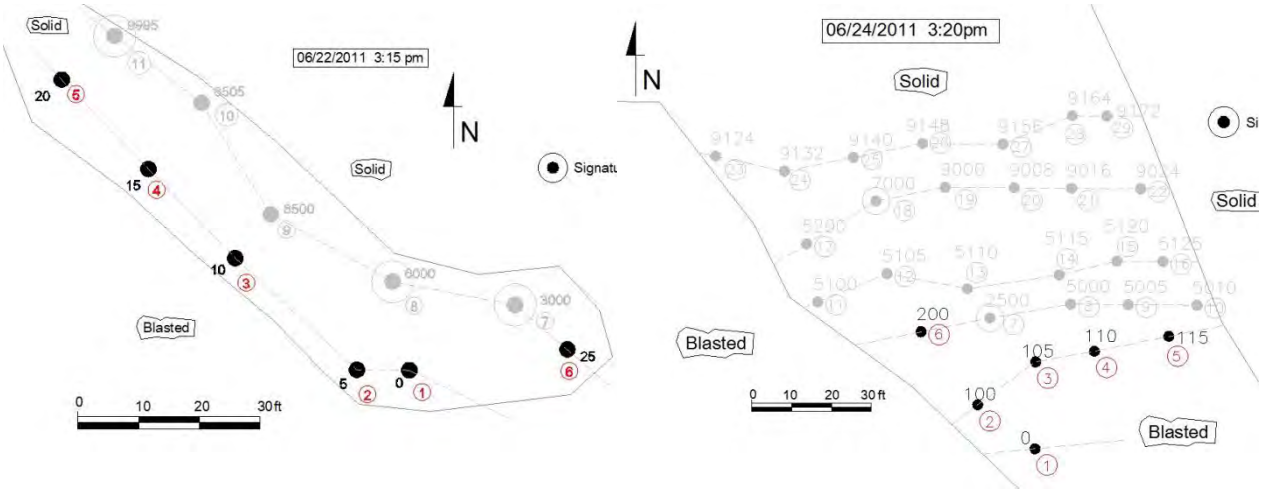

a) Test No. 10 b) Test No. 12

Figure 92 Plan layout Tests No. 10 and 12.

In both tests, six holes were detonated with similar geometrical characteristics and similar load per hole. The primary differences between both tests were the distance from the blast to the seismograph and the timing used. For the ridge seismograph, the centroid of test No. 10 was located at a distance of 976ft, while for test No. 12 it was at 792ft. Scaled distance for test No. 10 was 42ft/lb$^{1/2}$ while for test No. 12 was 27ft/lb$^{1/2}$. If both tests were performed at the same area, it is expected that constants a and b in the scaled distance equation to predict (forecast) vibration levels be the same. Thus, higher vibration levels are expected for test No. 12 than for test No. 10. Using the database collected, the scaled distance equation to assess vibration levels for a production blast in this particular area of the mine is given by (see Figure 48):

$$PPV = 19.51 * SD^{-1.25}$$

Equation 22

Based on the data set equation 22 is for delays of 8ms or greater. Table 14 summarizes the main parameters of test No. 10 and 12 regarding ground vibration based on 5 ms delay intervals.

Table 15 Parameters tests No.10 and 12

	Expl/5 ms delay (lb)	Expl/8 ms delay (lb)	Distance seis (ft)	SD, 5ms ($ft/lb^{1/2}$)	SD, 8 ms ($ft/lb^{1/2}$)	PPV Eqn 22, 5ms (in/s)	PPV Eqn 22, 8 ms (in/s)	PPV Ridge seis (in/s)
Test No.10	539	1078	976	42	30	0.182	0.28	0.82
Test No.12	837	1674	792	27	19	0.317	0.49	0.62

When the 8 ms scaled distance is used to estimate PPV for the 5 ms per delay shots, the results are under estimated compared to the measured values. The same is true for 8 ms intervals. This suggests that the measured PPV will be greater than the calculated using either delay

One of the main weaknesses of scaled distance or vibration prediction is that the sequence and initiation timing are not involved in the calculations. This research proves that timing and sequence have a large effect on the vibration levels.

As indicated in Figure 92, in both tests, the delay between holes was 5ms, however in test No. 10 there was no delay between rows (it was 5ms in series), while in test No.12 a delay of 100ms between rows was used. The radial component for those six holes in both tests is included in Figure 93.

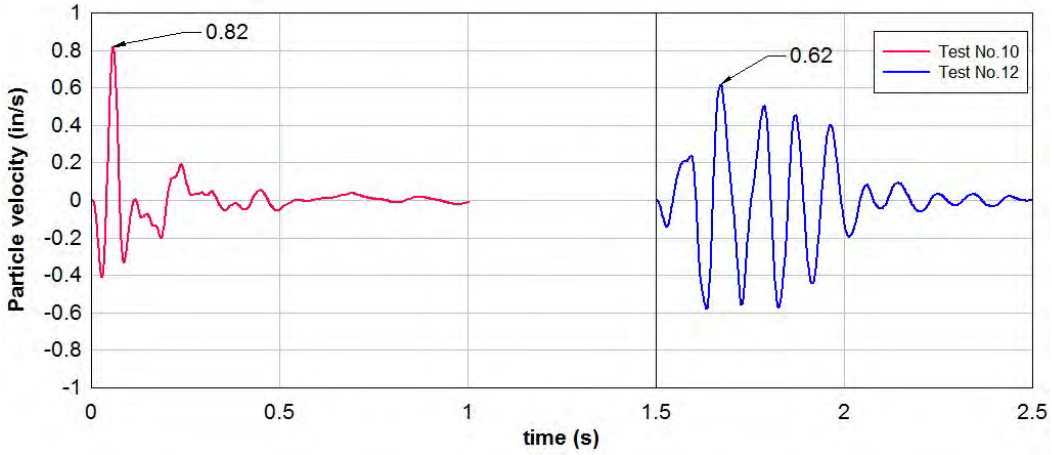

Figure 93 Radial component tests No. 10 and No. 12, ridge seismograph

The influence of the timing in vibration production and in the peak particle velocity is evident when Figure 93 is analyzed. Maximum peak particle velocity occurs for test No. 10; however, the energy of the signal (calculated using Equation 21) is bigger in the case of test No. 12. This is evident when the power spectra of the signals are compared in Figure 94.

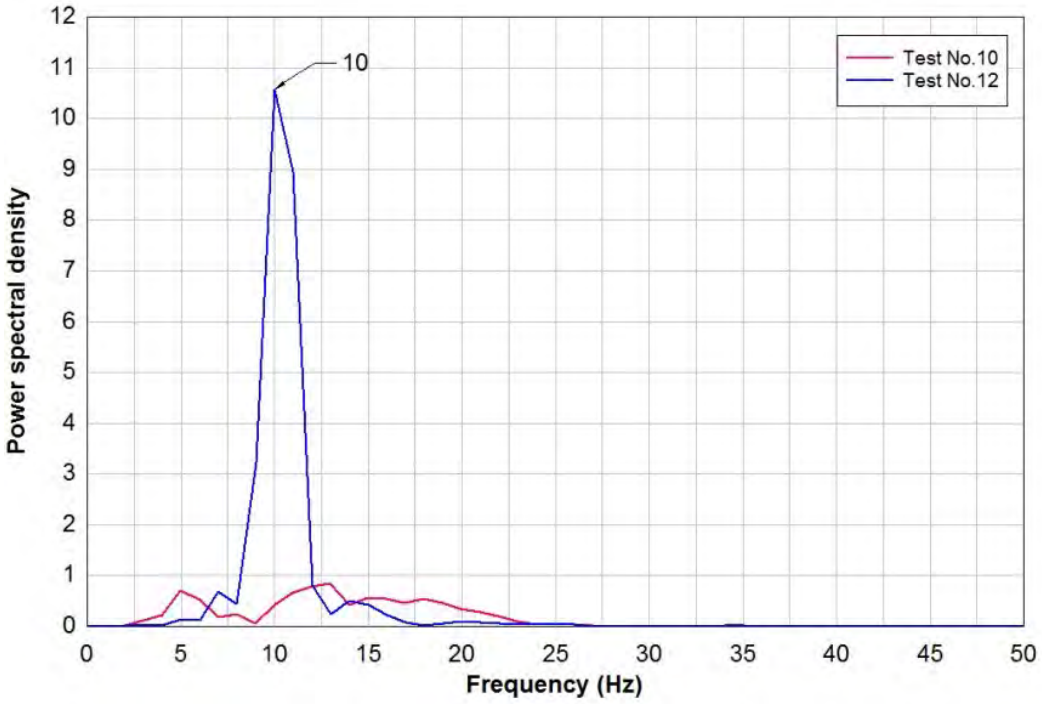

Figure 94 Power spectral density for tests No. 10 and 12, ridge seismograph.

When test No. 10 and 12 are compared in the frequency domain, the difference between them regarding the main frequency is less than 3 Hz.

Considering Figures 78, 79, and 80, the natural frequency of the ground strongly influences the vibration frequency of the production blast. For each case, dominant frequency is almost the same independent of timing. When power spectra density is analyzed in Figure 94, the main change in the spectrum is related to the distribution of the energy around the main frequency. The timing is affecting vibration amplitude at the monitoring location more than changing or controlling the main frequency of vibration event. When peak particle velocity and timing is analyzed, there is a range of optimum timing configurations within which the reduction in peak particle velocity values is negligible with respect to the changes in the delay timing. In other words, rather than one specific delay configuration, there is a range of delays that would produce similar results. This provides for a target area in which timings can be adjusted to optimize fragmentation and other productivity and cost based metrics. The concept is illustrated in Figure 95.

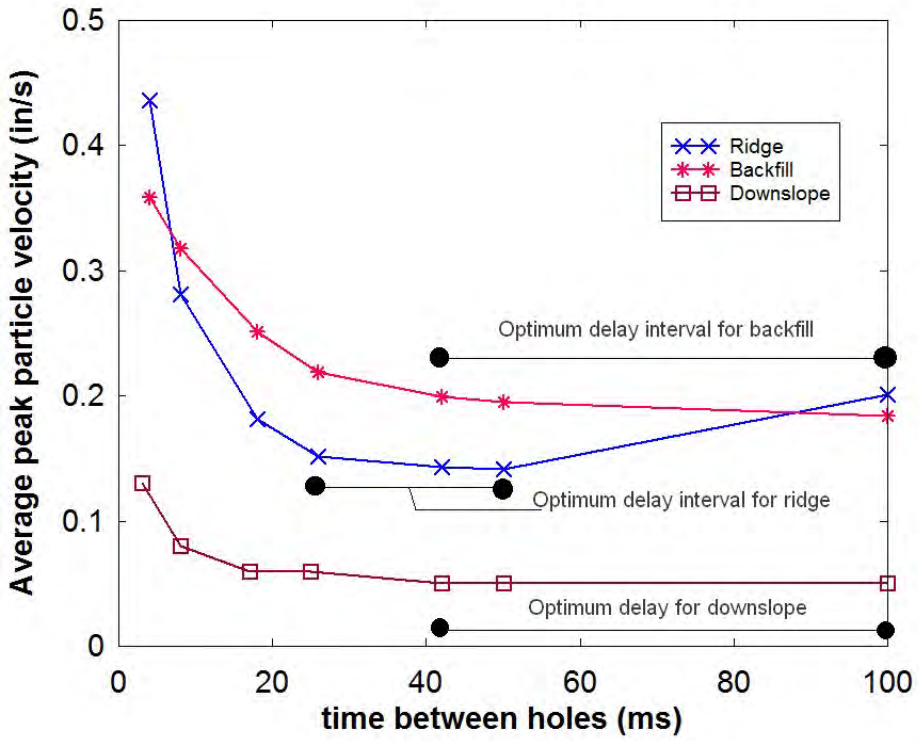

Figure 95 Concept of optimum delay interval for ridge, backfill and downslope (different locations)

The optimum delay interval is site specific and depends on the vibration characteristics of the monitoring location. The optimum delay interval for minimizing peak particle velocity is different for low velocity (unconsolidated or backfill and downslope) and high velocity (consolidated or ridge) sites.

In order to answer the question of what is a delay, from the ground vibration point of view, several aspects need to be address:

- Distance from the monitoring point to the production blast and different materials at the monitoring point affect the optimum delay timing of a production blast.
- Changes in main frequency of vibration. It is difficult to change the main frequency of ground vibration at a specific point through the change in the sequence of initiation. In other words, the main frequency of vibration remains almost constant or in a narrow range of frequencies for different combinations of initiation delays at the same point. This can be explained if it is considered that the characteristics of the vibration at a specific place depends on the dynamic properties of the place where the vibration takes place more than the dynamic properties of the place where the blast is generated.
- Tools to assess vibration levels. It is clear that through the application of the usage of scaled distance methodology and the implicit 8ms minimum delay

between charges it is impossible to study different timing combinations. It is necessary to migrate to another technique such as the Silva-Lusk Modified Signature Hole Technique proposed in this document. Other probabilistic methods are under development as well within the blast vibration research community. Through the use of these tools it is possible to establish a timing configuration with optimum delay intervals to minimize the ground vibrations.

Considering these aspects for a given blasthole geometry (one blasthole) and quantity of explosive detonated at the same time, an optimum delay can be defined as a timing configuration and blasthole sequence giving the minimum possible ground vibration levels for a specific monitoring point. The optimum configuration will distribute the energy around the main vibration frequency (avoiding energy concentrations around a main value) and it is expected that the vibration energy will be in lower ranges when compared to other timing configurations. At this site for the ridge, downslope, and backfill seismograph locations, 42 ms delays between holes in a row are optimum.

4.4 Direct Comparison Case Study

The practical consequence of the dependence of vibration levels with timing is related to near and far measurements. If only distance is analyzed (independent of the type of material were the vibration measurement is taking place), at a close monitoring point, electronic detonators are recommended. For a monitoring point far from the blast source, it was observed that the delay accuracy is not the major variable that controls vibration levels. In other words, similar levels of vibrations are expected from electronic or non-electric detonator systems for events far from the source. The previous statement is illustrated using tests No. 14 and 15. The plan view diagrams for each of these blasts is included in Figure 96.

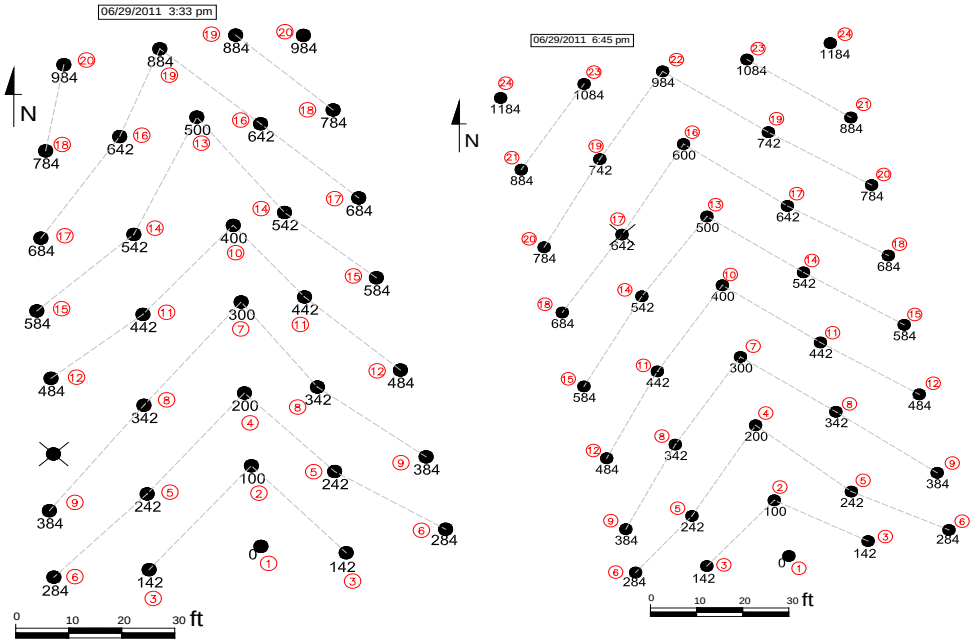

a) Test No. 14 b) Test No. 15

Figure 96 Plan layout tests No. 14 (pyrotechnic) and 15 (Electronic)

Tests No. 14 and 15 were adjacent blasts, they differ only by four holes (34 holes test No. 14 and 38 holes test No. 15). In both tests, the same nominal initiation sequence was used (delay timing was used based on 42 and 100ms delays). Assuming that the energy released by the four missing holes is not significant when compared to the entire blast, the electronic initiations system should lead to higher particle velocity values, because two holes are detonated at the same nominal time (142, 242, 342ms etc). This should be more critical for electronics than for pyrotechnics because lower scatter in electronics increases the likelihood of two holes detonating at the same time. The ridge vibration levels did reflect this prediction. However, for downslope and backfill this did not hold true. For example, seismograph 3599 (downslope) which is an average of 1440ft from the source, the complete vibration waveform, the peak particle velocity and the main frequency of the signals are almost the same for both tests, as shown in Figure 97 and 98.

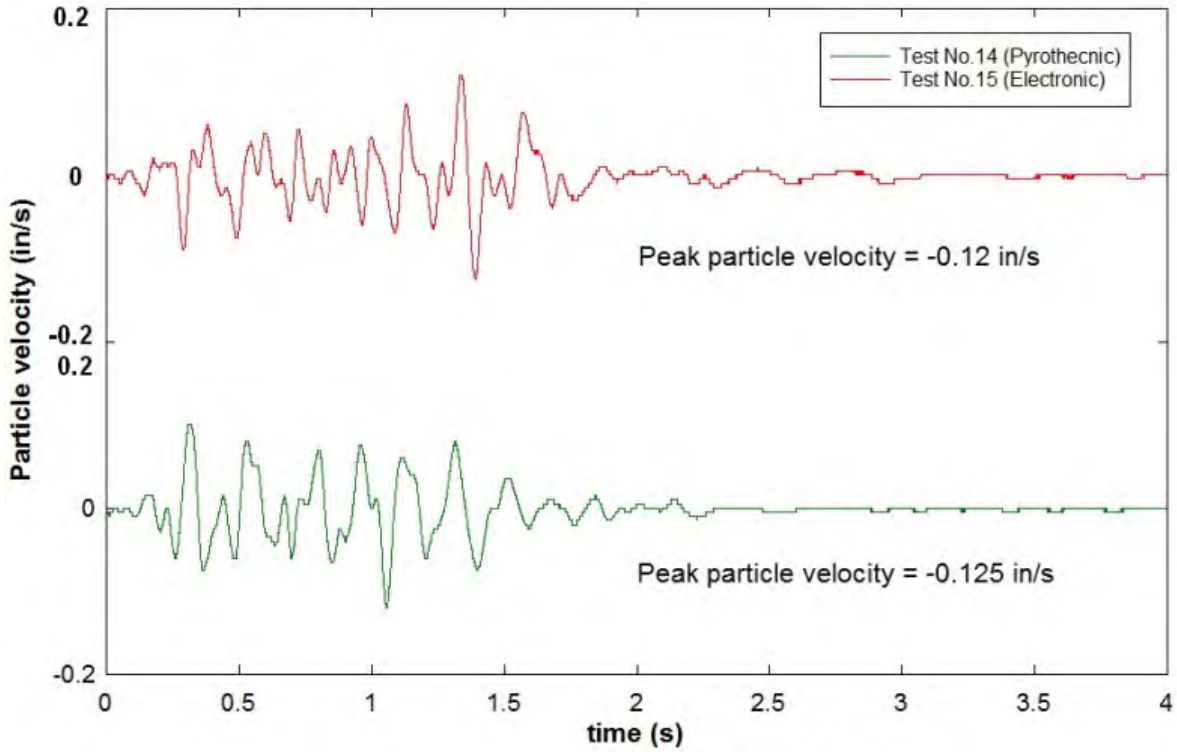

Figure 97 Waveform comparison test No. 14 vs test No. 15 transversal component (seismograph 3599) (downslope seismograph)

In this case, the difference in peak particle velocity is only 0.05in/s. Figure 98 shows that the frequency content is very similar for each test as well.

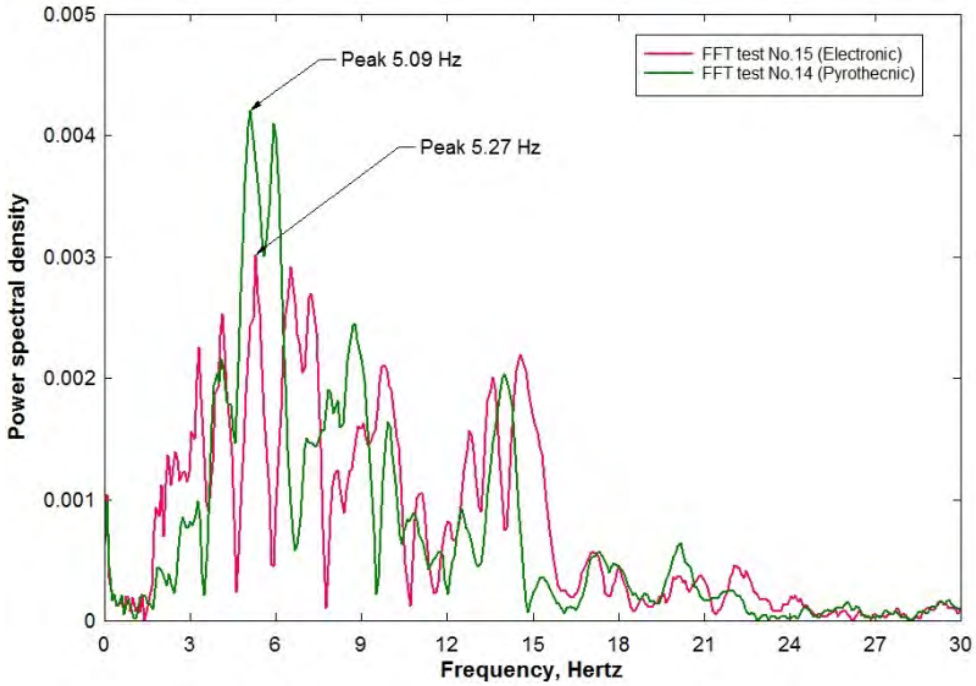

Figure 98 Frequency domain comparison test No. 14 vs test No. 15, seismograph 3599, (downslope seismograph)

Similar trends were observed for the other seismographs beyond 1440ft and downslope from the mine. The actual readings of the peak values for all the seismographs in test No. 14 and 15 are included in Table 15.

Table 16 Results test No.14 and No.15 particle velocity peak values (actual readings)

Seismograph	Distance Average (ft)	Test 14: PPV (in/s) Rad.	Test 15: PPV (in/s) Rad.	Test 14: PPV (in/s) Vert.	Test 15: PPV (in/s) Vert.	Test 14: PPV (in/s) Trans.	Test 15: PPV (in/s) Trans.
Ridge4906	711	0.365	0.820	0.235	0.600	0.450	0.600
Downslope3599	1440	0.115	0.120	0.095	0.095	0.120	0.125
Backfill4762	1946	0.175	0.175	0.095	0.095	0.105	0.120
Valley3857	2627	0.020	0.025	0.025	0.025	0.025	0.030
house180	3160	0.020	0.035	0.020	0.020	0.015	0.025

Note: Test 14: Pyrotechnic delay system
Test 15: Electronic delay system

When using "traditional" nominal delay timing (in this case 100 and 42ms) in this particular mine, there is no difference between electronic and non-electric initiation system regarding the peak particle velocity for seismographs beyond 1440ft (Table 15).

Similar results between the actual readings and the Silva-Lusk simulations were found at the downslope seismograph 3599 location (1440ft from the blast). When modeling, for test No. 14 (nonel), a Transverse peak particle velocity of 0.206 in/s and standard deviation of 0.035, compared to 0.206 in/s and standard deviation of 0.032 for test No. 15 (electronic).

In order to analyze if this result is explained based on the scatter introduced by the travel time of waves or due to the initiation timing system, a model including only the scatter of both initiation systems was used. In other words, the traveling time due to the distance (source – seismograph 3599) was not included in the calculations. Results are included in Figure 99.

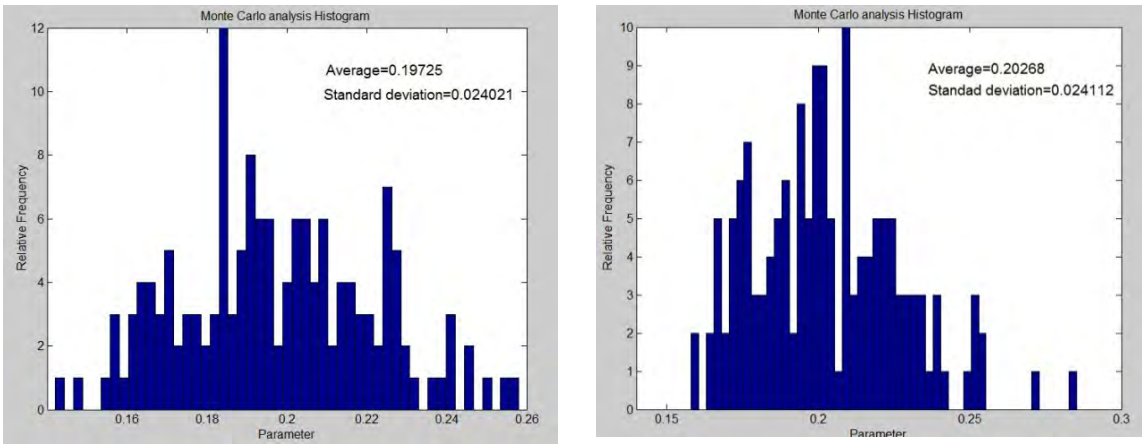

a) Pyrotechnic b) Electronic

Figure 99 Test No.15 simulating both initiation systems and including only time delay due to initiation sequence.

Figure 99 shows once again that in this case there is not a considerable difference for seismographs beyond 1440ft when pyrotechnic and electronic initiation systems are used. Other timing combinations for the location of downslope seismograph 3599 were analyzed in order to see any possible trend between nominal timing and the initiation system; the results are included in Table 16.

Table 17 Delay timing and initiation system simulation downslope seismograph

Timing	Electronic	Pyrotechnic
100/42ms	$\lvert\bar{v}\rvert = 0.20\,{}^{in}/_{s}$ $\sigma = 0.024$	$\lvert\bar{v}\rvert = 0.19\,{}^{in}/_{s}$ $\sigma = 0.024$
42/17ms	$\lvert\bar{v}\rvert = 0.20\,{}^{in}/_{s}$ $\sigma = 0.040$	$\lvert\bar{v}\rvert = 0.20\,{}^{in}/_{s}$ $\sigma = 0.040$
25/9ms	$\lvert\bar{v}\rvert = 0.25\,{}^{in}/_{s}$ $\sigma = 0.031$	$\lvert\bar{v}\rvert = 0.25\,{}^{in}/_{s}$ $\sigma = 0.034$
17/9ms	$\lvert\bar{v}\rvert = 0.38\,{}^{in}/_{s}$ $\sigma = 0.034$	$\lvert\bar{v}\rvert = 0.37\,{}^{in}/_{s}$ $\sigma = 0.040$
10/5ms	$\lvert\bar{v}\rvert = 0.60\,{}^{in}/_{s}$ $\sigma = 0.058$	$\lvert\bar{v}\rvert = 0.61\,{}^{in}/_{s}$ $\sigma = 0.055$

To create Table 16, the detonation sequence used in tests No. 14 and 15 were maintained (with two holes detonating at the same time). According to the results of Table 16, when using different nominal timing sequence there is no difference between electronic and pyrotechnic initiation system, however when lower delay timing is used an increase in the peak particle velocity is observed in the location of downslope seismograph 3599 (1440ft from blast).

To analyze the influence of the initiation sequence (the order how the holes are detonated) in the value of the peak particle velocity, the last timing scenario of Table 16 was modeled assuming an arrangement in series and using 5ms delay between holes. The result and the comparison between both arrangements is included in the next table:

Table 18 Sequence comparison for 5ms delay, downslope simulation

Timing	Echelon arrangement	Series arrangement
10/5ms	$\|\bar{v}\| = 0.60\ ^{in}/_{s}$ $\sigma = 0.058$	$\|\bar{v}\| = 0.32\ ^{in}/_{s}$ $\sigma = 0.045$

This result indicated that not only the delay between holes controls the amplitude of the generated peak particle velocity also the sequence is important in vibration produced by mining blast.

When ridge seismograph (No.4906) is analyzed, some important differences exist in peak particle velocity between tests No. 14 and 15. The difference in peak particle velocity generated by the two initiation systems is around 1.5 and 2.5 times for all components, always greater PPV values when electronic initiation system is used. A sample waveform from each blast is shown in Figure 100 and the peak values for other components are included in Table 15.

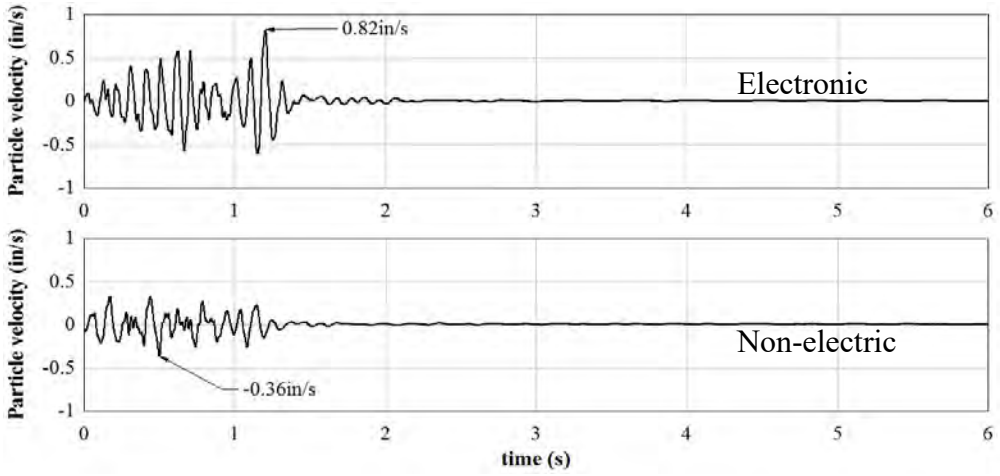

Figure 100 Influence of detonator type and timing for a close event, seismograph 4906, (ridge seismograph)

5. CONCLUSIONS

The current methodology used to assess blast vibrations from blasting (scaled distance) presents important disadvantages and inaccuracies.

- A reliable and extensive database is required to address site specific conditions
- Relies wholly on the record keeping capabilities of blasting personnel

- Theoretical and physical support of the equations is often weak.
- Actual delay times in a blast are not considered. Generally, the estimates are made on only the 8 ms rule. The scaled distance method provides no information about how different initiation timing affects the vibration levels.

The first disadvantage is related to the requirement of a confident and extensive database to calculate the site specific geological constants in the scaled distance equation. This fact makes this methodology impossible to apply for some areas at the mine if no vibration information was collected near the site where vibration levels are a concern. Even if the data are available, the records are mostly viewed as a regulatory compliance tool and can lack sufficient detail for research purposes. Another disadvantage is the weak theoretical and physical justification regarding the square root of the weight of explosive used in the scaled distance calculations Blair (2004). Scaled distance methodologies don't take into account the initiation sequence timing when vibration levels are calculated.

The emergence of electronic detonators as viable products for use in mine blasting has enabled blasting professionals to rethink the traditional blast design methodologies that pertain to timing.

This research determined the accuracy of two commercially available electronic detonators and non-electric shock tube systems. The study quantified the accuracy of two electronic and two non-electric systems during which 674 detonators were tested. Each system was tested at a low, medium, and high delay. Statistical models were then applied to quantify the scatter present in each system.

The two electronic initiation systems performed with considerably greater accuracy than non-electric detonators. No two adjacent delays should be less than 2ms apart when using Electronic Detonators A and short delay times, 1000ms and shorter, to ensure that there will be no overlap with 99% confidence. For delay times near the 8000ms time, no two adjacent delays should be less than 10ms apart.

When using Electronic Detonators B and short delay times, 1000ms and shorter, no two adjacent delays should be less than 1ms apart to ensure that there will be no overlap with 99% confidence. For longer delay times near the 8000ms time, no two adjacent delays should be less than 2ms apart. This allows blasters and engineers to be confident in the use of novel and nontraditional timing when using electronic detonators.

Figure 100 shows the normal distribution when electronic and non-electric initiation systems for Detonators A are compared for short delays (10 and 9ms).

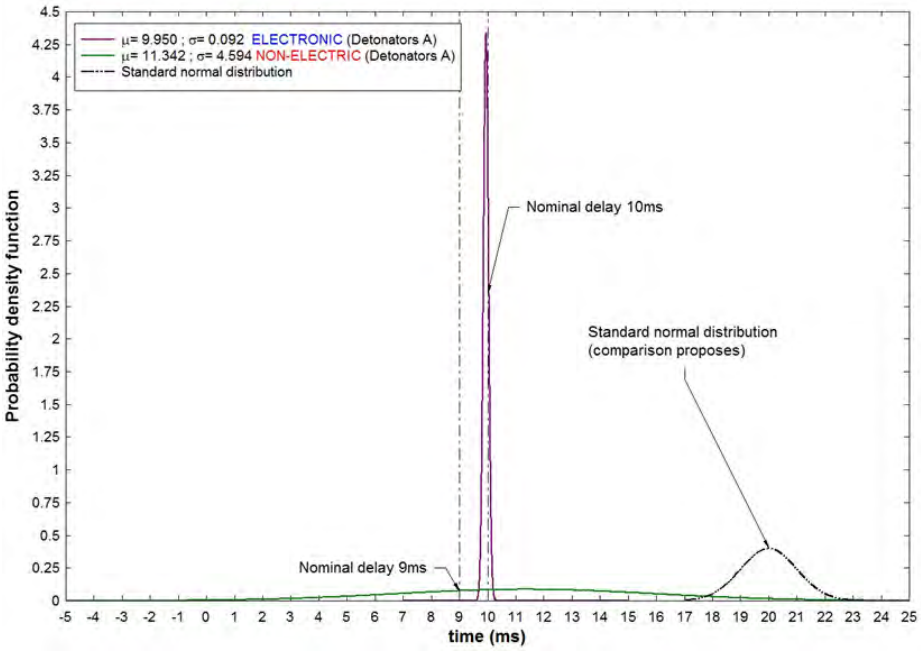

Figure 101 Comparison between electronic and non-electric initiation systems

Figure 100 shows the contrast in performance between the electronic and non-electric detonators. Timing flaws with the 9 ms non-electric detonators A were discovered originating from problems in accuracy, precision, or both. The accuracy of conventional pyrotechnic delay has however improved to some degree since Bajpayee's work in the 1980's. Although Bajpayee tested electric detonators and this study tested non-electric shocktube detonators both achieve a delay time through the burning of an internal pyrotechnic column.

Then building on the electronic detonator accuracy study, a new methodology based on the signature hole technique is introduced. Current signature hole techniques assume the invariability of the signature waveform hole to hole (linear superposition). While the invariability of the signature waveform can be true under some exceptional conditions, like a rock mass containing few or no joint systems and a massive rock layer, in general the geological conditions change. This can occur even between holes affecting the signature waveform that each hole generates. In this research, the a methodology was developed to modify the current signature hole technique based in a probabilistic approach. The methodology allows the change of the signatures hole to hole in a random fashion using Fourier series to generate different signatures for each hole. Through this mathematical tool variations in geology, geometry hole to hole, different explosives, contamination, change in the distance etc. are considered implicitly in the model.

The Silva-Lusk equation based on Fourier Series to introduce random behavior in the signatures hole to hole is given by:

$$f(t)i \approx \left[c_o + \sum_{n=1}^{m} ASF_n * \{A_n * \sin(2\pi * frequency_n * t + \emptyset_n)\} \right] * e^{+rise\ factor * t}_{-\ decay\ factor * t}$$

where:

$f(t)_i$:	synthetic signature waveform for hole (i)
ASF_n:	amplification scale factor for frequency n.
$\mathrm{c_o}$:	first term in the Fourier series
m:	number of frequencies chose to approach the measured signature waveform.
A_n:	amplitude coefficient for frequency n in the Fourier series
$\mathrm{frequency}_n$:	frequency value chose to approach the measured signature waveform.
t:	time
$\emptyset_n$:	phase for frequency n
decay factor:	factor related to the attenuation energy in that particular monitoring point.
rise factor:	factor related to the attenuation energy in that particular monitoring point.

The probabilistic methodology developed in this research using a Monte Carlo scheme, allows the design of the initiation timing in mining blasts. According to the initiation sequence and timing selected for different scenarios, using this methodology it is possible to predict or calculate vibration levels a location based on the signature of one hole with the same geometrical characteristics as the production holes.

The usage of signature holes recorded along with production holes is a practice that improves the quality of the results and confidence of the signature methodologies used in the assessment of vibration levels. This is because the signatures become more representatives of the geological conditions and the structural conditions of the rock mass where the explosions occur.

Based on field tests conducted in this research it can be concluded that the initiation timing and its influence on vibration levels is more important for some locations than others. This fact is commonly assumed by the blasting community, but in this research this situation was demonstrated. The data did not allow for determination of the more dominant contributing factor, but distance (near field vs far field) and site conditions at the monitoring point contributed to the differences identified during this project.

For a given quantity of explosive detonated at the same time, a delay can be defined as a timing configuration and detonation sequence giving the minimum possible ground vibrations levels for a specific monitoring point. Such configuration will distribute the energy around the main vibration frequency (avoiding energy concentrations around a main value) and it is expected that the vibration energy be in lower ranges when compared to other timing configurations. At this site, 42 ms was shown to provide minimized vibration levels. This is shown very well in Figure 95 for many conditions and locations.

The signature modified model, using Silva-Lusk equation can be used to predict vibration in many types of site conditions and different distances. This statement is supported by the model development for seismographs ridge, downslope and backfill.

Practical application of the results of this study will allow for better control of vibration at points of interest surrounding a blast site. In the beginning phases of blasting, site response characteristics can be assessed. During this process seed waveforms can be collected to allow for simulation of vibration results at key interest points such as homes, schools, or historic structures. The initial blasts can also provide real time data for model validation. After the modeling process has been completed, the results can be used to determine an optimum delay interval to be used for the duration of the project.

6. REFERENCES

Anderson, D. A. (2008). Signature Hole Blast Vibration Control- Twenty Years Hence and Beyond. The Journal od Explosives Engineers. September/Octuber., pp 6-14.

Blair, D.P., 1993, "Blast vibration control in the presence of delay scatter and random fluctuations between blastholes," International Journal for Numerical and Analytical Methods in Geomechanics, Vol. 17: pp 95–118, February.

Blair, D.P. (2004). Charge weight Scaling Laws and the Superposition of Blast Vibrations Waves. Fragblast Vol.8. No.4, pp. 221-239.

Bourbie, T., Coussy, O., Zinszner, B., (1987), Acoustics of Porous Media, Gulf Pub. Co.

Chi-Tsong Chen (2004). Signals and Systems 3th edition. Oxford University Press

Crenwelge Jr., O.E. and Peterson T. A., (1986). Overburden blasting vibrations: Analysis, prediction, and control. International Society of Explosives Engineers, General proccedings., pp 269-281.

Lusk, B., Worsey, P., Oakes, K., Chambers, J., Crabtree, S., Brasier, T., and Wheeler R., (2006). Destructive Wave Interference in Underground Blasting Utilizing Precise Timing. International Society of Explosives Engineers General Proceedings,. Vol. 1.

Siskind, D.E,. Stagg, M.S., Kopp, J.W., and Dowding, C.H. (1980b). Structure response and damage produced by ground vibration from surface mine blasting. U.S. Bureau of Mines RI 8507.

Spathis, A.T., 2010, A brief review of measurement, modeling and management of vibrations produced by blasting. Vibrations from blasting: Proceedings and Monographs in Engineering, Water and Earth Sciences, Taylor & Francis Group.